TESIS

Universidad de Jaén

Escuela Politécnica
Superior de Linares

Mejora en microrredes de CC basada en el acoplamiento serie de convertidores CC/CC

Autor: Enrique Javier Lanagrán Vargas

Director de la tesis: Manuel Ortega Armenteros
Francisco Jurado Melguizo

Departamento: Ingeniería eléctrica

Fecha: 08/04/2024

ISBN:

RESUMEN

Esta tesis se centra en la mejora de las microrredes de CC mediante el uso de una nueva estructura basada en el acoplamiento serie de fuentes y de sistemas de almacenaje. Actualmente existen varías arquitecturas para las microrredes de CC y todas toman como base dos configuraciones: la unipolar, que utiliza dos conductores (más usada) y la bipolar, que utiliza tres conductores. En todas ellas las fuentes y los sistemas de almacenaje se acoplan en paralelo.

En las zonas remotas o rurales, donde no existe posibilidad de interconexión con la red principal o esta es muy débil, y además las fuentes de energía renovable son de pequeña y mediana potencia con tensiones bajas, el acoplamiento en paralelo presenta algunos inconvenientes. Debido al nivel bajo de las tensiones de las fuentes y sobre todo de los sistemas de almacenaje, el área de influencia de las microrredes es muy limitada y la potencia de acoplamiento también está bastante limitada. Para resolver estos problemas se propone un sistema modular basado en el acoplamiento serie de las fuentes y de los sistemas de almacenaje. Este acoplamiento se lleva a cabo a través de convertidores de fuente de impedancia.

En un acoplamiento clásico (acoplamiento paralelo), normalmente el nivel más bajo de tensión lo tienen los sistemas de almacenaje (baterías o supercondensadores) y las pilas de combustible, siendo estos los que más influyen en el nivel de tensión de la barra del acoplamiento. Para conseguir tensiones de distribución entre 350 y 450V recomendadas por la IEC SEG4 para la distribución residencial y comercial, son necesarios convertidores con muy alta ganancia (sobre todo en los sistemas de almacenaje). Sin embargo, hay que tener en cuenta que, en los convertidores, la potencia convertida es inversamente proporcional a la ganancia, también estos son más caros a medida que aumenta la potencia convertida y la ganancia. Además, en el acoplamiento paralelo, cada convertidor (de fuente o sistema de almacenaje) necesita su propio control de corriente para poder aportar potencia al acoplamiento. Otros problemas del acoplamiento paralelo son: el estrés de tensión y el de corriente. Cuando se necesita alta ganancia, a medida que se eleva la potencia convertida, también se eleva la corriente a la que trabajan los dispositivos del convertidor, y sobre todo en el lado de baja tensión del convertidor, donde los dispositivos (diodos y transistores) encuentran su límite físico

quedando la potencia convertida muy limitada, por lo tanto, esto supone un problema desde el punto de vista de la potencia convertida, ya que con valores de tensión bajos la potencia convertida está muy limitada y la longitud de distribución también queda limitada a distancias muy cortas, siendo la fuentes o sistemas de almacenaje de más baja tensión los que imponen las restricciones al acoplamiento paralelo.

Un acoplamiento serie de convertidores de fuente de impedancia tiene ventajas claras sobre uno clásico. Las tensiones de salida de cada uno de los convertidores de acoplamiento se suman, siendo la tensión de la barra de acoplamiento de CC la suma de todas las tensiones de salida de los convertidores de acoplamiento (de las fuentes o sistemas de almacenaje) que están aportando a la barra de CC en cada momento. Con este sistema de acoplamiento se reducen los problemas de ganancia de tensión, de estrés de tensión y de corriente. De este modo, la fuente o sistema de almacenaje con menos tensión no afecta al conjunto de elementos acoplados y la tensión de la barra de CC no está limitada por una sola fuente, como sucede en el acoplamiento paralelo. El sistema de acoplamiento serie es modular y la tensión de la barra de acoplamiento no está limitada. La potencia convertida total se obtiene sumando la potencia convertida de cada convertidor a través de la suma de las tensiones de salida de los convertidores acoplados.

Las redes de impedancia de cada convertidor pueden ser diseñadas para limitar la potencia convertida y las corrientes, tanto en la entrada como en la salida de este (incluso en caso de cortocircuito en la salida del convertidor). Esto evita el estrés de corriente en los dispositivos y en la fuente, incluso en caso de falta. Los convertidores de fuente de impedancia también se pueden diseñar para un rango de tensiones determinado con una dependencia casi lineal del ciclo de trabajo en la zona de trabajo. Esto facilita mucho el acoplamiento, de modo que todos los convertidores pueden ser controlados por un solo controlador de tensión, que hace que la tensión del acoplamiento (tensión en la barra de CC) se mantenga muy próxima a su referencia, evitando que las perturbaciones que se producen en las fuentes renovables alcancen la barra de CC. El controlador actúa sobre todos los convertidores del acoplamiento activos en cada momento.

La ganancia de tensión de cada convertidor no depende de la tensión de la fuente ni de la tensión de la barra de acoplamiento (barra de CC), como sucede en el acoplamiento paralelo, esto hace que el estrés de corriente de los dispositivos no suponga ningún problema, pudiendo ser conectadas fuentes y sistemas de almacenaje con

tensiones muy distintas y potencias muy distintas, sin afectar esto al acoplamiento. Esto no es posible en los sistemas tradicionales de acoplamiento.

En cuanto a la gestión, también se simplifica mucho, ya que el acoplamiento tiende a obtener la potencia de la fuente que más potencia tiene disponible. Para conseguir esto, se requiere diseñar cada convertidor y su red de impedancia para la fuente que va a ser acoplada, teniendo en cuenta las fuentes que intervienen en el acoplamiento y los parámetros del acoplamiento. También hay que diseñar un controlador promedio que puede actuar sobre el ciclo de trabajo de todos los convertidores al mismo tiempo. Por último, si se quiere optimizar la gestión de energía del acoplamiento, es necesario un sistema de gestión para la toma de decisiones sobre el acoplamiento de fuentes en función de la potencia generada, consumida y almacenada en los sistemas de almacenaje o disponible a través de cualquier otro recuso.

Los resultados más significativos de esta tesis son: el estudio y obtención de un acoplamiento en serie que es capaz mantener un suministro estable en la carga a pesar de las variaciones aleatorias que se producen en las fuentes renovables. Con un diseño adecuado de los sistemas de almacenaje y una buena combinación de fuentes de energía renovable, se puede conseguir una microrred compuesta de fuentes renovables distribuidas de pequeña y mediana potencia, que acopladas en ramas en serie, sean capaces de conservar un suministro estable y de calidad, no dependiente de una red principal.

Esta tesis se justifica con el acoplamiento de varias fuentes y sistemas de almacenaje presentado en el capítulo 2. El estudio del modelo dinámico del convertidor usado en el acoplamiento, que nos permite obtener el controlador para el acoplamiento, es presentado en el capítulo 4. También, la técnica del acoplamiento en serie ha sido aplicada a un gasificador de biomasa en el capítulo 3. Debido a la inercia de las reacciones químicas que se producen en un gasificador de biomasa, cuando el gasificador pretende trabajar en isla, presenta problemas para el seguimiento de las variaciones de carga, obteniendo un suministro de baja calidad, que no es capaz de hacer un buen seguimiento de la carga en todo el rango de potencia. Mediante la técnica de acoplamiento en serie a través de convertidores de fuente de impedancia, los problemas han sido eliminados y se ha conseguido un suministro de calidad con el gasificador trabajando en isla.

ABSTRACT

This thesis focuses on the improvement of DC microgrids through the use of a new structure based on the serial coupling of sources and storage systems. Currently there are several architectures for DC microgrids and all of them are based on two configurations: the unipolar using two conductors (most commonly used) and the bipolar using three conductors. In all of them the sources and storage systems are coupled in parallel.

In remote or rural areas, where there is no possibility of interconnection with the main grid or it is very weak, and in addition the renewable energy sources are of small and medium power with low voltages, parallel coupling presents some disadvantages. Due to the sources low voltage level and especially of the storage systems, the area of microgrids influence is very limited and the coupling power is also quite limited. To solve these problems, a modular system based on the serial coupling of the sources and the storage systems is proposed. This coupling is carried out through converter of impedance source.

In a classical coupling (parallel coupling), typically the lowest voltage level is provided by storage systems (batteries or supercapacitors) and fuel cells, which have the greatest influence on the voltage level of the coupling bus. To achieve distribution voltages between 350 and 450V recommended by IEC SEG4 for residential and commercial distribution, converters with very high gain are necessary (especially in storage systems). But it should be noted that in converters, the converted power is inversely proportional to the gain, also these are more expensive as the converted power and gain increases. In addition, in parallel coupling, each converter (for source or storage system) needs its own current control in order to provide power to the coupling. Other problems of parallel coupling are voltage stress and current stress. When high gain is needed, as the converted power rises, so does the current at which the converter devices work, and especially on the low voltage side of the converter, where the devices (diodes and transistors) find their physical limit leaving the converted power very limited, therefore, This is a problem from the point of view of the converted power, since at low voltage values the converted power is very limited and the distribution length is also

limited to very short distances, being the lowest voltage sources or storage systems the ones that impose the restrictions to the parallel coupling.

A series coupling of impedance source converters has distinct advantages over a classical one. The output voltages of each of the coupling converters are summed, with the DC coupling bus voltage being the sum of all the output voltages of the coupling converters (from the sources or storage systems) that are contributing to the DC bus at any given time. With this coupling system, voltage gain, voltage stress and current problems are reduced. In this way, the source or storage system with less voltage does not affect the set of coupled elements and the DC bus voltage is not limited by a single source, as is the case in parallel coupling. The series coupling system is modular and the coupling bus voltage is not limited. The total converted power is obtained by summing the converted power of each converter through the sum of the output voltages of the coupled converters.

The impedance networks of each converter can be designed to limit the converted power and currents, both at the input and output of the converter (even in case of short-circuit at the converter output). This avoids current stress on the devices and on the source, even in case of a fault. Impedance source converters can also be designed for a given voltage range with an almost linear dependence on the duty cycle in the duty zone. This makes coupling much easier, so that all converters can be controlled by a single voltage controller, which keeps the coupling voltage (DC bus voltage) very close to its reference, preventing disturbances occurring in the renewable sources from reaching the DC bus. The controller acts on all the coupling converters active at any given time.

The voltage gain of each converter does not depend on the voltage of the source or the voltage of the coupling bus (DC bus), as is the case in parallel coupling. This means that the current stress of the devices is not a problem, and sources and storage systems with very different voltages and very different powers can be connected without affecting the coupling. This is not possible in traditional coupling systems.

In terms of management, it is also greatly simplified, since the coupling tends to obtain the power from the source that has the most power available. To achieve this requires designing each converter and its impedance network for the source to be coupled, taking into account the sources involved in the coupling and the coupling parameters. It

is also necessary to design an average controller that can act on the duty cycle of all converters at the same time. Finally, if the energy management of the coupling is to be optimized, a management system is needed to make decisions on the coupling of sources according to the power generated, consumed and stored in the storage systems or available through any other resource.

The most significant results of this thesis are the study and obtaining of a series coupling that is able to maintain a stable supply in the load despite the random variations that occur in renewable sources. With a proper design of the storage systems and a good combination of renewable energy sources, it is possible to achieve a microgrid composed of distributed renewable sources of small and medium power, which coupled in series branches, are able to maintain a stable and quality supply, not dependent on a main grid.

This thesis is justified by the coupling of several sources and storage systems presented in chapter 2. The study of the converter dynamic model used in the coupling, which allows us to obtain the controller for the coupling, is presented in chapter 4. Due to the inertia of the chemical reactions that take place in a biomass gasifier; when the gasifier pretends to work in island, it presents problems for the tracking of the load variations, obtaining a low quality supply, which is not able to make a good tracking of the load in all the power range. By means of the series coupling technique through impedance source converters, the problems have been eliminated and a quality supply has been achieved with the gasifier working in island.

AGRADECIMIENTOS

En primer lugar, quiero agradecer este trabajo a mi familia, los cuáles son mis ejemplos de amor, constancia, trabajo y buen hacer. Sin sus consejos no habría llegado a ser la persona que soy hoy día, han sido mis maestras y maestros, y me han aportado en todos los niveles de mi vida, porque ellas y ellos además de mi ejemplo, son mi refugio. Por supuesto, agradecerle a mi esposa, quien es mi compañera, amiga y confidente. Me ha acompañado durante todo el camino desde que comenzamos en el mundo de la ingeniería, apoyándome, ayudándome y cuidándome.

A mis amigas y amigos con los que hemos pasado muy buenos momentos.

También me gustaría agradecer a mis directores de tesis Francisco Jurado Melguizo y Manuel Ortega Armenteros por su tiempo, conocimientos y ayuda.

En general agradecer a todo aquel que ha estado junto a mí en estos años ya que en mayor o menor medida me han aportado algo que es de agradecer.

Quisiera dedicar este trabajo a mi esposa, la persona más importante de mi vida y que sin ella este trabajo no habría visto la luz, pues fue ella la que me introdujo en el mundo de la ingeniería.

Gracias a todas y todos por tanto.

ÍNDICE DE CAPÍTULOS:

CAPÍTULO I: Objetivos y planteamiento de la Tesis Doctoral..... 1

CAPÍTULO II: Design and integration of Z-source converters for energy management with series operation: Applied to DC microgrid 54

CAPÍTULO III: Design of an energy management system applied to an electric power plant based on a biomass gasifier 93

CAPÍTULO IV: Improvement of the coupling of renewable sources through Z-source converters based on the study of their dynamic model 136

CAPÍTULO V: Conclusiones aportaciones originales de la tesis y futuras líneas de investigación……..... 171

CAPÍTULO I: Objetivos y planteamiento de la Tesis Doctoral

ÍNDICE CAPÍTULO I:

1.1 GENERALIDADES Y ANTECEDENTES 6

1.1.1 Breve clasificación de los convertidores de CC/CC 9

1.1.2 Clasificación de las topologías elevadoras basadas en la red de impedancia 11

1.2 REDES DE CORRIENTE CONTINUA 18

1.2.1 Polaridad de la tensión en microrredes de CC 19

1.2.2 Arquitectura de las microrredes de corriente continua 22

1.2.3 Problemas de calidad de energía en microrredes de cc 30

1.3 LA GASIFICACIÓN COMO FUENTE DE ENERGIA CONTROLABLE 34

1.3.1 Situación actual de la gasificación 38

1.3.2 Problemática: aplicación y velocidad de respuesta para sistemas aislados 39

TABLA DE FIGURAS DEL CAPÍTULO I:

Fig. 1.1. Clasificación general de convertidores de CC/CC 11

Fig 1 2.Relaciones entre topologías de condensador + condensador 13

Fig 1 3.Topologías basadas en redes de impedancia 14

Fig 1.4. Forma de RZ usada en el convertidor de fuente de impedancia utilizado en esta tesis. 15

Fig 1 5. Estructura genérica de un convertidor de fuente de impedancia bidireccional. 16

Fig 1.6. Ejemplo de un inversor de fuente de impedancia trifásico 17

Fig 1.7: Configuración de una red de CC unipolar 20

Fig 1.8: Configuración de microrred de CC bipolar..... 21

Fig 1.9. Microrred de DC con arquitectura radial. 23

Fig 1.10. Arquitectura radial configuración serie..... 24

Fig 1.11.Arquitectura radial configuración paralelo. 24

Fig 1.12. Microrred CC con arquitectura en anillo. 25

Fig 1.13: Arquitectura de microrred de CC tipo malla..... 27

Fig.1.14. Arquitectura de microrred en CC de tipo zonal 28

Fig 1.15: Proceso de gasificación..... 35

Fig 1.16.Respuesta de un gasificador de 10 kW para diferentes variaciones de carga. 41

Fig 1.17.Detalle del incremento de carga uno..... 41

Fig 1.18.Detalle del incremento de carga dos. 42

Fig 1.19.Detalle del incremento de carga tres. 42

GLOSARIO DE SÍMBOLOS Y TÉRMINOS

BT	Baja tensión
CEM	Compatibilidad electromagnéticas
EMI	Interferencias electromagnéticas
ESS	Sistemas de almacenamiento de energía
FC	Pila de combustible
HVDC	Sistema de CC de alto voltaje
IED	Dispositivo electrónico inteligente
MTDC	Microrred de CC tipo malla
MV	Multiplicador de tensión
PLC	Comunicación a través de línea eléctrica
PV	Paneles solares fotovoltaicos
PWM	Modulación por ancho de pulso
RESs	Fuentes de energía renovable
RZ	Red de impedancia
SC	Condensador conmutado
SI	Inductor conmutado
SoC	Estado de carga
TL	Topología de tres niveles

VS	Estrés de tensión
WT	Aerogenerador o turbina de viento
ZS	Fuente de impedancia
ZTDC	Microrred de CC tipo zonal

1.1 GENERALIDADES Y ANTECEDENTES

En la actualidad el uso de energías renovables se está incrementando cada vez más debido a los problemas, cada vez más urgentes, que están surgiendo a consecuencia del cambio climático. Este se está manifestando con un aumento generalizado de la temperatura del planeta, que va unido al deshielo de los glaciares, eventos climáticos extremos cada vez más recurrentes y cambios en los patrones meteorológicos. Estos hechos tienen impactos muy significativos en la biodiversidad, el medio ambiente y, por consecuencia, en el ser humano. Ante esta problemática hay que buscar métodos paliativos.

Actualmente, en los países desarrollados la energía eléctrica es clave e imprescindible, de la que somos totalmente dependientes y vivimos completamente interconectados. Los avances de cualquier país o sociedad están directamente asociados al fomento de la energía eléctrica. Para evitar seguir contribuyendo al cambio climático es importante la actualización de los métodos de generación de energía que utilizan combustibles fósiles y otros elementos tan nocivos para el medio ambiente. Además, cada vez son más necesarios suministros electicos permanentes, estables y de calidad, sin contaminación armónica, ni perturbaciones que afecten a las cargas. De hecho, el desarrollo de la economía de un país tiene gran dependencia de su plan energético, debiéndose garantizar los puntos anteriormente citados sin que la energía tenga un coste desorbitado.

La generación mundial de energía utilizando fuentes renovables está creciendo rápidamente. La capacidad que tienen las tecnologías renovables para permitir una rápida transición a un sistema energético con bajas emisiones de carbono depende en gran medida de la energía que deben "consumir" durante su ciclo de vida. Según sugieren los resultados de [1] la energía eólica tiene los costes energéticos más bajos, seguida de la termosolar y la fotovoltaica. A pesar de que el coste de las energías renovables primarias sea bajo, la realidad es que llevar a cabo la integración de varias fuentes a gran escala plantea grandes y nuevos retos en las conexiones de dichas fuentes y sobre todo poder mantener un suministro permanente a las cargas desde energías renovables, así como adaptar los niveles de tensión de las fuentes a los de las cargas. En estos puntos es donde

toman gran relevancia los convertidores de potencia, ya que son de gran importancia a la hora de resolver problemas que se plantean en estas nuevas conexiones [2].

Aún a día de hoy se puede afirmar que la organización de la generación eléctrica es jerárquica, con relativamente pocos generadores de gran potencia (aunque esto ya está cambiando poco a poco). Estos grandes generadores son los que trabajan para abastecer una demanda muy poco flexible de forma generalizada. Sin embargo, las fuentes primarias de energía renovable están marcadas por las condiciones meteorológicas y pueden utilizarse descentralizadas. Debido a la aleatoriedad de estas fuentes y para garantizar el suministro es muy común combinarlas con el uso de sistemas de almacenaje de energía (ESSs), los cuales están siendo objeto de investigación [3].

Por otro lado, el mercado eléctrico a día de hoy marca el precio de la energía para grandes áreas geográficas y no engloba la producción relacionada con la generación distribuida ni con las microrredes [4]. Debido al incremento de las fuentes energéticas distribuidas que se está llevando a cabo desde hace algunos años, una opción a considerar sería el fomentar el control descentralizado para gestionar el sistema y la complejidad que acarrea [5]. Los sistemas de generación renovable pueden estar desconectados de la red de forma permanente usando elementos de almacenaje de energía con baterías (sistemas aislados), o pueden estar conectados a la red compartiendo energía con ella, siendo la red la que se encarga de absorber los excedentes y de proporcionar el suministro cuando hay falta en las renovables, esto es muy utilizado en suministros domésticos e industriales de países con redes eléctricas potentes [6]. Los sistemas aislados son muy beneficiosos para zonas alejadas, ya que pueden crearse microrredes para tener abastecimiento energético sin necesidad de ampliar la red eléctrica tradicional [6].

En entornos con limitaciones energéticas, donde la capacidad de las fuentes de energía renovable (RESs) es significativa y los ESSs reemplazan parte de la capacidad de generación, es esencial que estos contribuyan a garantizar el suministro durante los períodos de tiempo de baja generación de las fuentes de energía renovable aleatoria. Al diseñar los ESS, es crucial considerar el equilibrio entre los costos asociados con la generación de energía excedente y el riesgo de escasez [7]. Además, los ESSs en las microrredes deben operar de manera que mantengan un estado de carga (SOC) lo suficientemente alto para cubrir los períodos de alta demanda, al mismo tiempo que

mantienen un SOC lo suficientemente bajo durante los períodos de alta generación de las renovables para minimizar el desperdicio de energía. Este logro es complejo y requiere un diseño cuidadoso de los convertidores, así como el uso de un sistema de gestión que consigan optimizar el funcionamiento del proceso teniendo en cuenta la demanda y la aleatoriedad de las fuentes renovables en la zona de ubicación de los generadores [8].

En las diversas fuentes de energías renovables, encontramos distintos tipos que generan tanto en CC como en CA [9]. Por lo general, estas fuentes renovables producen energía de manera dependiente de la variabilidad del recurso energético, como el viento o la radiación solar. Es común que, por sí mismas y sin necesidad de un apoyo externo, estas fuentes no logren mantener constante su tensión de salida frente a cambios en los recursos energéticos primarios, así como ante variaciones en la carga. Por esta razón, se hace necesario desarrollar y utilizar convertidores de potencia [10], junto con técnicas de control y gestión adecuadas. Estas herramientas nos permitirán aprovechar de manera eficiente la energía de estas fuentes limpias, asegurando un suministro estable incluso en situaciones de generación y carga variables.

Los convertidores de potencia desempeñan un papel esencial y necesario, sin ellos sería imposible una buena gestión de las energías renovables. Entre las topologías clásicas de convertidores de CC destacan los de fuente de tensión [11] y los de fuente de corriente [12], que son muy usados para potencias bajas y medias con tensiones bajas, los de fuente de corriente son más adecuados para trabajar en modo elevador,

cuando se quiere elevar la potencia convertida y la tensión de salida del convertidor son más adecuados los convertidores de CC/CC con estructura de puente completo y transformador de alta frecuencia [13]. Estos últimos presentan problemas asociados con la inductancia de fugas del transformador y sobre todo cuando se necesitan tensiones de salida elevadas, esto nos obliga a adoptar soluciones constructivas de intercalado de bobinados primario y secundario para disminuir las inductancias de fugas mediante la compensación de las inductancias de ambos bobinados, [14]. Aunque existen varios tipos de convertidores, estos deben de ser elegidos en función de sus características y de la aplicación a la que van a ser destinados.

Por ejemplo, la pila de combustible (FC) es una fuente de energía con corriente elevada y tensión baja, siendo su tensión el motivo que hace aumentar sus pérdidas en la

entrada del convertidor que adapta su potencia. También presenta una respuesta lenta frente a variaciones de la carga. Su tensión de salida sufre variaciones importantes (comparadas con su tensión nominal) cuando la carga experimenta fluctuaciones o cambios bruscos, es por ello que la FC no puede mantener estable su tensión de salida (experimenta perturbaciones). Por lo tanto, se requieren convertidores CC/CC capaces de interconectar la FC con una barra o red de CC, que puedan conservar su tensión con valores estables y no se vea afectada por las perturbaciones sufridas en la tensión de salida de la FC, producidas por los cambios en la carga [15]. Estos convertidores también llevan asociada una gran ganancia de tensión debido a que la tensión de salida de la FC es baja.

Algunos estudios han propuesto métodos para implementar la conversión de energía en pilas de combustible, trabajando de manera aislada mediante el uso de convertidores CC/CC con configuraciones push-pull de puente completo, ya sea alimentados por tensión o por corriente[16].

En los sistemas de generación de energía renovable es posible cargar y descargar los ESSs haciendo uso de convertidores bidireccionales CC/CC[17]. Esto se realiza con el fin de almacenar la energía sobrante en las horas de gran generación de energía renovable para luego aprovecharla cuando la demanda lo solicite en las horas de escasa generación, de manera que se pueda conservar el suministro de calidad la mayor cantidad de tiempo posible y mantener constante la tensión en la barra de CC [18]. También nos podemos encontrar sistemas de AC con enlaces bidireccionales en CC [19]. Además, ciertos convertidores bidireccionales logran una eficiencia notable con un número reducido de elementos de conmutación, y su capacidad de aumentar significativamente la ganancia de tensión se facilita mediante el uso de un inductor acoplado [20].

1.1.1 Breve clasificación de los convertidores de CC/CC

La red de impedancia (RZ) ha sido aplicada a muchos tipos de convertidores donde son varias las estructuras usadas para estos convertidores [21]. Se puede hacer una clasificación de los convertidores que trabajan como elevadores según si tienen aislamiento galvánico o no lo tienen. Para conseguir el acoplamiento es necesaria una

estructura de acoplamientos tal como un trasformador de alta frecuencia. Dentro de los convertidores sin aislamiento se puede hacer una clasificación entre convertidores CC/CC con inductor acoplado y de red de impedancia [22].

Para realizar la elevación de tensión en los convertidores de CC/CC se introduce un transformador de alta frecuencia entre las dos etapas de continua CC/CA/CC, de modo que el aislamiento se consigue mediante el transformador, Igualmente, el transformador permite conseguir una gran ganancia de tensión dependiendo esta de los números de espiras de sus bobinados, pero el aumento del número de espiras es inversamente proporcional a la eficiencia y a la potencia convertida [23], ya que se produce un aumento en la inductancia de fugas, por lo que cuando se necesitan grandes ganancias de tensión, este tipo de convertidores puede plantear problemas.

También se puede conseguir mejorar la ganancia de tensión mediante la topología de inductor acoplado, que consiste en añadir un inductor a un convertidor con trasformador, pero de este modo desaparece el aislamiento galvánico del convertidor [24]. Cuando se aumenta la ganancia mediante el incremento del número de espiras, se puede usar un circuito amortiguador adicional para el convertidor de inductor acoplado, aunque esto supone un sobrecoste, además de hacer el convertidor más complejo y voluminoso [25] [26],[14].

Por otra parte, existen los convertidores de CC/CC no aislados que son más sencillos, no tienen los problemas de la inductancia de fugas y en esta categoría encajan varios de los convertidores tradicionales con pocos dispositivos [14], Sin embargo, estos convertidores elevadores no tienen un ciclo de trabajo limitado, ya que su funcionamiento depende de varios parámetros constructivos y de la carga, de modo que estos convertidores no pueden obtener una ganancia elevadora muy grande[27], [28].

Otro tipo de convertidores son los de RZ, donde existen varias configuraciones de redes de impedancia, compuestas por inductores, condensador, diodos y conmutadores. Desde un punto de vista general los convertidores basados en RZ no presentan problemas de picos de tensión y tienen una capacidad de potencia convertida alta. En la Fig 1.1 se muestra una clasificación general de topologías elevadores de convertidores de CC/CC.

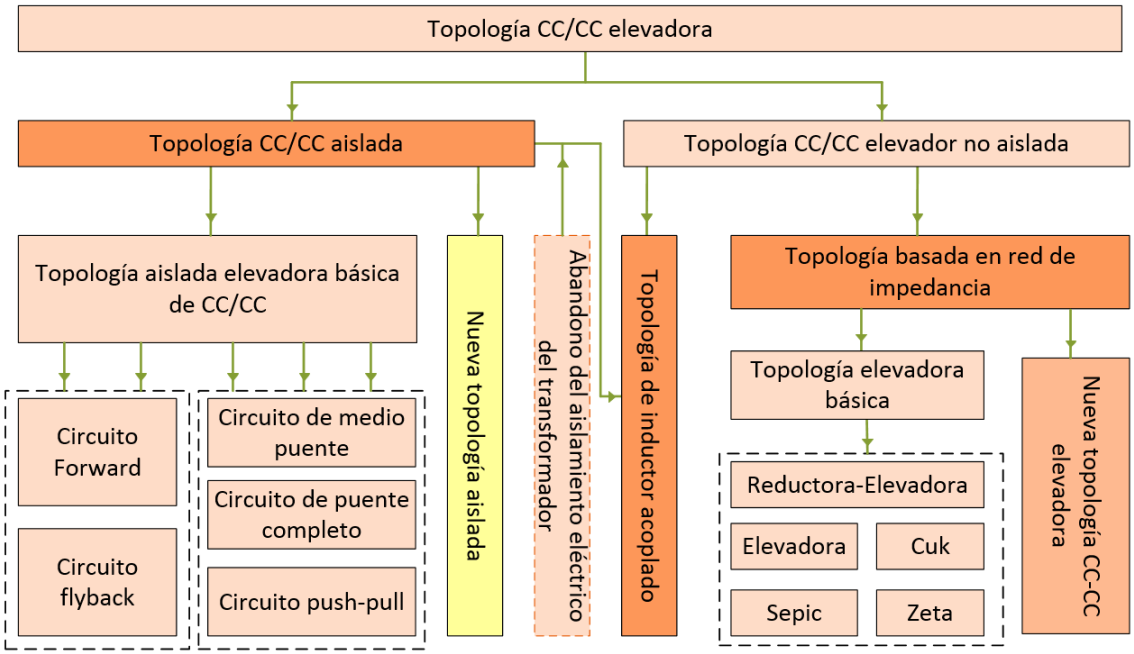

Fig. 1.1. Clasificación general de convertidores de CC/CC

1.1.2 Clasificación de las topologías elevadoras basadas en la red de impedancia

Los convertidores basados en RZ combinan elementos de almacenamiento de energía (inductor y condensador) junto con diodos y dispositivos de conmutación [29], que conmutados y teniendo en cuenta los cuatro principios siguientes, pueden obtenerse estructuras de convertidores CC/CC basadas en redes de Z.

Principio 1: Para conseguir ganancias de tensión elevadoras, la carga de los inductores y condensadores se hace desde la fuente en paralelo. La descarga se debe de llevar a cabo colocando los elementos energizados en serie, de modo que cuando descargan sus energías sobre la carga o sobre la barra de CC suman sus tensiones, de este modo se amplifica la ganancia elevadora.

Principio 2: Para conseguir una ganancia elevada es imprescindible disponer de un almacenaje de energía inicial antes de comenzar la conmutación, de modo que la conmutación inicia con un intercambio de energía entre condensadores e inductores en el

momento que el transistor es cerrado, y cuando está abierto, tanto los inductores como la fuente de alimentación, suministran energía a la carga conjuntamente.

Principio 3: Para aumentar la ganancia es necesario intercalar condensadores e inductores sin violar las leyes del circuito en cada etapa de conmutación.

Principio 4: Para reducir el estrés de tensión (VS) de los componentes, el condensador debe añadirse a la red de impedancia, formando un circuito cerrado con un interruptor, un diodo y una carga.

Por otra parte, el diseño de los componentes nos permite ajustar una red de impedancia para conseguir una ganancia de tensión y una potencia convertida determinadas.

Se distinguen varios tipos de redes de impedancia:

- Estructura (Tipo1): configuración (inductor + inductor).

Dos inductores se combinan según el Principio 1, y sus estados de funcionamiento dependen de los estados de los diodos y conmutadores. Esta es la estructura de inductor conmutado (SI). Cuando la corriente de entrada está basada en pulsos, para obtener un rizado de corrientes a la entrada lo más reducido posible, se hace un desplazamiento de fase de los inductores, de modo que los inductores se cargan y descarga de forma alterna. Por lo tanto, cuando un inductor se carga el otro se descarga.

En la etapa de carga de cada inductor, su diodo de descarga se conserva polarizado inversamente. Si se utilizan condensadores, de forma que los dos inductores y el condensador funcionen según el Principio 1, se obtiene la estructura del interruptor conmutado combinada con una bomba de carga.

- Estructura (Tipo2): Configuración (condensador + condensador)

Cuando dos condensadores se combinan según el Principio 1, dependiendo sus estados de funcionamiento de la posición de los conmutadores (abierto o cerrado). se obtiene así la estructura de condensador conmutado (SC). Según el Principio 2, se puede obtener un multiplicador de tensión (MV).

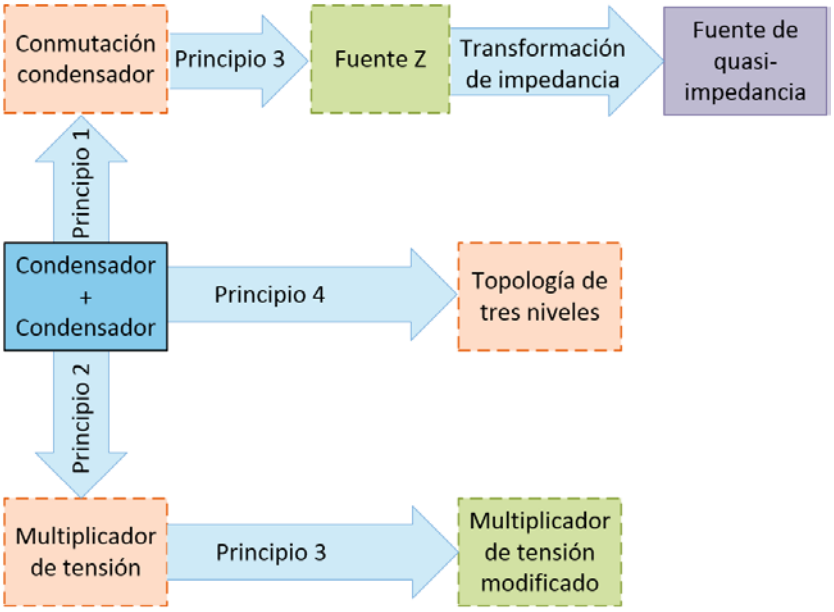

Fig 1 2.Relaciones entre topologías de condensador + condensador

La estructura de fuente Z puede obtenerse modificando la estructura de condensador conmutado según el Principio 3. La estructura de fuente q-Z puede obtenerse mediante la transformación de la impedancia de la estructura de fuente Z. La estructura modificada del multiplicador de tensión puede obtenerse haciendo la modificación según el Principio 3. También se puede obtener una topología de tres niveles (TL) combinando dos condensadores según el Principio 4. La relación entre las topologías de condensador + condensador se muestra en la Fig. 1.2.

Estructura (Tipo3): configuración (inductor + condensador)

Según el Principio 1, las topologías basadas en redes de impedancia pueden obtenerse combinando un inductor con un condensador.

Estructura (Tipo4): configuración (hibrido en cascada)

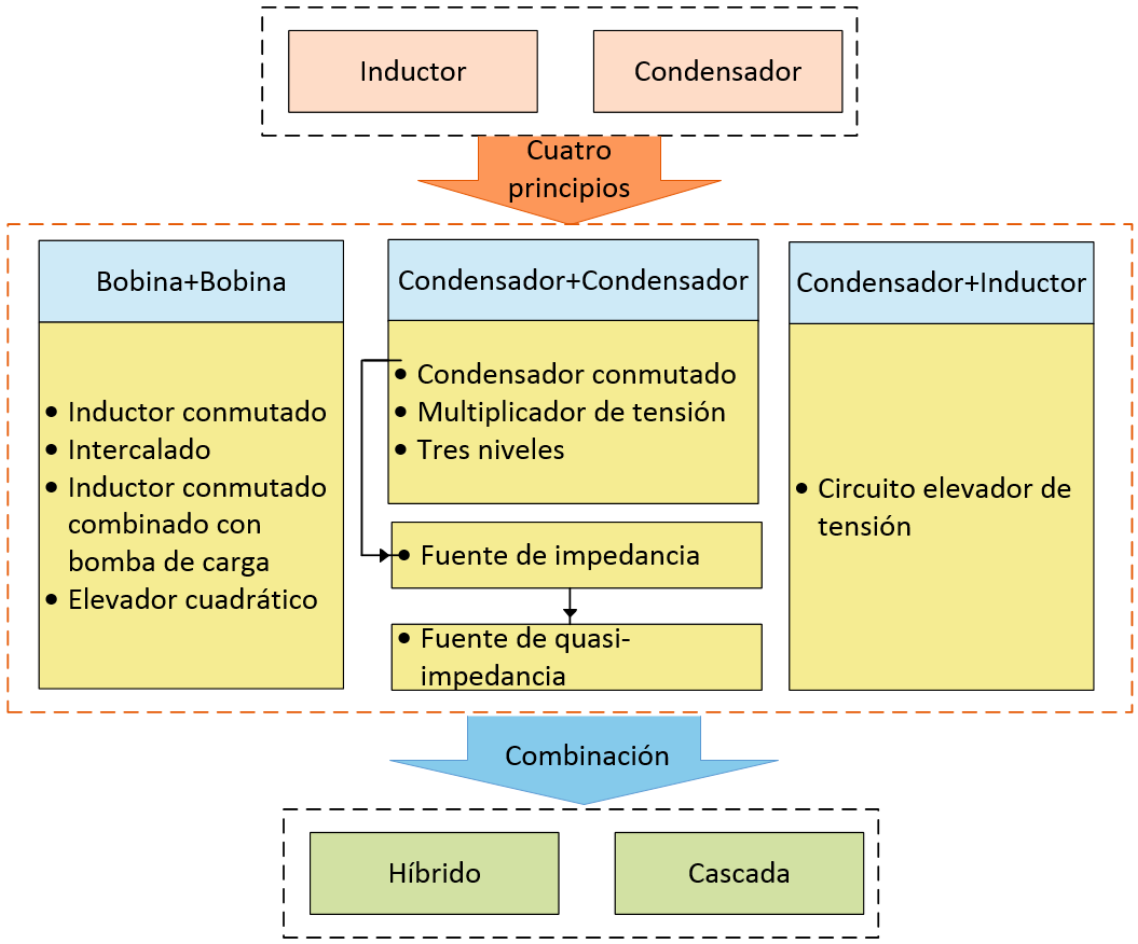

Fig 1 3.Topologías basadas en redes de impedancia

Mediante la conexión en cascada e integración de redes de impedancia se puede conseguir convertidores de CC/CC con mejores características en cuanto a eficiencia, ganancia de tensión, estrés de corriente, además de obtener convertidores de CC/CC con topologías nuevas.

La clasificación de topologías basadas en la red de impedancia, se muestra en la Fig 1.3.

1.1.2.1 Convertidores de fuente de impedancia

Los convertidores de fuente de impedancia [ZS] son un subgrupo de los convertidores de RZ, que se encuentran entre los últimos convertidores desarrollados y, posterior mente, haciendo modificaciones a la fuente de impedancia, surgen los de fuente de cuasi impedancia. Ambos son muy parecidos, pero presentan algunas diferencias, que les confieren utilidades también diferentes.

La investigación del convertidor de fuente de impedancia comenzó con el estudio del inversor de fuente de impedancia basándose en la red de impedancia [30]. Estos inversores se pueden configurar en modo elevador o en modo reductor utilizando únicamente una etapa de conmutación, lo cual presenta una ventaja frente a otros convertidores de fuente de tensión o de corriente. La principal característica que tiene es que está formado por condensadores, bobinas, diodos e interruptores semiconductores y con ellos se consigue reducir o elevar tensión. También presenta mayor compatibilidad con cargas variables, por las propiedades de la RZ. En los últimos años, los convertidores de fuente de impedancia han sido usados para la etapa de elevación de inversores, también en la implementación de convertidores de CC/CC tanto unidireccionales como bidireccionales [31], etc.

La base de un convertidor de fuente de impedancia es su red de impedancia, siendo la red clásica la mostrada en la Fig 1.1. Se trata de una red de dos puertos que incorpora dos inductores, L1 y L2, y dos condensadores, C1 y C2, dispuestos de manera cruzada como se muestra en la Fig 1.1. Los inductores y condensadores son los que configuran la red Z. Con el diseño adecuado de los elementos componentes L y C se le pueden aportar unas propiedades específicas y ya prefijadas a un convertidor de SZ. En la, esta puede utilizarse de forma bidireccional y también puede conmutarse en los modos elevador y reductor en ambas direcciones. Aunque se puede definir una estructura genérica de los convertidores de SZ, pero los elementos en cada convertidor deben de ser dispuestos y configurados según los objetivos buscados por cada convertidor.

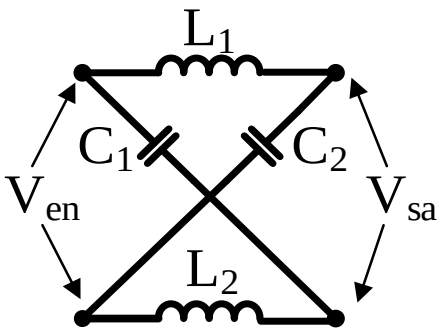

Fig 1.4. Forma de RZ usada en el convertidor de fuente de impedancia utilizado en esta tesis.

Una de las aplicaciones clásicas de la fuente de impedancia es la etapa de elevación de acondicionamiento de tensión en la barra de CC del inversor, usando una ZS se puede obtener una tensión adecuada en la barra de CC del inversor para conseguir en la salida de corriente alterna la tensión adecuada.

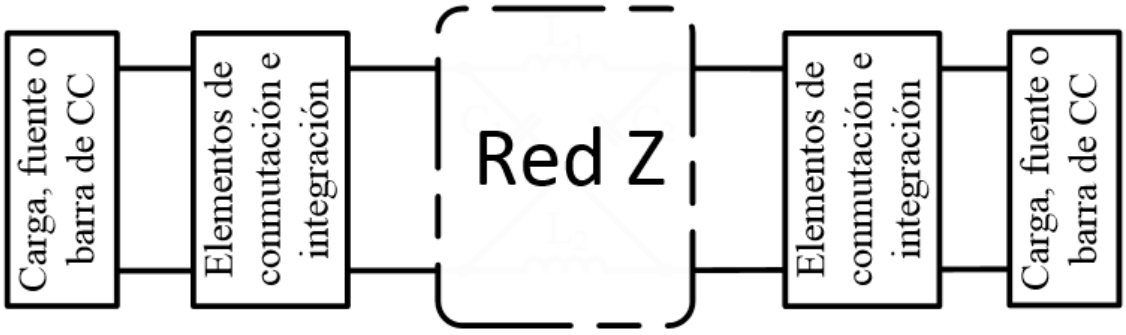

Fig 1 5. Estructura genérica de un convertidor de fuente de impedancia bidireccional.

En la Fig 1.6 se muestra el circuito de potencia de un inversor de medio puente trifásico, con acondicionamiento de tensión de la barra de CC basado en ZS. En un inversor de fuente de tensión trifásico convencional que tiene ocho estados, seis estados activos y dos estados cero ([000] y [111]). Si se hace un acondicionamiento de la tensión de entrada mediante una ZS, también tiene que ser modificada la conmutación del inversor y además de los ocho estados propios del inversor de fuente de tensión (seis estados activo y dos estados cero), son posibles siete estados adicionales que activan simultáneamente los dispositivos superior e inferior de cualquier tramo de una fase, dos fases o todos los tramos de tres fases [30], [15]. Estos estados de disparo directo están prohibidos en un inversor de fuente de tensión convencional, ya que podrían causar un cortocircuito en la fuente. Estos estados directos son intercalados entres los estados propios de la conmutación del inversor en fuente de tensión y de este modo se consigue ajustar el nivel de tensión a la salida de la ZS.

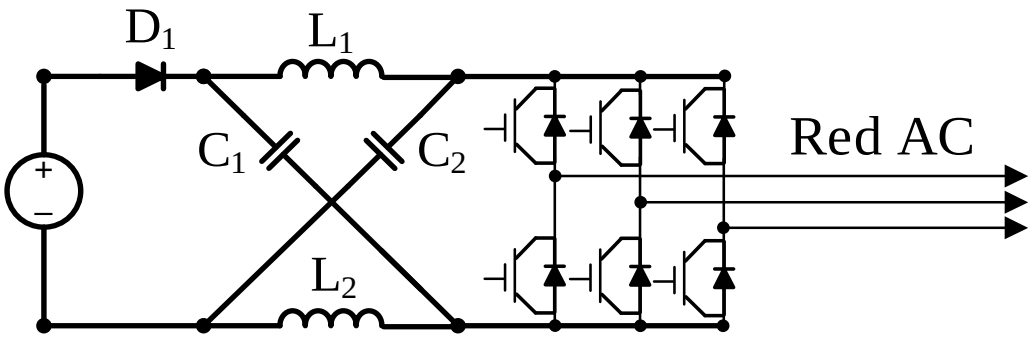

Fig 1.6. Ejemplo de un inversor de fuente de impedancia trifásico

La ZS y los estados de disparo directos, intercalados en la secuencia de disparos con los disparos activos, proporcionan una característica única que llega a mejorar el inversor de fuente de tensión, aunque la conmutación se está haciendo integrada en la del inversor, pero, los estados de disparo directos afectan a la ZS, de modo que con ellos se regula la tensión de salida de la misma. Esto permite regular el valor de tensión de la salida de la ZS mediante la regulación del tiempo de duración de los estados de disparo directo o de cortocircuito. De esta manera, es posible conseguir tensiones de salida superiores a las de la entrada, una función imposible de lograr con un inversor de fuente de tensión convencional.

La ZS agrega un refuerzo a la regulación de tensión que se consigue controlar con los estados de cortocircuito. Todas las técnicas de conmutación de inversores típicas como la PWM de vectores espaciales [31], PWM sinusoidal [32], pueden ser modificadas para conmutar y controlar al mismo tiempo la ZS y los transistores de potencia del puente del inversor. De este modo, las relaciones teóricas que existen entre la entrada y la salida siguen siendo válidas. Las técnicas de conmutación clásicas han sido fusionadas con estados que activan la ZS (disparo directo o de cortocircuito) y se han desarrollado nuevos métodos PWM como el control de impulso máximo, control de impulso simple, control de impulso constante máximo y modulación de vectores espaciales [33]**.** Otra característica que le aporta la ZS al inversor, es que protege a la fuente de CC que él conecta con la red o la carga de AC, de modo que con un diseño adecuado de la RZ, la fuente de CC queda inmunizada frente a cortocircuitos que ocurran aguas abajo de la RZ,

esto es debido al cortocircuito que se produce en una de las etapas de conmutación del convertidor que le proporciona inmunidad a las fuentes que están conectadas a él.

El convertidor utilizado en esta tesis doctoral, es un convertidor CC/CC bidireccional basado en fuente de impedancia de una sola etapa, el cual ha sido estudiado [2]. Aporta las ventajas propias de un convertidor de ZS, pero debido a su diseño se ha conseguido una respuesta lineal (en toda la zona de trabajo) de su salida respecto a su ciclo de trabajo, además de que se caracteriza por tener altas ganancias en los modos elevador y reductor. También tiene un aprovechamiento total del ciclo de trabajo, necesitándose muy pocos elementos pasivos y semiconductores para la implementación del convertidor.

En general, en las redes de CC, unos de los elementos principales e imprescindibles son los convertidores de CC/CC para interconectar los ESSs y los generadores con la barra de CC, ya que los convertidores de CC/CC puede garantizar un nivel de tensión y de corriente de salida controlable. Usando convertidores unidireccionales se pueden integrar en una misma microred varios generadores de distintos tipos y con características nominales diferentes (potencia, tensión, etc.). También, si se usan convertidores bidireccionales se pueden integrar ESSs diferentes y con valores de SoC distintos.

1.2 REDES DE CORRIENTE CONTINUA

A día de hoy, en el área residencial y comercial se utilizan equipos conectados a la red como ordenadores, sistemas de iluminación, y cargadores de baterías los cuales utilizan corriente continua. Las redes actuales solo aportan energía en corriente alterna, lo que obliga a los usuarios a hacer una conversión a continua de la corriente alterna que recibe en su suministro, lo cual reduce la eficiencia global y la fiabilidad de los sistemas, ya que estos dispositivos necesitan una etapa de conversión AC/CC para conectarse a la red de AC. Algunas de estas etapas de conversión pueden sustituirse por un convertidor de CC/CC de alta eficiencia si estos dispositivos se conectaran directamente a una red de corriente continua.

Una microrred es una red eléctrica de baja tensión (BT) que contiene fuentes de energía distribuida, como son paneles fotovoltaicos, microturbinas eólicas, pilas de combustible y ESSs. La idea de las microrredes surgió como una solución para satisfacer la demanda de energía local conectando fuentes de energía distribuida a redes de distribución sin necesidad de ampliar las redes centralizadas (ya que es muy costoso).

Las microrredes de CC son una tecnología atractiva en el sistema de redes eléctricas modernas debido a su interfaz natural con fuentes de energías renovables, cargas eléctricas y ESSs. En los últimos años ha habido un aumento de los trabajos de investigación en el área de las microrredes de CC [34], [35], lo que hace que la aplicación práctica de este tipo de tecnología esté cada vez más cerca, siendo una muy buena solución para áreas aisladas[35].

Igual que en corriente alterna, en las microrredes de CC para la conexión de cargas, también se usan dos niveles de tensión.

1.2.1 Polaridad de la tensión en microrredes de CC

En las redes de AC la energía eléctrica se puede distribuir mediante dos cables (monofásicos) o cuatro cables (sistemas trifásicos con neutro). En las redes de CC sucede algo similar. Se pueden usar los sistemas de dos hilos (unipolares) y de tres hilos (bipolares) [36]. Siendo la diferencia entre estas dos configuraciones de red de CC el número de niveles de voltaje disponibles y por tanto la capacidad de suministro de potencia a las cargas conectadas a esa red.

1.2.1.1 Microrred con configuración unipolar de CC

En las microredes de CC, las fuentes y cargas están conectadas entre los polos positivo y negativo de la barra de CC como se ilustra en la Fig 1.7. La energía se transmite a través de la barra de CC con un nivel de tensión; por lo tanto, la selección del nivel de tensión de la barra de CC es clave en este sistema, ya que esta tensión es común para

todas las fuentes y cargas, de modo que todas ellas tienen que conectarse con ella directamente o a través de convertidores. Si se usa una tensión más elevada, aumenta la capacidad de transmisión de energía del sistema, en cuanto a distancia de transmisión y a potencia transmitida, pero se requieren convertidores con mayor ganancia de tensión, normalmente esto supone convertidores con mayores pérdidas y más caros. Además, un nivel de tensión más alto también aumenta los riesgos de seguridad.

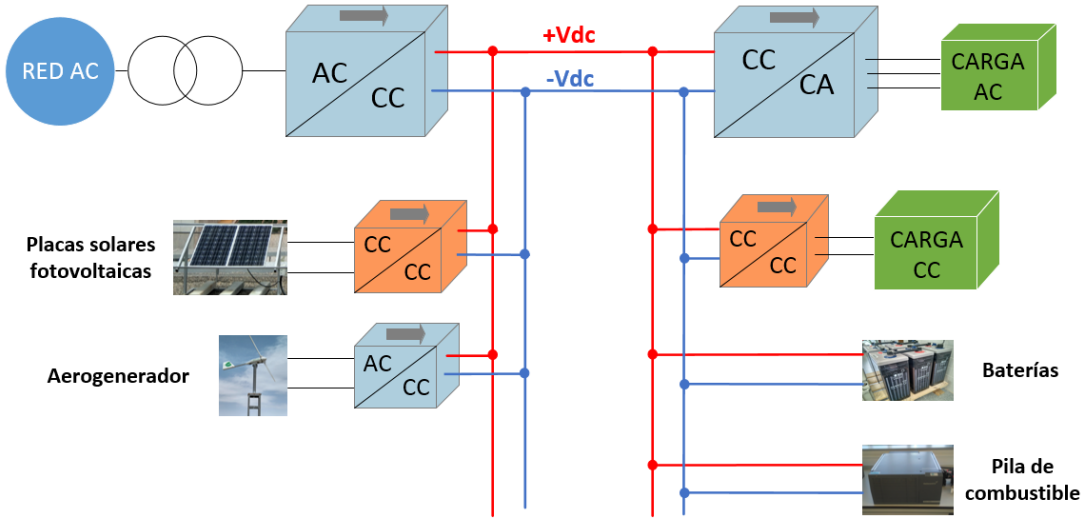

Fig 1.7: Configuración de una red de CC unipolar

Con niveles de voltaje bajos, la capacidad de transmisión del sistema se limita a una distancia más corta. Pero, si en la barra de CC se elige un nivel de voltaje bajo, se puede evitar la instalación de una gran cantidad de convertidores CC-CC para los distinto equipos (fuentes o cargas) que se conectan a esta barra CC.

El sistema unipolar mostrado en la Fig 1.4 es viable en zonas rurales remotas para viviendas aisladas de la red eléctrica, donde no existe infraestructura de red pública. Recientemente se han implementado sistemas unipolares de 48V en CC con la integración de paneles fotovoltaicos en microrredes para casas aisladas de la red en zonas rurales de la India [37].

1.2.1.2 Microrred bipolar de CC

Un sistema bipolar puede superar las limitaciones del sistema unipolar. Este sistema también es conocido como sistema de barra de CC de tres cables, cuyas tensiones son $+V_{dc}$, $-V_{dc}$ y una línea neutra, como se muestra en la Fig 1.5. En esta configuración, los clientes tienen la opción de elegir tres niveles de tensión diferentes: $+V_{dc}$, $-V_{dc}$. y $2V_{dc}$. Además, en caso de fallo en uno de los polos de CC, la energía aún puede ser suministrada por los otros dos cables (bipolares) y un convertidor auxiliar. Por lo tanto, la confiabilidad, disponibilidad y calidad de la energía del sistema aumentan durante condiciones de falla. Este sistema bipolar requiere de convertidores especiales denominados balanceadores de voltaje, que son los convertidores que interconectan la parte de la microred unipolar con la bipolar.

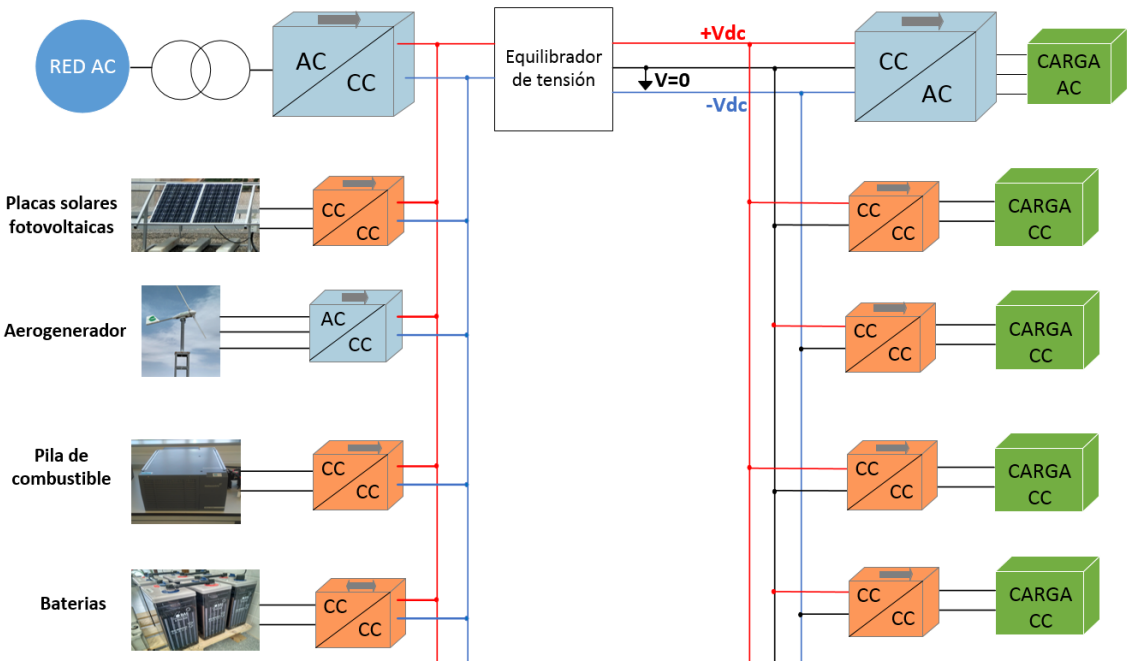

Fig 1.8: Configuración de microrred de CC bipolar

Los diferentes niveles de tensión ofrecen más flexibilidad a los clientes para conectar cargas a varios niveles de tensión, pero al mismo tiempo se pueden producir desequilibrios en el sistema, debido a una distribución desigual de las cargas. Por lo tanto, en este tipo de sistemas es muy recomendable un circuito equilibrador de tensión o un sistema de control adecuado para los convertidores de potencia en el lado de la fuente[38]

Las topologías unipolares y bipolares son la base para las futuras arquitecturas en las microrredes de CC.

1.2.2 Arquitectura de las microrredes de corriente continua

La capacidad de los sistemas distribuidos de energías renovables es muy variable e incierta debido a su dependencia de las condiciones climáticas. Por lo tanto, una interfaz con la red de AC es muy importante para mejorar la fiabilidad y disponibilidad de energía en una microrred de CC. Hay algunas opciones para interconectar una microrred de CC con una red de CA, como:

- Configuración radial.
- Configuración de anillo o bucle.
- Configuración interconectada.

1.2.2.1 Configuración radial

En esta configuración, la barra de CC está interconectada con una red de CA en un extremo y la energía fluye a lo largo de un único camino hacia las cargas. Por lo tanto, solo hay una ruta disponible entre cada carga y la interfaz de la red de AC. En la Fig 1.4 se muestra un diagrama unifilar del sistema de la microrred radial de CC, donde fuentes de energía, ESS y cargas (tanto de CA como de CC) están conectados en paralelo a la barra de CC. Esta barra puede ser unipolar o bipolar, dependiendo de las aplicaciones y requisitos. Esta arquitectura se puede utilizar en edificios residenciales, donde se prefiere la barra de CC de baja tensión para igualar el nivel de tensión de muchos electrodomésticos y evitar etapas adicionales de conversión CC/CC. También en tales sistemas, las cargas y la interfaz de la red de CA pueden ubicarse cerca entre sí para reducir las pérdidas de distribución.

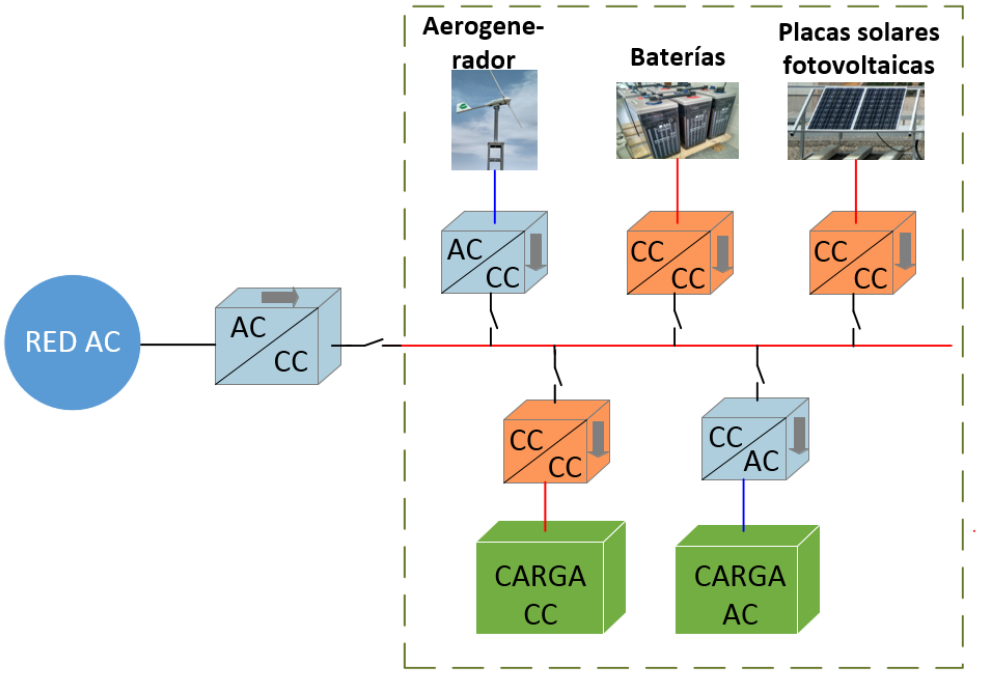

Fig 1.9. Microrred de DC con arquitectura radial.

El mismo concepto se puede extender a un sistema de microrred de CC múltiple, como un edificio de varios pisos o una comunidad, donde cada microrred puede tener RES y ESS junto con diferentes cargas. En dichos sistemas, la barra de CC de cada microrred puede interconectarse en serie o en paralelo dependiendo de la disposición física de los edificios o comunidades. De esta forma, cada edificio actúa como un conjunto dentro de la microrred y es capaz de consumir o inyectar energía a las microrredes vecinas. La arquitectura radial paralela puede aumentar la confiabilidad del sistema al aislar solo las barras defectuosas en caso de fallas, permitiendo así que las barras en buen estado continúen con su funcionamiento normal. La arquitectura radial en serie puede tener algunos problemas de estabilidad durante los modos en isla.

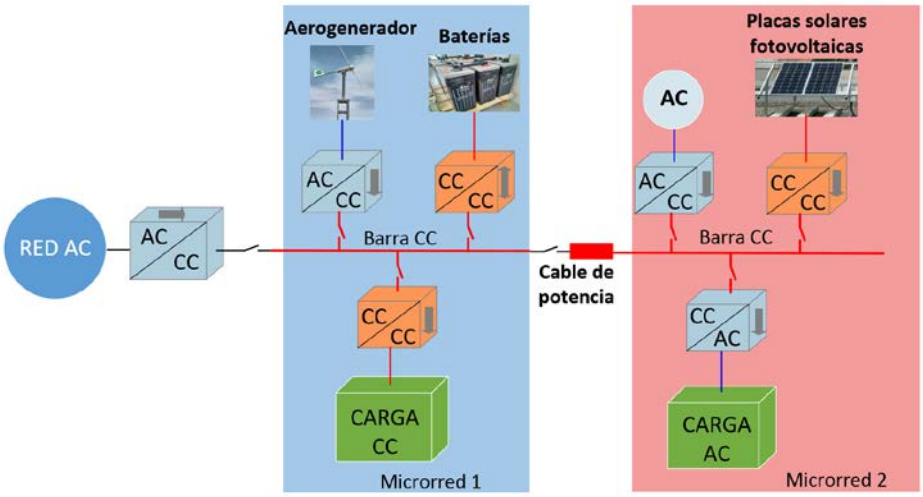

Fig 1.10. Arquitectura radial configuración serie.

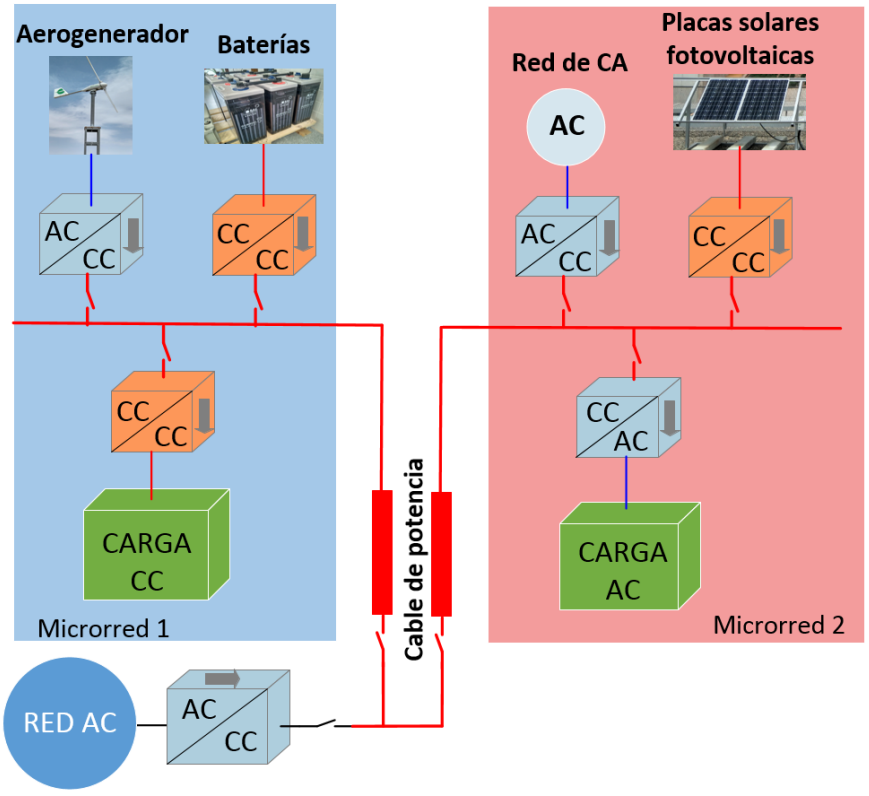

Fig 1.11.Arquitectura radial configuración paralelo.

Las configuraciones radiales de microrredes de CC pueden ofrecer una serie de ventajas como simplicidad, nivel de tensión múltiple (en bipolar) y capacidad de

compartir la energía de entre barras vecinas (en arquitectura multi-barra). Sin embargo, la arquitectura radial en serie no es flexible durante condiciones de falla. Por ejemplo, una única falla puede afectar a todos los usuarios conectados a un único sistema de barra. En el caso de un sistema multibarra radial en serie, cuando una barra defectuosa está aislada mediante disyuntores, las barras posteriores y anteriores a la barra defectuosa no tendrán la posibilidad de compartir su energía con todo el sistema, lo cual supone un inconveniente.

1.2.2.2 Configuración en anillo

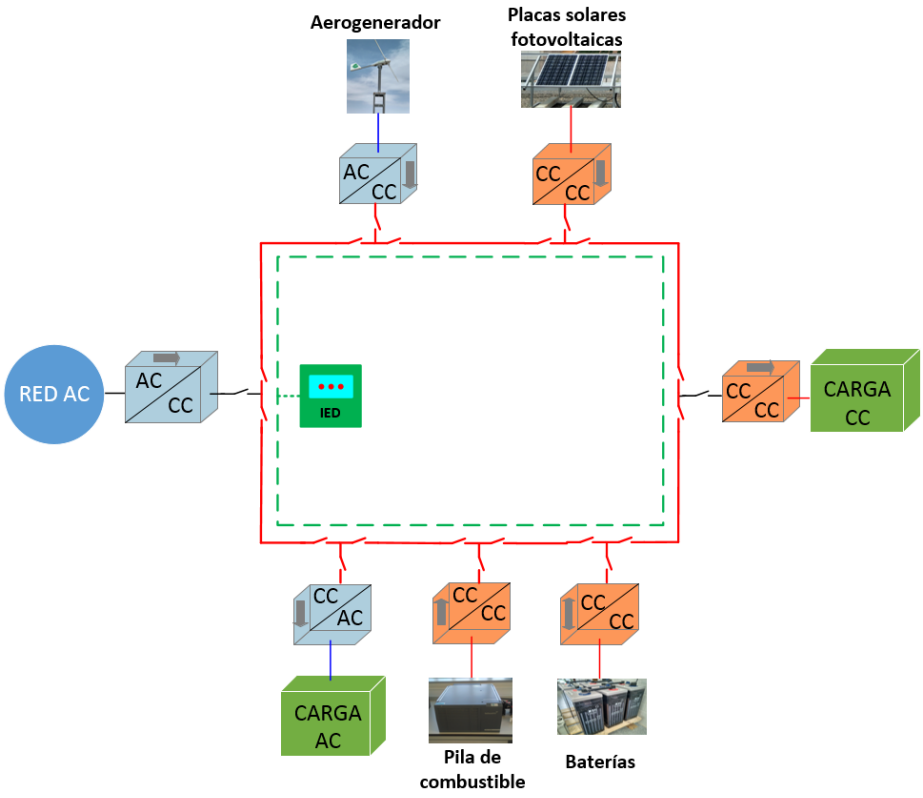

Fig 1.12. Microrred CC con arquitectura en anillo.

Para superar las limitaciones de la configuración radial, se puede utilizar un sistema de distribución de tipo anillo o bucle. Esta configuración consta de dos o más rutas entre la interfaz de la red de AC y los clientes, como se muestra en la Fig 1.5. Se colocan interruptores extra-rápidos de CC en ambos extremos de cada barra de CC, que ofrecen la flexibilidad de aislar la barra defectuosa del sistema.

Se utiliza un dispositivo electrónico inteligente (IED) para controlar cada barra y su interfaz con otras barras colaterales [39]. Cuando se encuentra una falla en cualquier barra, el IED primero detecta y aísla el barra defectuosa del sistema y luego proporciona una ruta alternativa para suministrar energía a los clientes. Este tipo de sistema de distribución se puede utilizar en entornos urbanos e industriales.

El sistema de distribución tipo anillo es más fiable en comparación con el sistema radial, pero ambos sistemas de microrredes dependen del suministro de red de AC. Si ocurre alguna falla en el alimentador de CA, el sistema de microrred de CC no tiene ninguna posibilidad de obtener el suministro requerido de la red de CA.

1.2.2.3 Configuración interconectada

La confiabilidad del sistema de microrred de CC se puede mejorar garantizando un suministro alternativo a los clientes desde la red de CA, de esta forma, en caso de falla de uno o más alimentadores no se interrumpe el servicio eléctrico a los usuarios. Esto se puede hacer interconectando la barra de CC con más de un suministro de la red de CA. Son posibles dos arquitecturas diferentes:

- Sistema de microrred CC tipo malla.
- Sistema de microrred CC de tipo zonal.

a) MICRORREDES TIPO MALLA DE CC (MTDC)

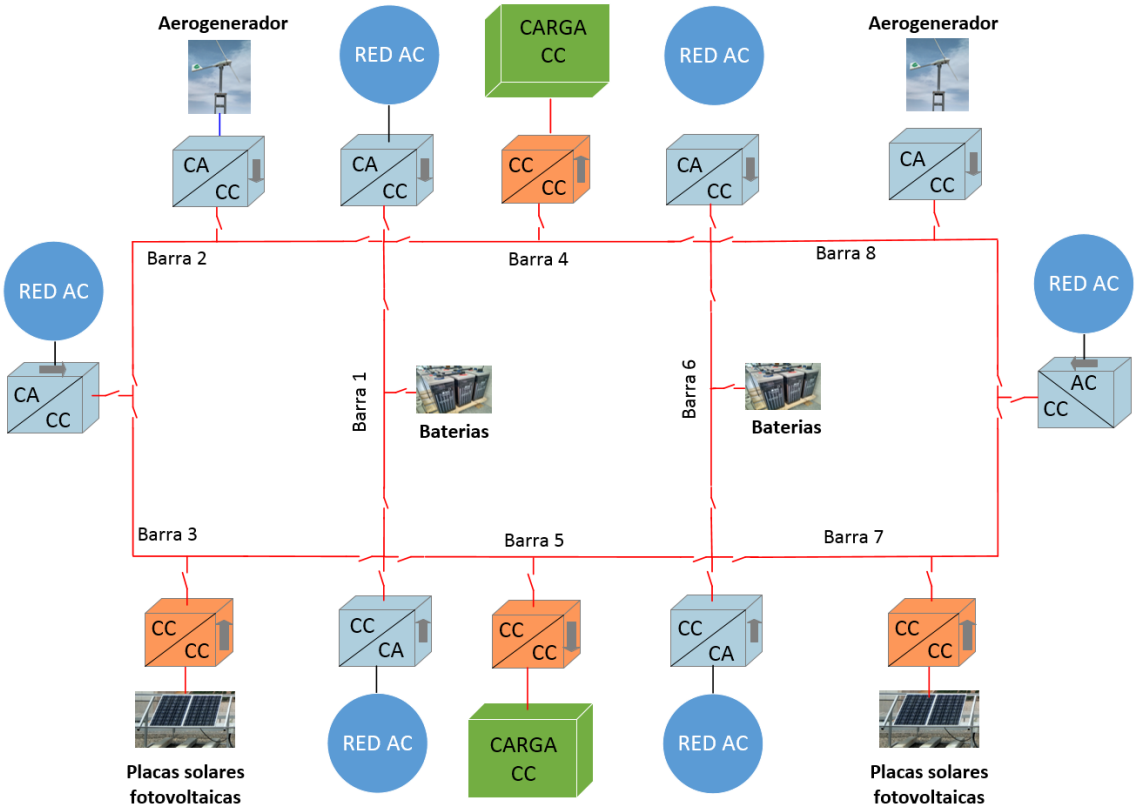

Fig 1.13: Arquitectura de microrred de CC tipo malla

En una microrred de CC de tipo malla (también conocida como red de terminales múltiples), ver Fig 1.13, más de una interfaz de la red de CA está conectada a la microrred de CC, cada una a través de un convertidor CA/CC. Existe la posibilidad de diferentes arquitecturas de microrredes de CC basadas en esta configuración donde varias fuentes de alimentación de CC y CA están conectadas a los alimentadores de CC. La MTDC es más fiable en comparación con las redes de CC radiales o en anillo debido a la disponibilidad de otros alimentadores para poder inyectar energía a varias partes del sistema. En sistemas de corriente continua de alto voltaje (HVDC), como parques eólicos marinos y sistemas subterráneos de transporte y distribución urbana, también son usadas arquitecturas similares [39], [40].

En [41] se ha propuesto un método para localizar la barra defectuosa de CC, aislándola posteriormente del resto de la microred. Restaurando la MTDC con la nueva configuración de la barra aislada y alimentando las cargas desde otras barras, para ello no usa ninguna comunicación interna dentro de los

convertidores CA/CC del sistema. En [42] se tratan los sistemas de transmisión de CC multiterminales desde el punto de vista del control y de la protección.

b) SISTEMA DE MICRORRED TIPO CC ZONAL (ZTDC)

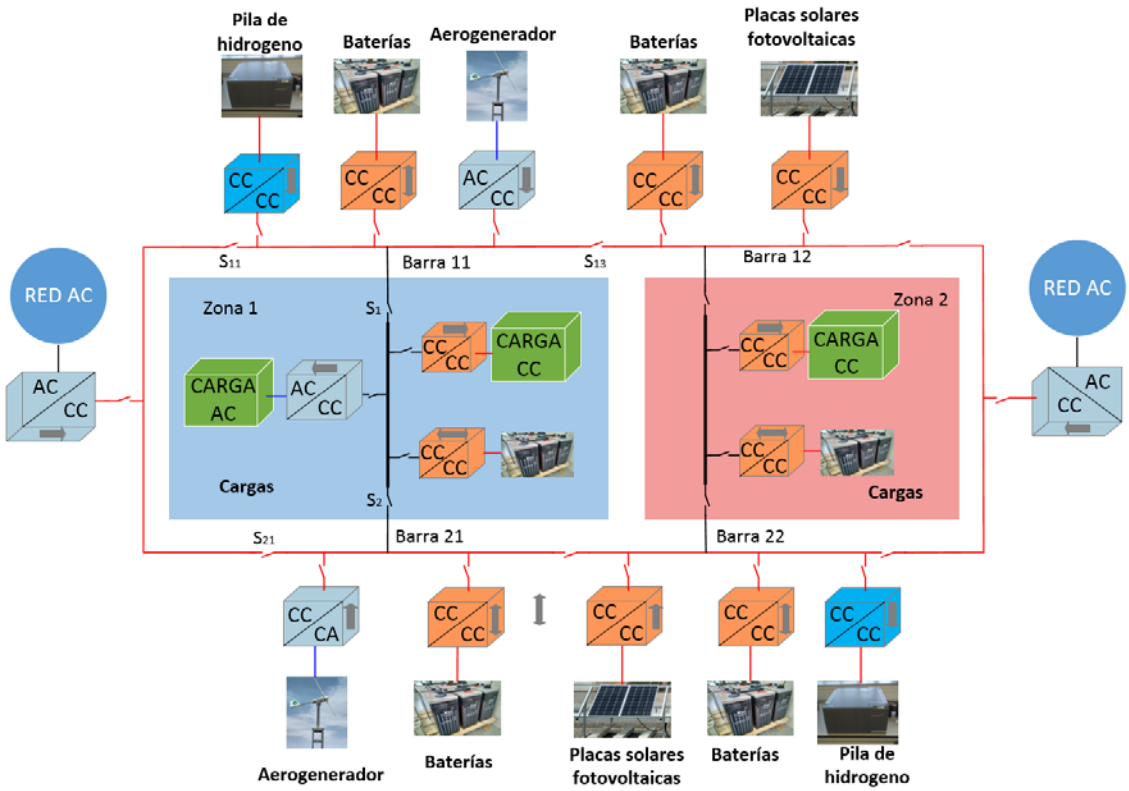

Fig.1.14. Arquitectura de microrred en CC de tipo zonal

Para mejorar aún más la fiabilidad de la microrred, se ha propuesto un sistema de distribución eléctrica zonal en[43], [44], donde la microred se divide en varias zonas (que pueden llegar a ser independizadas). Cada zona tiene un sistema de barras de CC compuesto por dos barras redundantes, como se muestra en la Fig 1.14. De hecho, esta arquitectura de red de CC se puede decir que está compuesta de varias microrredes de CC en cascada con una configuración simétrica.

Este tipo de microred al, igual que las expuestas anteriormente, puede utilizar distintos elementos de potencia, como convertidores de CC/CC y CA/CC, ESSs, generadores de energías renovables primarias (placas solares y

aerogeneradores), generadores de energía renovables secundarias como la FC, etc. También necesita aparamenta eléctrica para la conexión y desconexión de los distintos elementos (fuentes, ESSs y cargas). Cada zona está conectada con dos barras de CC redundantes alimentadas por la red de CA y fuentes de energía distribuidas de CC y CA. Este tipo de arquitectura proporciona una mayor fiabilidad y disponibilidad para las cargas que pueden ser alimentadas a través de uno de los alimentadores.

Por ejemplo, suponiendo que ocurra una falta en barra 11 de la Zona-1, los interruptores S_{11} y S_{13} se desconectarán mientras que la barra 21 y el interruptor S_2 se conservarán activos, de modo que en esta situación la energía llega a las cargas a través de la barra 21 y del interruptor S2. Además, como cada zona también puede tener conectada sus propias RESs y ESSs, en el supuesto de producirse varias faltas en las barras o en los interruptores extrarrápidos de alimentación tanto superiores como inferiores, el sistema puede quedar dividido en zonas o secciones independientes que pueden ser alimentados por sus propias fuentes.

Esta configuración se presenta más flexible y modular debido al mayor número de interruptores, esto le confiere mayor capacidad para la gestión en caso de faltas, además de ser más adecuada para la planificación de la distribución. Por tanto se puede afirmar que la red ZTDC ofrece múltiples opciones para suministrar energía a las cargas. La energía se puede suministrar desde múltiples barras de CC simultáneamente o solo desde una barra exclusivamente.

Sin embargo, hay que tener en cuenta que cuando se pretende extraer energía desde múltiples barras simultáneamente, se pueden llegar a complicar consierablemente los diseños de: la maniobra, los enclavamientos de los distintos elementos, así como la integración de las protecciones, para conseguir una buena operación del sistema de distribución[45].

Por este motivo, en [46] se ha propuesto una estrategia de selección de barras, según la cual, una carga extrae energía de la barra con el nivel de voltaje más alto (solo un barra alimenta a la carga).

Sin embargo, la carga puede cambiar a otra barra cuando cambian las condiciones de suministro. Este tipo de configuración se utiliza comúnmente en fuentes de alimentación a bordo [47], [48].

1.2.3 Problemas de calidad de energía en microrredes de cc

Las redes de corriente alterna son afectadas por diversos problemas relacionados con la calidad de la energía (armónicos, fluctuaciones de tensión, variaciones en la frecuencia de la línea, distorsión en tensiones y corrientes, etc.). A menudo, no se tienen en consideración estos problemas en las redes de CC, sobre todo en lo referente a los armónicos. Dado que las microrredes de CC basadas en energías renovables son una de las tecnologías emergentes más prometedoras, sobre todo para las zonas aisladas, varios grupos de investigadores en todo el mundo han estado y siguen trabajando en esta tecnología para conseguir un servicio de la calidad con redes de CC basadas en energías renovables [49], [50].

Para llevar esta tecnología de la fase de investigación a la aplicación práctica, es crucial abordar los problemas asociados con la calidad de la energía. A pesar de que la mayoría de las investigaciones recientes destacan las ventajas de las redes de corriente continua sobre las redes de corriente alterna convencionales, son escasos los trabajos que tratan específicamente los problemas de calidad de la energía en las redes de corriente continua.

Las microrredes de CC si se diseñan adecuadamente pueden operar de manera aislada o estar conectadas a una red de CA. Durante el funcionamiento normal de la red de CC, está puede estar consumiendo energía de la red de CA o suministrando energía a la red de CA. Por lo tanto, los problemas de calidad de la energía en las microrredes de CC pueden surgir internamente o ser exportados desde la red de CA. Algunos de los problemas eléctricos más comunes en estos sistemas incluyen:

- Transitorios de tensión de la red de corriente alterna.
- Generación de armónicos debido a resonancias y convertidores de electrónica de potencia.
- Problemas de compatibilidad electromagnéticas (CEM) con interferencias.
- Fallos en las comunicaciones.

- Corrientes de arranque.
- Faltas en la barra de CC.
- Desequilibrio de tensión en la barra de corriente continua bipolar.
- Corrientes circulantes.

Los transitorios de tensión son frecuentes en las redes de corriente alterna, principalmente debido a la conmutación de baterías de condensadores, que conmutan cuando ocurren cambios en la carga y fluctuaciones de potencia en sistemas de energía renovable conectados a la red. Un estudio reciente en aplicaciones de centros de datos ha mostrado que los transitorios de tensión podrían hacer vulnerables a las redes de CC [51].

Hay que tener en cuenta que las futuras líneas y redes públicas de suministro eléctrico en CC serán más complejas que las redes actuales, debido a la integración de sistemas de energías renovables y sistemas de almacenaje de forma distribuida. Esto hace que se busquen enfoques distintos a los actuales más armonizados, para el desarrollo de normas que regulen la calidad de la energía y que aseguren la compatibilidad entre los distintos tipos de cargas y fuentes existentes en las redes eléctricas que están en constante cambio.

Esto obliga a normalizar la tensión en CC que todavía está pendiente, aunque existen unos niveles de tensión preferidos para aplicaciones de potencia, obtenidos en los resultados del estudio IEC SEG4 para la tensión nominal y las bandas de tensión basados en la descripción del caso utilizado [52].

De modo que para los fabricantes de material eléctrico como: componentes eléctricos, enchufes, clavijas, contactares, protecciones, etc. Los límites estándar de tolerancia y las perturbaciones transitorias de tensión se vuelven cruciales. La mayoría de los productos y sistemas, como los dispositivos basados en USB, sistemas de iluminación LED, ordenadores de sobremesa y sistemas de tracción eléctrica en CC, como los sistemas ferroviarios, ya cuentan con sus propios límites estándar de tolerancia, referidos a los niveles de tensión y a las perturbaciones transitorias. Aunque para las aplicaciones en CC la mayoría de estas normas se fundamentan en el uso convencional de la energía de CC y las redes futuras presentan nuevos retos a los que se tiene que hacer frente.

En las microrredes puras de CC, como no existen convertidores de potencia de CA/CC, no surgirán problemas debido a los armónicos de baja frecuencia. Sin embargo,

el uso creciente de convertidores CC/CC, que cada vez utilizan frecuencias de conmutación más elevadas, podrían llegar causar interferencias electromagnéticas (EMI) en los dispositivos electrónicos de la microrred.

En una microrred de CC, se utilizan múltiples convertidores con su conmutación basada en modulación por ancho de pulso (PWM) con condensadores de CC a ambos lados del convertidor. Estos condensadores en el lado de CC y la impedancia del cable de la barra CC o del alimentador pueden originar diversas frecuencias de resonancia [53]. Si una de estas frecuencias de resonancia se sintoniza en cualquier rango de frecuencias en que el convertidor esté conmutando, pueden ocurrir problemas significativos de calidad como sobretensiones debidas a las resonancias, que pueden influir sobre la estabilidad del enlace de CC. El rango de frecuencia que debe existir en una microrred de CC puede variar desde frecuencias muy bajas (inferiores a 9 kHz) hasta frecuencias muy altas, como sucede en la transmisión, realizada en las bandas de 9-150 kHz y 150 kHz-30 MHz.

La comunicación a través de línea eléctrica (PLC) se emplea en aplicaciones de smart grid para señalización [54], [55]. Los sistemas PLC se suelen utilizar sobre infraestructuras de cables eléctricos, por los que se hace la transmisión de datos entre un sistema de control central y las cargas [56]. En una microrred de CC, donde se utilizan varios convertidores que conmutan sus elementos de potencia a alta frecuencia, estos generan ruido y armónicos de baja y alta frecuencia, que pueden interferir sobre la transmisión de datos del sistema PLC y afectar el funcionamiento del control de la microrred. Por lo tanto, las futuras microrredes de CC, requieren un análisis exhaustivo del ruido, así como un filtrado adecuado de los armónicos para asegurar un funcionamiento de los sistemas de PLC correctos.

Los convertidores electrónicos de potencia están equipados con filtros EMI que cumplen con todas las normativas de CEM. Estos convertidores están conectados a la barra de CC y cuanto se activan, la corriente convertida circula a través de los filtros EMI. Esta corriente puede producir oscilaciones de tensión en la barra de CC, debido a las oscilaciones de la caída de tensión interna de los convertidores, afectando así el funcionamiento de otros equipos conectados a la misma barra de CC [57]. La corriente de carga también puede ocasionar caídas de tensión en la barra de CC.

En una microrred de CC, si ocurre una falta en la barra de CC, esta corriente de falta o parte de ella puede circular a través de los convertidores, de las fuentes de energía o de la capacitancia. Luego la corriente de falta queda limitada por: la corriente máxima permitida por los convertidores, la potencia de las fuentes de energía, la energía almacenada en los ESS y también por la energía almacenada en los condensadores de la barra de CC. Aunque los elementos de protección en una microrred de CC pueden no ser activados por una corriente de falta leve, pero debido a faltas pequeñas no eliminadas, en otras partes distintas de la zona de la falta también pueden surgir perturbaciones de tensión [58]. También hay que tener en cuenta que debido a la menor sensibilidad de las protecciones en CC, la configuración y colocación de las protecciónes donde no existe diferencia significativa entre la falta y la carga pesada, podría ser una situación complicada para ser detectada por la protección si la corriente de falta tiene una magnitud baja [59]. Además, teniendo en cuenta que la tensión en continua no es periódica y por tanto no tiene cruces por cero, que son naturales en las redes de CA. En las redes de CC pueden ocurrir faltas que podrían desarrollar un arco auto sostenido difícil de detectar y por tanto de extinguir [53].

Transitorios importantes pueden aparecer en la barra de CC ocasionados por la conexión y desconexión frecuente de cargas [60]. Para paliar esta situación y compensar estos transitorios, en muchas microrredes de CC se conectan varios dispositivos (por ejemplo, baterías), pero a pesar de esto, siguen ocurriendo algunas oscilaciones en el barra de CC.

Cuando las microrredes de CC están conectadas a la red de CA, El desequilibrio de la tensión puede ocurrir en la red de CA y transmitirse a la de CC. También en sistemas de distribución bipolar de CC, el desequilibrio puede ser debido a una distribución desequilibrada de cargas monofásicas o fuentes de generación distribuida [61].

Cuando en una barra de CC varios convertidores están conectados en paralelo para verter energía o para alimentar sus cargas, pueden surgir problemas debido a la corriente circulante, la cual puede aparecer entre los convertidores, cuando existe un punto de tierra común en ambos lados de los convertidores[62], [63].

Entre las energías renovables más comunes tenemos la obtenida del sol y del viento que son las energías primarias más abundantes, pero estas no son controlables por el ser

humano y tienen un alto grado de aleatoriedad. Si se quieren conseguir microrredes con un suministro estable e independiente de la red principal, que puedan trabajar en zonas aisladas. En el mix de energías renovables se necesita la contribución de energías renovables controlables por el ser humano, de este modo se reduce significativamente la cantidad de ESSs, pues se puede generar energía cuando hay escasez de renovables primarías. En este tipo de energías renovables no aleatorias destacan dos, la obtenida con hidrogeno a través de pila de combustible (FC) y la obtenida con plantas de gasificación. Las plantas de gasificación producen energía eléctrica a partir de residuos orgánicos o de madera, por ejemplo, uno de los residuos utilizados es el alperujo obtenido como subproducto de la producción del aceite de oliva, además después de gasificar el pellet de alperujo se obtiene biochar que se utiliza para mejorar las propiedades de los suelos agrícolas. Por ejemplo, los suelos con aportación de biochar cuando se le aplica fertilizantes vegetales incrementan la actividad microbiana, regula el pH y sus propiedades físicas y químicas mejoran.

1.3 LA GASIFICACIÓN COMO FUENTE DE ENERGIA CONTROLABLE

La integración de la gasificación en las redes de CC como fuente controlable puede ser una buena solución para mejorar la calidad del servicio. La tecnología de la gasificación de biomasa ha alcanzado un nivel de madurez considerable y se encuentra en uso en numerosos países para la generación de energía eléctrica y térmica de manera renovable mediante la cogeneración. Aunque la gasificación tiene una eficiencia ligeramente menor que la combustión, con rendimientos de conversión que pueden llegar hasta el 85% a escala industrial, esta tecnología a menudo reemplaza a las centrales térmicas de carbón [64]. La gasificación también presenta una mayor versatilidad en su aplicación que la combustión, ya que puede utilizar biomasa con un contenido de humedad y cenizas más elevado (hasta un 60% y un 25%, respectivamente, en reactores updraft). También se consigue una reducción de las emisiones de CO_2, partículas e incluso NOx, debido a que la temperatura de reacción es inferior que la que requiere la combustión [65].

En la gasificación se obtiene un gas compuesto principalmente por H_2, CO, CH_4, H_2O, N_2 y CO_2. A este gas se le denomina syngas o gas de sístesis, el proceso por el que se obtiene es un proceso termoquímico de conversión en el cual un combustible sólido (madera, cascara de arroz, alperujo, etc.) se transforma en gas, que entre otras cosas puede ser utilizado para la generación de energía térmica, eléctrica o ambas simultáneamente. También se puede usar en la producción de biocombustibles como el biometano, H_2, metanol, entre otros [66]. Para llevar a cabo esta conversión, se requiere que en el proceso intervenga un oxidante, que se denomina agente gasificante, este elemento produce una serie de reacciones exotérmicas y endotérmicas que llevan a cabo la transformación de la biomasa en gas de síntesis (véase Fig 1. 15: Proceso de gasificación) [66].

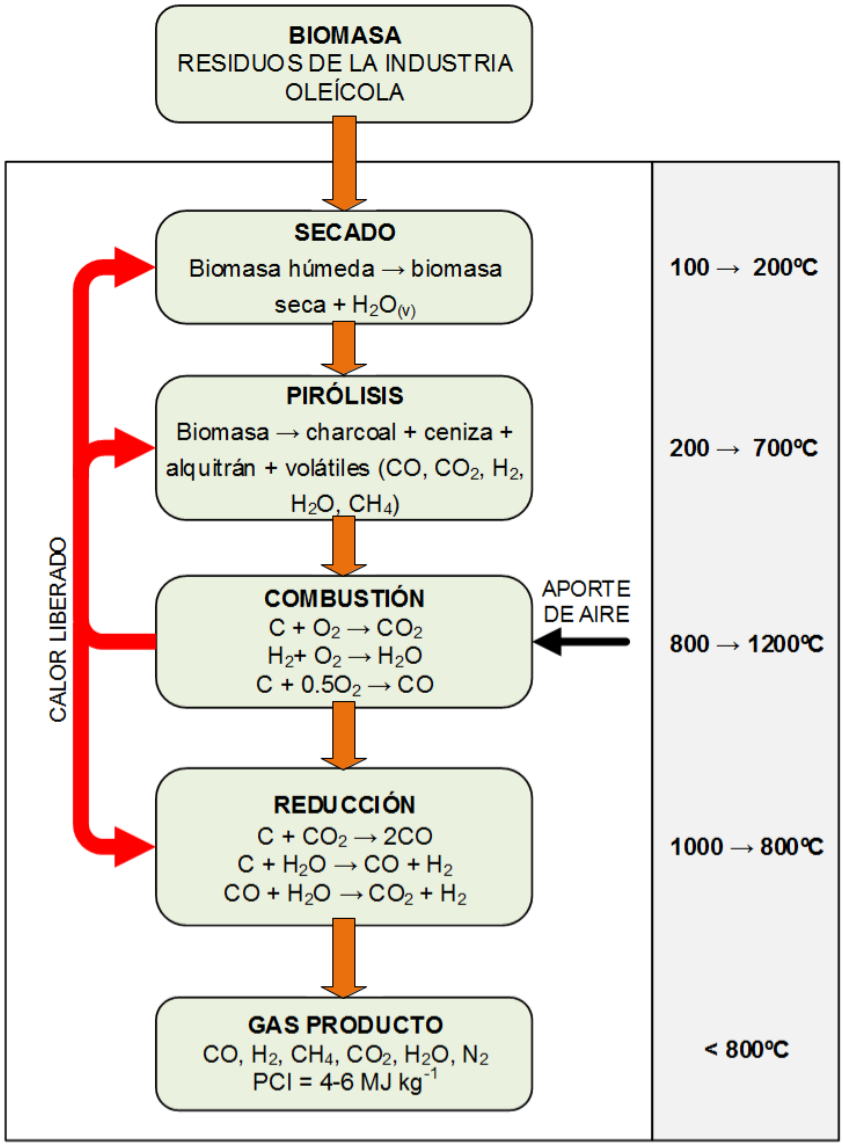

Fig 1.15: Proceso de gasificación

Dentro del reactor, cuando se está llevando a cabo el proceso de gasificación, se distinguen varias etapas, ver Fig 1.15, que están claramente definidas por la temperatura a la que se esta producción cada una de ellas. Las etapas son: secado, pirólisis, combustión y reducción. Hay que resaltar que la gasificación es un proceso auto-térmico, luego las reacciones de combustión (exotérmicas) son las encargadas de aportar la energía necesaria para que puedan ocurrir las reacciones endotérmicas, que son las responsables de la formación del gas de síntesis final.

Según la Fig 1.15, en el interior del reactor se desarrollan varias reacciones químicas para llevar a cabo el proceso completo de la gasificación, estas se dividen en cuatro etapas, denominadas: secado, pirólisis, reducción y combustión.

El proceso de gasificación es auto-térmico, el cual se produce de modo que las reacciones de combustión (exotérmicas) suministran energía a las reacciones endotérmicas que son las reacciones que hace posible la formación del syngas.

El proceso de **secado** es necesario, ya que la cantidad de humedad que tiene la biomasa es muy variada. Residuos agrícolas como la cascara de arroz tienen una humedad entre el 10% y 15%, en la industria del olivar nos encontramos residuos como la poda y hojas del olivo con una humedad entre el 5% y el 15%, por otra parte, también existen residuos como el orujo que puede llegar 70%. Esto no es recomendable para el proceso, sobre todo cuando se trata de aplicaciones para la obtención de energía, ya que parte de la energía generada se invierte en el proceso de secado del propio combustible, de modo que son necesarios 2.260 kJ de energía para evaporar cada kilogramo de humedad. Por este motivo, antes de iniciar el proceso de gasificación es necesario llevar a cabo un secado previo de modo que la biomasa quede con un grado de humedad inferior al 20%.

El secado final ocurre en la etapa de secado, después de la entrada de la biomasa en el gasificador, donde es calentada por la corriente ascendente de gases calientes y la transmisión térmica, ambas recibidas de partes inferiores del reactor. De modo que esta biomasa colocada en la parte superior del reactor es secada, liberando vapor de agua cuando se encuentra por encima de los 100°C, entonces la biomasa se descompone en sus compontes volátiles. Las temperaturas a las que ocurre esta fase están entre 70 y 200 °C.

La siguiente etapa de la gasificación es la **pirólisis**, que es un proceso esencial en el que no interviene el agente gasificante. Esta etapa se considera que ocurre en la zona del reactor donde la biomasa supera los 200ºC, en esta temperatura se produce la descomposición de las moléculas grandes que componen la biomasa en moléculas cuyo peso molecular es menor sin apenas reaccionar con el aire o cualquier otro agente gasificante.

Si hablamos de la gasificación de la biomasa, entre los 200 y los 280ºC la hemicelulosa se descompone en CO_2, CO, H_2O, C_2H_2, entre otros, y una pequeña proporción de alquitrán.

Si se llega hasta los 350ºC se logra la descomposición de la celulosa de la biomasa. En este momento se genera alquitrán, que se compone principalmente de benceno, ácido acético, compuestos fenólicos, hidrocarburos aromáticos y agua. La parte sólida recibe el nombre de char, el cual se compone principalmente de carbón. Este se genera a temperaturas entre 280 y 500ºC. El contenido de alquitranes que tenga el gas producto final es un factor a tener en cuenta, ya que si no es eliminado puede ocasionar grandes daños en el sistema de generación térmica y eléctrica.

En la etapa de **reducción**, cuando los productos de la pirólisis atraviesan las zonas más calientes del reactor, los componentes volátiles principalmente reaccionan con el vapor de agua (H_2O) y dióxido de carbono (CO_2), generando CO y H_2.

Estas reacciones son muy exotérmicas y son la precursoras de la generación del gas de síntesis, que básicamente es una mezcla de CO y H_2, para su obtención se han sintetizado diversos productos químicos y combustibles.

Esta fase en un gasificador de biomasa es esencial para la producción de gas de síntesis, en ella se llevan a cabo una serie de reacciones complejas que transforman los productos volátiles de la biomasa en gases útiles, empleados en diversas aplicaciones industriales y energéticas.

En la etapa de **combustión** la mayoría de reacciones de reducción son endotérmicas. La energía necesaria para estas reacciones, además de la requerida para los procesos de secado y pirólisis de la biomasa, proviene de las reacciones de combustión del char, las

cuales son todas exotérmicas (liberan energía durante su ocurrencia). La reacción es la más apropiada para este caso, ya que es la que más energía libera por kmol de carbón consumido. La segunda reacción que contribuye significativamente a la energía en el entorno de gasificación es la también genera parte del gas producto deseado (CO).

Cuando el char (C) toma contacto con el oxígeno, ambas reacciones tienen lugar dentro del reactor. El grado de producción entre ambas depende en gran medida de la temperatura alcanzada. Las reacciones de combustión tienen una velocidad de reacción superior a las de reducción bajo condiciones de presión y temperatura iguales. Con un tamaño de partícula del char de alrededor de 6 mm y una temperatura de gasificación de 900°C, la velocidad de las reacciones de combustión es 15 veces mayor que la de las reacciones de gasificación. Este ratio aumenta significativamente (aproximadamente 60) a medida que disminuye el tamaño de partícula del char

1.3.1 Situación actual de la gasificación

La gasificación de biomasa ha sido estudiada por gran cantidad de autores, pero estos estudios han sido planteados desde un punto de vista teórico buscando su aplicación energética [67], [68], [69], [70], [71], [72], [73], [74].

También, han sido llevados a cabo numerosos estudios de simulación sobre plantas de potencia, que utilizan como combustible gas de síntesis, obtenido con gasificadores (principalmente de lecho fijo, downdraft). Por otra parte, han sido estudiadas tecnologías de generación distribuida como son las microturbinas de gas [75], motores de gas [76] [74], turbinas de combustión externa [77] y máquinas de vapor basadas en ciclos orgánicos de Rankine [68].

Todos estos trabajos están enfocados a la optimización de sistemas de generación eléctrica y térmica a pequeña-mediana escala. Aunque ésta tecnología tiene un rendimiento de generación eléctrica relativamente bajo (en torno al 15-20%), pero el rendimiento de cogeneración pude superar el 50%, además de la obtención de otros productos que aportan valor como el biochar.

En términos de viabilidad experimental y pruebas demostrativas, la aplicación de la gasificación de biomasa a sistemas de generación eléctrica de pequeña y mediana potencia (menos de 1 MW eléctrico) se encuentra actualmente en desarrollo comercial en algunos países como China, EE.UU. e India. Hay fabricantes como Ankur Scientific Energy Technologies y All Power Labs que pueden suministrar diferentes tipos de gasificadores para distintos niveles de potencia eléctrica, que van desde unos pocos kW hasta varios cientos de kW. Estos sistemas básicamente suelen estar compuestos por un reactor, un sistema de limpieza y enfriamiento de gas, y una unidad de potencia. El reactor es principalmente de lecho fijo downdraft, la temperatura de salida del gas generado está entre los 400 y 500°C. Las partículas sólidas y los alquitranes son eliminados mediante el sistema de limpieza y enfriamiento. Para la construcción de la unidad de potencia se utiliza un motor de combustión interna alternativo, normalmente se suele usar un motor de gas natural o gasolina (ciclo Otto) [76], [78], [79], [74].

1.3.2 Problemática: aplicación y velocidad de respuesta para sistemas aislados

La generación de energía eléctrica y térmica, así como la producción de biocombustibles como el amoniaco o el H_2, son los temas más estudiados en la literatura mediante el uso de plantas de gasificación. Hay que destacar que, en cuanto a la generación eléctrica mediante plantas de gasificación, la mayoría de los trabajos se enfocan en plantas conectadas a la red eléctrica, ya sea para media o grande potencia, o en aplicaciones de pequeña potencia integrado en las redes de forma distribuida. Sin embargo, el uso de sistemas de gasificación en aplicaciones aisladas o autónomas todavía está en una etapa incipiente. Debido a la gran inercia de las reacciones químicas involucradas en el proceso de gasificación, que hace que la respuesta del gasificador no sea lo suficientemente rápida para soportar las variaciones de carga cuando este trabaja en isla, otro elemento que contribuye a no mejorar la velocidad de respuesta es la pequeña inercia del conjunto motor-alternador. Cuando el gasificador está aportando energía eléctrica a la red de forma aislada y ocurren variaciones en la carga, estas son seguidas de forma lenta por el gasificador, lo que limita las variaciones de carga alrededor del 20%, incluso así, tampoco se consigue un suministro de calidad cuando el gasificador trabaja

en isla. Para la electrificación sin conexión a la red, la mayoría de los trabajos tienen un enfoque económico y no existen sistemas que resuelvan el problema de la calidad del suministro para las plantas de biomasa sin conexión a la red.

Se procede a justificar el comportamiento de un gasificador mediante pruebas experimentales.

En la Fig 1.16 se muestran una prueba experimental de la planta de gasificación acoplada a un motor de combustión interna y a un generador eléctrico aislado de la red. La marca del motor-generador es un modelo NPT con una potencia nominal de 10 kW (aunque su potencia real de trabajo puede superar los 11 kW). El motor-generador se conectó a un banco de cargas resistivo con una posibilidad de cambios instantáneos de carga de 0,6 kW (funcionamiento en modo sin conexión a la red). La prueba experimental dura 5 horas de funcionamiento continuo. Durante la prueba, el gasificador estuvo funcionando y adaptándose a la carga hasta aproximadamente el 70% de su potencia nominal (6-7 kW), la carga cambió del 0% al 30% (Fig 1.17, incremento uno) y posteriormente al 70% (Fig 1.18, incremento dos), durante estos cambios de carga, el gasificador se adapta a la nueva carga sufriendo bajadas de tensión, pero consigue su nuevo punto de trabajo con cierta dificultad, especialmente en el paso del 30% (incremento uno). Sin embargo, cuando el gasificador está funcionando al 70% de la potencia nominal y sufre un aumento de carga superior al 25% (tiempo = 200 min, incremento tres), la velocidad del motor empieza a disminuir hasta que se desconecta la carga del alternador, que se vuelve a conectar al cabo de más de dos minutos. El motor-generador alcanza el nuevo punto de carga de más de 10.500 W con gran dificultad, y muy mala calidad de suministro durante el transitorio, el suministro se desconectó durante más de dos minutos para que el sistema gasificador-motor-generador pudiera soportar el aumento de potencia (incremento tres). Además, para potencias suministradas inferiores al 70% de la potencia nominal de la planta, se producen transitorios durante los cambios de la potencia suministrada, en los que la calidad del suministro es baja. Pero con cargas de funcionamiento superiores al 70% de la potencia nominal del gasificador, los aumentos de carga elevados provocan problemas de parada del generador, véanse las Fig 1.16 y Fig 1.19. Además, cuando la potencia suministrada es inferior al 70% de la potencia nominal de la planta de gasificación, los cambios de potencia que se producen disminuyen la calidad del suministro durante la duración del transitorio, véanse las Fig 1.17 y Fig 1.18.

Ninguno de los cambios es instantáneo, que es lo que debe de ocurrir en un suministro de calidad. Por ejemplo, el cambio de la Fig 1.17 (incremento uno) tarda algo menos de dos minutos.

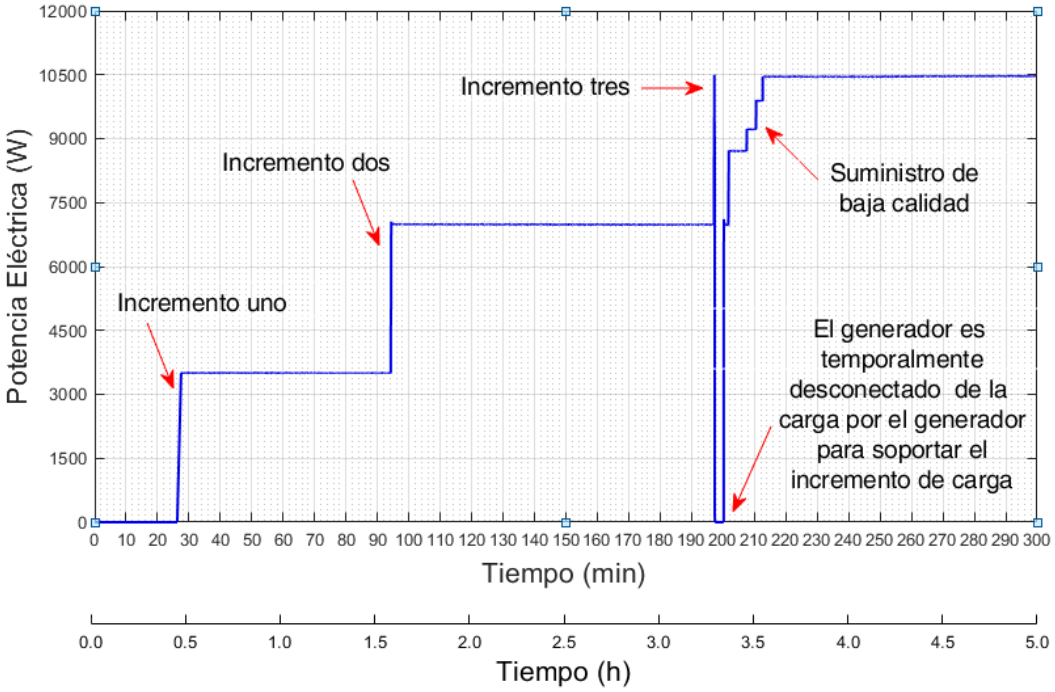

Fig 1.16.Respuesta de un gasificador de 10 kW para diferentes variaciones de carga.

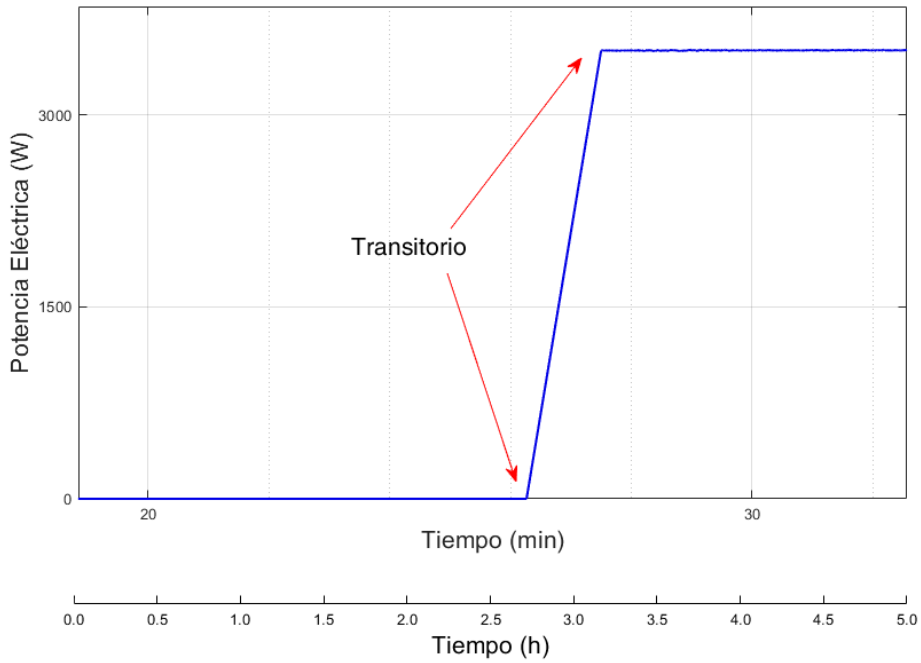

Fig 1.17.Detalle del incremento de carga uno.

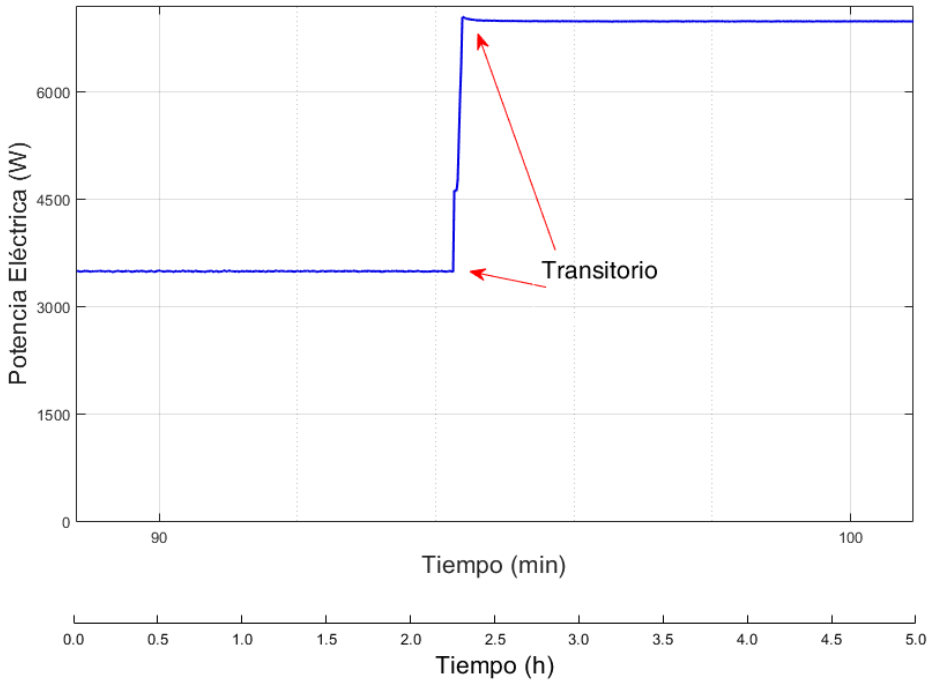

Fig 1.18.Detalle del incremento de carga dos.

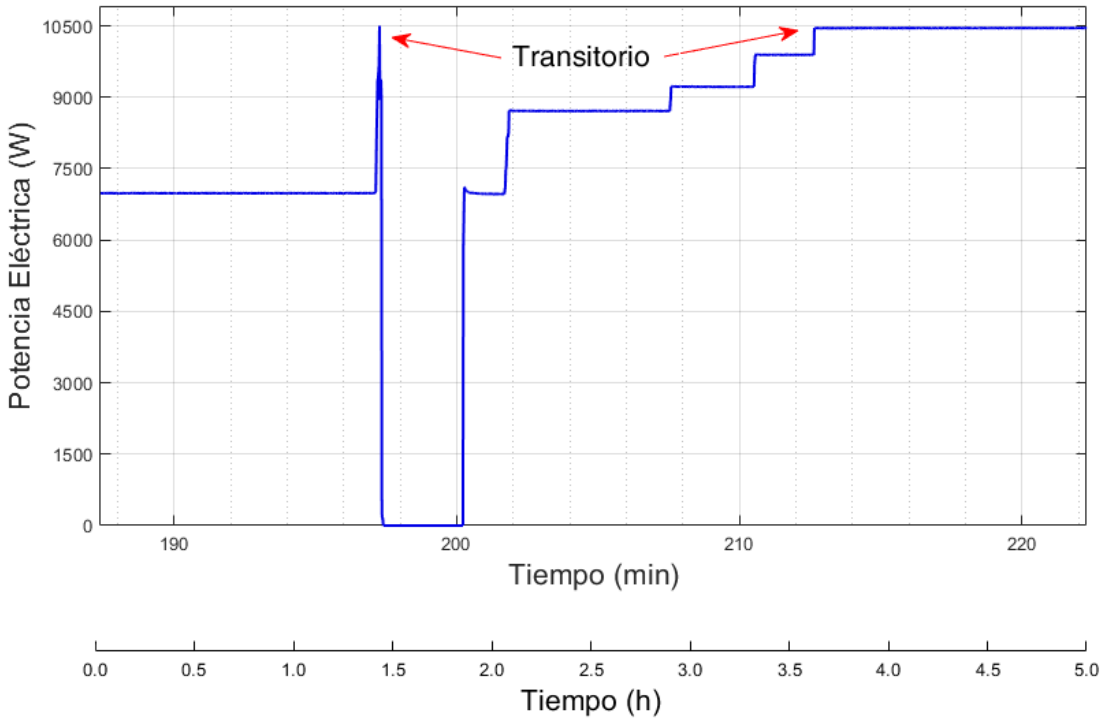

Fig 1.19.Detalle del incremento de carga tres.

Este funcionamiento puede crear problemas en algunos tipos de cargas, como las existentes en los sectores industriales agroalimentarios de muchos países, donde estos sistemas serían de gran utilidad en la generación de electricidad, si se disponen de materias primas para gasificar.

Para la solución del problema expuesto, en el capítulo 3 se propone una técnica que permitirá aplicar la tecnología de la gasificación en sistemas aislados de manera que pueda adaptarse eficazmente a variaciones bruscas de carga y proporcionar un suministro de calidad en todo momento.

REFERENCIAS

[1] M. Dale, "A comparative analysis of energy costs of photovoltaic, solar thermal, and wind electricity generation technologies," *Appl. Sci.*, vol. 3, no. 2, pp. 325–337, 2013, doi: 10.3390/app3020325.

[2] M. Ortega, M. V. Ortega, F. Jurado, J. Carpio, and D. Vera, "Bidirectional DC–DC converter with high gain based on impedance source," *IET Power Electron.*, vol. 12, no. 8, pp. 2069–2078, 2019, doi: 10.1049/iet-pel.2018.5385.

[3] A. H. Fathima and K. Palanisamy, "Optimization in microgrids with hybrid energy systems - A review," *Renew. Sustain. Energy Rev.*, vol. 45, pp. 431–446, 2015, doi: 10.1016/j.rser.2015.01.059.

[4] E. Mengelkamp, J. Gärttner, K. Rock, S. Kessler, L. Orsini, and C. Weinhardt, "Designing microgrid energy markets: A case study: The Brooklyn Microgrid," *Appl. Energy*, vol. 210, pp. 870–880, 2018, doi: 10.1016/j.apenergy.2017.06.054.

[5] N. A. M. Kajaan, Z. Salam, and R. Z. R. M. Radzi, "Review of Market Clearing Method for Blockchain-Based P2P Energy Trading in Microgrid," *5th IEEE Conf. Energy Conversion, CENCON 2021*, pp. 202–207, 2021, doi: 10.1109/CENCON51869.2021.9627254.

[6] H. M. El Zoghby and H. S. Ramadan, "Isolated microgrid stability reinforcement

using optimally controlled STATCOM," *Sustain. Energy Technol. Assessments*, vol. 50, no. November 2021, p. 101883, 2022, doi: 10.1016/j.seta.2021.101883.

[7] Q. Zhou, H. Wang, Z. Meng, J. Hu, X. Fan, and H. Yao, "Research on a Customer-Side Energy Storage Business Model and Its Cost-Effectiveness under the Market-Based Tariff Mechanism," *2022 6th Int. Conf. Power Energy Eng. ICPEE 2022*, pp. 259–264, 2022, doi: 10.1109/ICPEE56418.2022.10050322.

[8] M. Zamani, A. Aghaie, A. Zamani, R. Tari, M. Abarzadeh, and S. H. Hosseini, "Design and Implementation of Nonisolated High Step-Up DC-DC Converter," *Int. Trans. Electr. Energy Syst.*, vol. 2023, 2023, doi: 10.1155/2023/4016996.

[9] O. Beik and A. S. Al-Adsani, "A Wind Turbine Generator Design and Optimization for DC Collector Grids," *IEEE J. Emerg. Sel. Top. Power Electron.*, vol. 10, no. 1, pp. 484–493, 2022, doi: 10.1109/JESTPE.2021.3066278.

[10] T. Siva Rajan and A. Jayachandran, "Hybrid Fuzzy Logic Multilevel Inverter for Cost Management in Wind Turbines," *Electr. Power Components Syst.*, vol. 51, no. 13, pp. 1288–1301, 2023, doi: 10.1080/15325008.2023.2196669.

[11] J. Isozaki, B. Veerasamy, W. Kitagawa, and T. Takeshita, "Duality between PWM strategies for suppressing DC ripples of current and voltage source AC/DC converters," *IEEJ J. Ind. Appl.*, vol. 4, no. 4, pp. 512–513, 2015, doi: 10.1541/ieejjia.4.512.

[12] P. J. Wolfs, "A Current-Sourced DC-DC Converter Derived via the Duality Principle from the Half-Bridge Converter," *IEEE Trans. Ind. Electron.*, vol. 40, no. 1, pp. 139–144, 1993, doi: 10.1109/41.184830.

[13] C. Bai, B. Han, B. H. Kwon, and M. Kim, "Highly Efficient Bidirectional Series-Resonant DC/DC Converter over Wide Range of Battery Voltages," *IEEE Trans. Power Electron.*, vol. 35, no. 4, pp. 3636–3650, 2020, doi: 10.1109/TPEL.2019.2933408.

[14] Q. Pan, H. Liu, P. Wheeler, and F. Wu, "High step-up cascaded DC-DC converter integrating coupled inductor and passive snubber," *IET Power Electron.*, vol. 12,

no. 9, pp. 2414–2423, 2019, doi: 10.1049/iet-pel.2018.5706.

[15] P. Thounthong, S. Raël, and B. Davat, “Test of a PEM fuel cell with low voltage static converter,” *J. Power Sources*, vol. 153, no. 1, pp. 145–150, 2006, doi: 10.1016/j.jpowsour.2005.01.025.

[16] D. R. Nayanasiri, G. H. B. Foo, D. M. Vilathgamuwa, and D. L. Maskell, “A switching control strategy for single- and dual-inductor current-fed push-pull converters,” *IEEE Trans. Power Electron.*, vol. 30, no. 7, pp. 3761–3771, 2015, doi: 10.1109/TPEL.2014.2348800.

[17] Z. Zhang, O. C. Thomsen, and M. A. E. Andersen, “Optimal design of a push-pull-forward half-bridge (PPFHB) bidirectional DC-DC converter with variable input voltage,” *IEEE Trans. Ind. Electron.*, vol. 59, no. 7, pp. 2761–2771, 2012, doi: 10.1109/TIE.2011.2134051.

[18] M. Ortega, F. Jurado, and D. Vera, “Novel topology for DC-DC full-bridge unidirectional converter for renewable energies,” *IEEE Lat. Am. Trans.*, vol. 12, no. 8, pp. 1381–1388, 2014, doi: 10.1109/TLA.2014.7014504.

[19] M. Ortega, F. Jurado, and J. Carpio, “Control of indirect matrix converter with bidirectional output stage for micro-turbine,” *IET Power Electron.*, vol. 5, no. 6, pp. 659–668, 2012, doi: 10.1049/iet-pel.2011.0210.

[20] R. J. Wai and J. J. Liaw, “High-efficiency-isolated single-input multiple-output bidirectional converter,” *IEEE Trans. Power Electron.*, vol. 30, no. 9, pp. 4914–4930, 2015, doi: 10.1109/TPEL.2014.2364817.

[21] X. Wu, J. Wang, Y. Zhang, J. Du, Z. Liu, and Y. Chen, “Review of DC-DC Converter Topologies Based on Impedance Network with Wide Input Voltage Range and High Gain for Fuel Cell Vehicles,” *Automot. Innov.*, vol. 4, no. 4, pp. 351–372, 2021, doi: 10.1007/s42154-021-00163-z.

[22] Y. Ji, H. Liu, Y. Feng, F. Wu, and P. Wheeler, “High Step-Up Y-Source Coupled-Inductor Impedance Network Boost DC-DC Converters with Common Ground and Continuous Input Current,” *IEEE J. Emerg. Sel. Top. Power Electron.*, vol. 8,

no. 3, pp. 3174–3183, 2020, doi: 10.1109/JESTPE.2019.2892499.

[23] Y. Zhang, C. Fu, M. Sumner, and P. Wang, “A Wide Input-Voltage Range Quasi-Z-Source Boost DC-DC Converter with High-Voltage Gain for Fuel Cell Vehicles,” *IEEE Trans. Ind. Electron.*, vol. 65, no. 6, pp. 5201–5212, 2018, doi: 10.1109/TIE.2017.2745449.

[24] M. N. H. Khan, M. Forouzesh, Y. P. Siwakoti, L. Li, T. Kerekes, and F. Blaabjerg, “Transformerless Inverter Topologies for Single-Phase Photovoltaic Systems: A Comparative Review,” *IEEE J. Emerg. Sel. Top. Power Electron.*, vol. 8, no. 1, pp. 805–835, 2020, doi: 10.1109/JESTPE.2019.2908672.

[25] M. Karimi Hajiabadi, A. Mosallanejad, and A. Salemnia, “Ultra-high gain quadratic boost DC–DC converter based on a three-winding coupled inductor with reduced voltage stress for fuel cell-based systems,” *IET Power Electron.*, vol. 16, no. 16, pp. 2666–2681, 2023, doi: 10.1049/pel2.12592.

[26] S. W. Lee and H. L. Do, “High Step-Up Coupled-Inductor Cascade Boost DC-DC Converter with Lossless Passive Snubber,” *IEEE Trans. Ind. Electron.*, vol. 65, no. 10, pp. 7753–7761, 2018, doi: 10.1109/TIE.2018.2803731.

[27] M. M. Haji-Esmaeili, E. Babaei, and M. Sabahi, “High Step-Up Quasi-Z Source DC-DC Converter,” *IEEE Trans. Power Electron.*, vol. 33, no. 12, pp. 10563–10571, 2018, doi: 10.1109/TPEL.2018.2810884.

[28] M. K. Nguyen, T. D. Duong, and Y. C. Lim, “Switched-capacitor-based dual-switch high-boost DC-DC converter,” *IEEE Trans. Power Electron.*, vol. 33, no. 5, pp. 4181–4189, 2018, doi: 10.1109/TPEL.2017.2719040.

[29] G. Zhang *et al.*, “A Five-Terminal Impedance Network Based Three-Port Converter,” *IEEE Access*, vol. 6, pp. 29474–29485, 2018, doi: 10.1109/ACCESS.2018.2840528.

[30] F. Z. Peng, “Z-source inverter,” *IEEE Trans. Ind. Appl.*, vol. 39, no. 2, pp. 504–510, 2003, doi: 10.1109/TIA.2003.808920.

[31] T. D. Duong, M. K. Nguyen, T. T. Tran, D. Van Vo, Y. C. Lim, and J. H. Choi, "Three-Phase Impedance-Source Inverter with Common-Mode Voltage Reduction," *IEEE Access*, vol. 9, pp. 164510–164519, 2021, doi: 10.1109/ACCESS.2021.3134996.

[32] D. Ghaderi, "THD minimization for Z-source-based inverters with a novel sinusoidal PWM switching method," *Turkish J. Electr. Eng. Comput. Sci.*, vol. 27, no. 4, pp. 3098–3113, 2019, doi: 10.3906/elk-1809-46.

[33] C. N. El-Khoury, H. Y. Kanaan, I. Mougharbel, and K. Al-Haddad, "Optimized modulation technique for series Z-Source Very Sparse Matrix Converter," *Proc. - 2018 IEEE 12th Int. Conf. Compat. Power Electron. Power Eng. CPE-POWERENG 2018*, pp. 1–6, 2018, doi: 10.1109/CPE.2018.8372575.

[34] G. DING, F. GAO, S. ZHANG, P. C. LOH, and F. BLAABJERG, "Control of hybrid AC/DC microgrid under islanding operational conditions," *J. Mod. Power Syst. Clean Energy*, vol. 2, no. 3, pp. 223–232, 2014, doi: 10.1007/s40565-014-0065-z.

[35] M. W. Altaf, M. T. Arif, S. N. Islam, and M. E. Haque, "Microgrid Protection Challenges and Mitigation Approaches-A Comprehensive Review," *IEEE Access*, vol. 10, pp. 38895–38922, 2022, doi: 10.1109/ACCESS.2022.3165011.

[36] H. Kakigano, Y. Miura, and T. Ise, "Low-voltage bipolar-type dc microgrid for super high quality distribution," *IEEE Trans. Power Electron.*, vol. 25, no. 12, pp. 3066–3075, 2010, doi: 10.1109/TPEL.2010.2077682.

[37] F. Wang, Z. Lei, X. Xu, and X. Shu, "Topology deduction and analysis of voltage balancers for DC microgrid," *IEEE J. Emerg. Sel. Top. Power Electron.*, vol. 5, no. 2, pp. 672–680, 2017, doi: 10.1109/JESTPE.2016.2638959.

[38] H. Kakigano, Y. Miura, T. Ise, and R. Uchida, "Voltage Control of the DC Micro-grid Quality," pp. 518–525, 2007.

[39] W. Lu and B. T. Ooi, "Multiterminal LVDC system for optimal acquisition of power in wind-farm using induction generators," *IEEE Trans. Power Electron.*,

vol. 17, no. 4, pp. 558–563, 2002, doi: 10.1109/TPEL.2002.800995.

[40] W. Lu and B. T. Ooi, “Multi-terminal HVDC as enabling technology of premium quality power park,” *Proc. IEEE Power Eng. Soc. Transm. Distrib. Conf.*, vol. 2, no. 1, pp. 719–724, 2002, doi: 10.1109/pesw.2002.985098.

[41] L. Tang and B. T. Ooi, “Locating and isolating DC faults in multi-terminal DC systems,” *IEEE Trans. Power Deliv.*, vol. 22, no. 3, pp. 1877–1884, 2007, doi: 10.1109/TPWRD.2007.899276.

[42] N. DiFonzo and P. Bordia, *Reproduced with permission of the copyright owner . Further reproduction prohibited without*, vol. 130, no. 2. 1998. [Online]. Available: http://dx.doi.org/10.1016/j.jaci.2012.05.050

[43] R. M. Cuzner and G. Venkataramanan, “The status of DC micro-grid protection,” *Conf. Rec. - IAS Annu. Meet. (IEEE Ind. Appl. Soc.*, pp. 1–8, 2008, doi: 10.1109/08IAS.2008.382.

[44] E. Tironi, M. Corti, and G. Ubezio, “Zonal electrical distribution systems in large ships: Topology and control,” *2015 AEIT Int. Annu. Conf. AEIT 2015*, 2015, doi: 10.1109/AEIT.2015.7415252.

[45] B. G. Dobbs and P. L. Chapman, “A multiple-input DC-DC converter topology,” *IEEE Power Electron. Lett.*, vol. 1, no. 1, pp. 6–9, 2003, doi: 10.1109/LPEL.2003.813481.

[46] R. S. Balog and P. T. Krein, “Bus selection in multibus DC microgrids,” *IEEE Trans. Power Electron.*, vol. 26, no. 3, pp. 860–867, 2011, doi: 10.1109/TPEL.2010.2094208.

[47] J. G. Ciezki and R. W. Ashton, “Selection and stability issues associated with a navy shipboard DC Zonal Electric Distribution System,” *IEEE Trans. Power Deliv.*, vol. 15, no. 2, pp. 665–669, 2000, doi: 10.1109/61.853002.

[48] P. Cairoli and R. A. Dougal, “New Horizons in DC Shipboard Power Systems: New fault protection strategies are essential to the adoption of dc power systems.,”

IEEE Electrif. Mag., vol. 1, no. 2, pp. 38–45, 2013, doi: 10.1109/MELE.2013.2291431.

[49] M. U. Shahid *et al.*, "A hierarchical control methodology for renewable dc microgrids supporting a variable communication network health," *Electron.*, vol. 7, no. 12, 2018, doi: 10.3390/electronics7120418.

[50] K. Higashikawa, W. Bian, T. Kiss, and S. M. Muyeen, "Energy Efficiency Improvement of Renewable-Rich DC Microgrids by SMES Cables," *IEEE Trans. Appl. Supercond.*, vol. 34, no. 3, pp. 1–5, 2024, doi: 10.1109/TASC.2023.3349361.

[51] E. Taylor, M. Korytowski, and G. Reed, "Voltage transient propagation in AC and DC datacenter distribution architectures," *2012 IEEE Energy Convers. Congr. Expo. ECCE 2012*, pp. 1998–2004, 2012, doi: 10.1109/ECCE.2012.6342567.

[52] "Implementing the Standardization Framework to Support the Development of Low Voltage Direct Current and Electricity Access, IEC SEG4, International Electromagnetic Commission, Geneva, Switzerland, Oct. 2016".

[53] S. Whaite, B. Grainger, and A. Kwasinski, "Power quality in DC power distribution systems and microgrids," *Energies*, vol. 8, no. 5, pp. 4378–4399, 2015, doi: 10.3390/en8054378.

[54] A. Bose, "Smart transmission grid applications and their supporting infrastructure," *IEEE Trans. Smart Grid*, vol. 1, no. 1, pp. 11–19, 2010, doi: 10.1109/TSG.2010.2044899.

[55] F. Li *et al.*, "Smart transmission grid: Vision and framework," *IEEE Trans. Smart Grid*, vol. 1, no. 2, pp. 168–177, 2010, doi: 10.1109/TSG.2010.2053726.

[56] A. Pinomaa, J. Ahola, A. Kosonen, and P. Nuutinen, "Noise analysis of a power-line communication channel in an LVDC smart grid concept," *ISPLC 2013 - 2013 IEEE 17th Int. Symp. Power Line Commun. Its Appl. Proc.*, pp. 41–46, 2013, doi: 10.1109/ISPLC.2013.6525822.

[57] K. Asakimori, K. Murai, T. Tanaka, and T. Babasaki, "Effect of inrush current

flowing into EMI filter on the operation of ICT equipment in HVDC system," *INTELEC, Int. Telecommun. Energy Conf.*, vol. 2014-Janua, no. January, pp. 1–5, 2014, doi: 10.1109/intlec.2014.6972194.

[58] A. Kwasinski, "Advanced power electronics enabled distribution architectures: Design, operation, and control," *8th Int. Conf. Power Electron. - ECCE Asia "Green World with Power Electron. ICPE 2011-ECCE Asia*, pp. 1484–1491, 2011, doi: 10.1109/ICPE.2011.5944475.

[59] G. C. Lazaroiu, E. Tironi, M. O. Popescu, O. Ghita, and V. Dumbrava, "Transient analysis of DG interfaced low voltage dc system," *ICHQP 2010 - 14th Int. Conf. Harmon. Qual. Power*, pp. 1–6, 2010, doi: 10.1109/ICHQP.2010.5625445.

[60] S. Rajagopalan, B. Fortenbery, and D. Symanski, "Power quality disturbances within DC data centers," *INTELEC, Int. Telecommun. Energy Conf.*, pp. 1–7, 2010, doi: 10.1109/INTLEC.2010.5525723.

[61] P. Prabhakaran and V. Agarwal, "Mitigation of voltage unbalance in a low voltage bipolar DC microgrid using a boost-SEPIC type interleaved DC-DC compensator," *2016 IEEE 2nd Annu. South. Power Electron. Conf. SPEC 2016*, pp. 1–6, 2016, doi: 10.1109/SPEC.2016.7846222.

[62] V. F. Pires, A. Cordeiro, C. Roncero-Clemente, S. Rivera, and T. Dragicevic, "DC-DC Converters for Bipolar Microgrid Voltage Balancing: A Comprehensive Review of Architectures and Topologies," *IEEE J. Emerg. Sel. Top. Power Electron.*, vol. 11, no. 1, pp. 981–998, 2023, doi: 10.1109/JESTPE.2022.3208689.

[63] M. Farhadi and O. A. Mohammed, "Real-time operation and harmonic analysis of isolated and non-isolated hybrid DC microgrid," *IEEE Trans. Ind. Appl.*, vol. 50, no. 4, pp. 2900–2909, 2014, doi: 10.1109/TIA.2014.2298556.

[64] H. A. M. Knoef, *Handbook Biomass Gasification Second Edition. Biomass Technology Group (BTG)*. 2012.

[65] P. Basu, *Design of Biomass Gasifiers*, First Edit. © 2010 Elsevier Inc., 2010. doi: 10.1016/b978-0-12-374988-8.00006-4.

[66] M. van der B. Christopher Higman, *Notes on the authors*. 2008. doi: 10.4337/9781845426835.00005.

[67] C. R. Altafini, P. R. Wander, and R. M. Barreto, "Prediction of the working parameters of a wood waste gasifier through an equilibrium model," *Energy Convers. Manag.*, vol. 44, no. 17, pp. 2763–2777, 2003, doi: 10.1016/S0196-8904(03)00025-6.

[68] B. de Mena, D. Vera, F. Jurado, and M. Ortega, "Updraft gasifier and ORC system for high ash content biomass: A modelling and simulation study," *Fuel Process. Technol.*, vol. 156, pp. 394–406, 2017, doi: 10.1016/j.fuproc.2016.09.031.

[69] L. Fryda, K. D. Panopoulos, and E. Kakaras, "Integrated CHP with autothermal biomass gasification and SOFC-MGT," *Energy Convers. Manag.*, vol. 49, no. 2, pp. 281–290, 2008, doi: 10.1016/j.enconman.2007.06.013.

[70] S. Jarungthammachote and A. Dutta, "Equilibrium modeling of gasification: Gibbs free energy minimization approach and its application to spouted bed and spout-fluid bed gasifiers," *Energy Convers. Manag.*, vol. 49, no. 6, pp. 1345–1356, 2008, doi: 10.1016/j.enconman.2008.01.006.

[71] A. Melgar, J. F. Pérez, H. Laget, and A. Horillo, "Thermochemical equilibrium modelling of a gasifying process," *Energy Convers. Manag.*, vol. 48, no. 1, pp. 59–67, 2007, doi: 10.1016/j.enconman.2006.05.004.

[72] A. Mountouris, E. Voutsas, and D. Tassios, "Solid waste plasma gasification: Equilibrium model development and exergy analysis," *Energy Convers. Manag.*, vol. 47, no. 13–14, pp. 1723–1737, 2006, doi: 10.1016/j.enconman.2005.10.015.

[73] M. J. Prins, K. J. Ptasinski, and F. J. J. G. Janssen, "Thermodynamics of gas-char reactions: First and second law analysis," *Chem. Eng. Sci.*, vol. 58, no. 3–6, pp. 1003–1011, 2003, doi: 10.1016/S0009-2509(02)00641-3.

[74] D. Vera, B. De Mena, F. Jurado, and G. Schories, "Study of a downdraft gasifier and gas engine fueled with olive oil industry wastes," *Appl. Therm. Eng.*, vol. 51, no. 1–2, pp. 119–129, 2013, doi: 10.1016/j.applthermaleng.2012.09.012.

[75] S. M. Camporeale, A. M. Pantaleo, P. D. Ciliberti, and B. Fortunato, "Cycle configuration analysis and techno-economic sensitivity of biomass externally fired gas turbine with bottoming ORC," *Energy Convers. Manag.*, vol. 105, pp. 1239–1250, 2015, doi: 10.1016/j.enconman.2015.08.069.

[76] L. I. Chaves *et al.*, "Small-scale power generation analysis: Downdraft gasifier coupled to engine generator set," *Renew. Sustain. Energy Rev.*, vol. 58, pp. 491–498, 2016, doi: 10.1016/j.rser.2015.12.033.

[77] D. Vera, F. Jurado, and J. Carpio, "Study of a downdraft gasifier and externally fired gas turbine for olive industry wastes," *Fuel Process. Technol.*, vol. 92, no. 10, pp. 1970–1979, 2011, doi: 10.1016/j.fuproc.2011.05.017.

[78] P. Gobbato, M. Masi, and M. Benetti, "Performance analysis of a producer gas-fuelled heavy-duty SI engine at full-load operation," *Energy Procedia*, vol. 82, pp. 149–155, 2015, doi: 10.1016/j.egypro.2015.12.007.

[79] M. Ouadi, J. G. Brammer, M. Kay, and A. Hornung, "Fixed bed downdraft gasification of paper industry wastes," *Appl. Energy*, vol. 103, pp. 692–699, 2013, doi: 10.1016/j.apenergy.2012.10.038.

CAPÍTULO II: Design and integration of Z-source converters for energy management with series operation: Applied to DC microgrid

(Publicado en International Journal of Electrical Power and Energy Systems, Volumen 128, Junio de 2021, DOI:10.1016/j.ijepes.2021.106781)

ÍNDICE DEL CAPÍTULO II:

2.1 INTRODUCTION 58

2.2 MICROGRID INTEGRATED WITH CASCADE DC CONVERTERS 59

2.3 OPERATION, SWITCHING TECHNIQUE AND OPERATION OF THE INTEGRATED CONVERTERS IN THE BRANCH 60

2.3.1. Converters operation 60

2.3.2. Switching technique and operation 63

2.4 ANALYSIS OF THE MODES OF OPERATION OF THE CONVERTER AND GAIN OF VOLTAGE. 65

2.4.1. Analysis of operating modes 65

2.4.2. Voltage gain in both modes 69

2.5 DESIGN OF THE CONVERTERS TO BE INTEGRATED IN THE BRANCH 71

2.6 CONTROL STRATEGY. 77

2.7 EXPERIMENTAL RESULTS 78

2.7.1. Design considerations 78

2.7.2. Branch results. 81

2.7.3. Advantages of the proposed system compared to conventional solutions. 87

2.8 CONCLUSIONS 87

2.9 REFERENCES 88

TABLA DE FIGURAS CAPÍTULO II:

Fig. 2.1. Classical structure and new branch structure integrated into the microgrid. 59
Fig. 2.2. Power circuit, switching and operation of converters. 62
Fig. 2.3.converter working area, power abacus, power converter by converter and I_{LT2} based on Z-source. 74
Fig. 2.4. Current and transmitted power. 76
Fig. 2.5. Root locus for open-loop and Bode diagrams, uncontrolled (open loop) and controlled (closed loop) G(s) step responses of plant. 78
Fig. 2.6. Experimental results. 83
Fig. 2.7.Experimental results with elimination of sources. 84
Fig. 2.8. Waveform in step up and step down modes 85
Fig. 2.9. Management, measurement, control system and laboratory system. 86

TABLA DE TABLAS CAPÍTULO II:

Table 2.1. Situation of the components in the different possible modes of work. .. 63
Tables 2.2. Design data for Uc and Bc boost and parameters obtained for design, Uc and Bc boost 79
Table 2.3. Design parameters obtained for the redactor Bc. 80

Design and integration of Z-source converters for energy management with series operation: Applied to DC microgrid

Manuel Ortega[1], Enrique Lanagrán, Maria Victoria Ortega[1], Francisco Jurado[1*],

[1]Department of Electrical Engineering, Escuela Politécnica Superior, University of Jaén, 23700 Linares, Spain.

Abstract: This paper presents a Z-source converter integration technique, with which the energy management of various renewable energy sources is achieved. With a single controller and with serial arrangement of converters, this innovative method connect in series several power sources, with different power and voltage conditions. In this way, the supply to the load can be maintained without alterations, despite the random variations that occur in renewable energy sources. The main innovation is the design of the converters, according to the power and voltage conditions of the sources, so they can be integrated into a common generation branch with a single controller for all converters. The results have been verified by building a laboratory prototype consisting of three unidirectional and two bidirectional converters, which integrate three renewable sources and two electric accumulators. The generation branch management has been implemented in an S7-1500 PLC, each converter has used a DSP TMS320F2812 for the implementation of its switching technique, the branch control has also been implemented in another DSP of the same type.

Keywords: Energy management; DC microgrid; Distributed generation; Renewable energy sources; Z-source converters

* *Corresponding author*. Tel.: +34 953 648518; fax: +34 953 648605. *E-mail address*: fjurado@ujaen.es (F. Jurado).

2.1 INTRODUCTION

Nowadays and increasingly, renewable energy sources are being used more worldwide. Many of these sources generate direct current (DC) [1] and does not have a connection with alternative current networks. This happens in fuel cells (FC) [2][3][4] or in photovoltaic systems [5][6]. One of the advantages of direct current is that energy can be stored in batteries when there is a surplus of production, for its subsequent use [7][8][9]. This requires a precise management of the energy conversion from DC to DC [10], making energy transfer between different voltage levels [4]. This power transfer may be necessary in one direction only, for which unidirectional DC/DC converters [11] are used, or in two directions using bidirectional DC/DC converters [12].

DC/DC converters have been designed using various techniques, there are several types of topologies, such as Current-fed DC/DC converters [13], Voltage-fed DC/DC converters that usually use a high-frequency transformer [14][15]. Both techniques have also been integrated into a single unidirectional DC/DC converter with soft switching, obtaining an improvement in efficiency [16][11]. Regarding high voltage applications, several topologies with high voltage gains have been proposed [17]. In [18] the impedance source was introduced, while the quasi-Z-Source circuit was designed making modifications on the Z-Source circuit [19]. These circuits, which at first glance seem different, are compatible with various switching techniques [20][21][22]. The impedance source has also been applied in DC/DC converters with high gain [4].

DC microgrids require converters. There are several works dealing with the energy management system in the microgrid [23] [24]. In [24] a review of DC microgrids is presented, where the architectures are key elements to improve the control of the system, being the dynamic response of the microgrid a function of the performance of the converters and their control loops. The proposed architecture is the classic one with all the sources in parallel feeding a common DC bus. In [25] the integration of photovoltaic (PV) systems is proposed using several quasi Z-source unidirectional converters in series, with low complexity of control of the cascade system.

This paper presents a new architecture for the integration of energy sources and accumulators in a DC microgrid. For this purpose, converters based on unidirectional and bidirectional Z-source, connected in series, are used. In this technique, the primary control is simplified and improvements are obtained compared to a classic architecture, if the converters are properly designed. The design method of the converters to be integrated in a specific microgrid is also presented.

2.2 MICROGRID INTEGRATED WITH CASCADE DC CONVERTERS

Most of the renewable energy sources produce electrical energy in the form of DC. However, wind turbine generates alternating current that can be easily rectified and transformed to DC. Renewable energy sources can work at different voltage levels and suffer random variations that are difficult to control. But, the electrical networks need a voltage as stable as possible, so that it does not depend on the randomness of the sources, for this reason converters must be used.

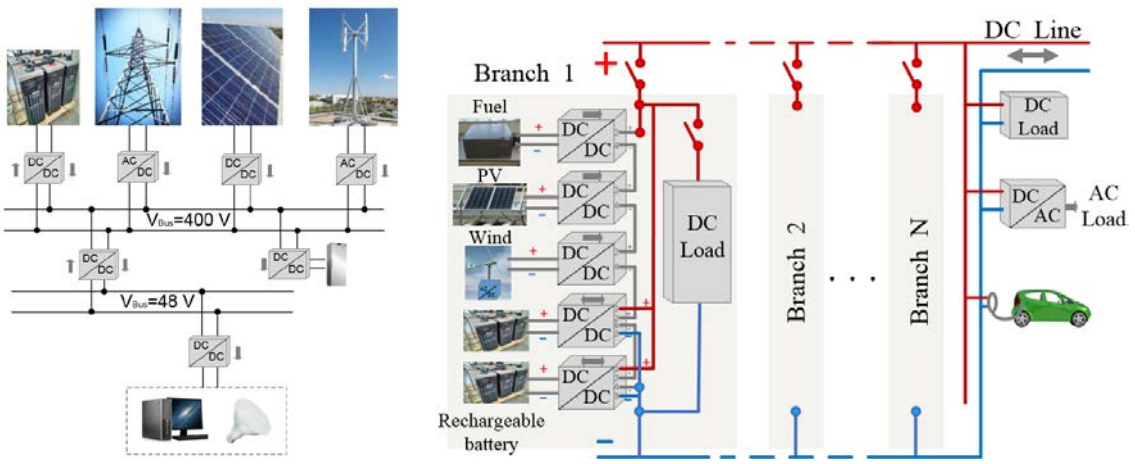

(a) Classical structure. (b) New branch structure integrated into the microgrid.

Fig. 2.1. Classical structure and new branch structure integrated into the microgrid.

In [23] [24] a classic microgrid structure is presented, see Fig 2.1(a). This paper presents a new configuration, where the energy sources as well as the storage systems can be connected in series, as indicated in Fig. 2.1(b).

To achieve the objectives, it is required to design the converters to be integrated in the branch. The proposed converters are presented in Fig. 2.2. If a source is integrated, a unidirectional converter (Uc) will be used, see Fig. 2.2(a). If a battery is integrated, a bidirectional converter (Bc) will be used, shown in Fig. 2.2(b). The design of the components of these converters is made based on the characteristics of the source that will be connect to the system and the number of sources that will intervene in each branch. The configuration of sources and energy storage systems can be done in many ways, this provides a very versatile system.

To demonstrate the technique, this paper presents an example with three sources and two storage batteries. In this example, each branch can be configured differently, and be composed of sources, storage batteries or a combination of both, where the number of components in each branch can be freely configured (from one component to several). In other words, it is a modular system. However, converters must be designed considering the type of elements to be integrated in the branch (source or accumulator) and the number of existing elements, so that all the energy generated by all sources can be extracted.

2.3 OPERATION, SWITCHING TECHNIQUE AND OPERATION OF THE INTEGRATED CONVERTERS IN THE BRANCH

2.3.1. Converters operation

Two Z-source based converters are introduced. In order to be integrated into the proposed system, this type of converters can be built in step-up mode (with a large gain of voltage) Fig. 2.2(a), and using step-up and step-down modes (with high voltage gain

in both modes) Fig. 2.2(b). In the two converters, the gains show a linear response with respect to the duty cycle. For their construction, they require very few components. However, integration in the proposed branch increases its constructive complexity somewhat, but overall the complexity of the management system is reduced. In addition, they use a very simple switching technique and very good efficiency is achieved.

- ***Unidirectional converter***, Fig. 2.2(a), this converter is used to integrate generating sources in the microgrid, in which the energy only moves from source to microgrid. The transistor S_{ce} connects the DC-source to the Z-source of the converter. The step-up duty cycle D_e actuates on the transistor S_e, if S_{ce} is deactivated the corresponding DC-source is disconnected from the branch; then the Z-source and C_a are de-energized on the load, and the branch current (from the other sources) passes through the diode D_a and the source disconnected from the branch does not provide power, remaining the rest of the sources suppling to the branch.

- *Bidirectional converter*, Fig. 2.2(b), this converter is used to integrate the energy storage system into the microgrid, which is loaded when there is excess energy generated and is discharged when the generation does not meet the needs of the demand. It can work in two modes. When it stores energy in the battery taking it is directly from the DC bus (step-down mode), this is achieved by activating S_{cr1} and S_{cr2}, and the step-down duty cycle D_r works on S_{rD}. The rest of the transistors are disconnected. Although the battery is being charged with energy from the microgrid, this converter via D_a allows current to circulate in the branch, with the rest of the sources supplying energy to the microgrid. When it is necessary to provide energy from the battery to the microgrid (step-up mode), S_{e1} y S_{e2} are activate during the entire period and D_e acts on S_e, the rest of the transistors are left deactivated, creating the voltage V_{Ca} at the ends of the C_a capacitor, which is the voltage that the battery contributes to the branch.

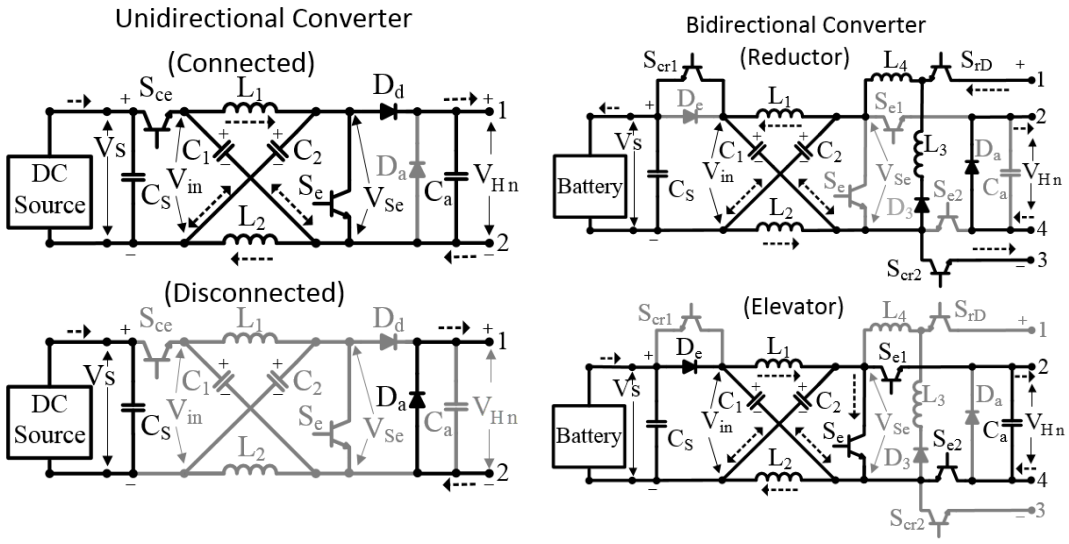

(a) Unidirectional converter (b) Bidirectional converter

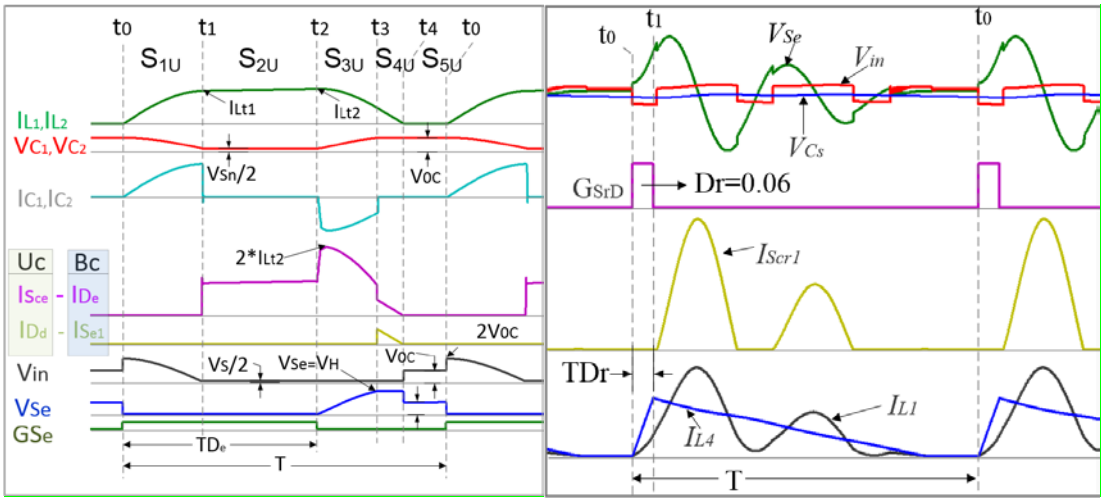

(c) Switching and operation in step-up mode (d) Switching and operation in step-down mode

Fig. 2.2. Power circuit, switching and operation of converters.

In Fig. 2.2 the converters are represented, with their operating modes and all the elements necessary to be integrated into the branch. The black lines show the active parts, the gray lines the non-active parts. Table 2.1 shows the location of the components in each working mode, on the transistors it is indicated whether or not they are active, for diodes the same symbology is used, but the exact conduction time is not defined (only the

time interval in which conduction occurs). The references used are: 0 disconnected all the period, T connected the whole period, TD active only the duty cycle time and (1-D)T disconnected during the duration of the duty cycle and active the rest of the time.

Table 2.1. Situation of the components in the different possible modes of work.

Unidirectional converter (Uc)									
Component	S_{ce}	S_e	D_d	D_a					
Connected	T	TD	(1-D)T	0					
Disconnected	0	0	0	T					
Bidirectional converter (Bc)									
Component	S_{cr1}	S_{cr2}	S_{rD}	D_3	D_e	S_{e1}	S_{e2}	S_e	D_a
Boost	0	0	0	0	TD	T	T	TD	0
Buck	T	T	DT	(1-D)T	0	0	0	0	T
Disconnected	0	0	0	0	0	0	0	0	T

2.3.2. Switching technique and operation

- **Step-Up mode.** This mode occurs in the Uc connected and Bc boost, Table 2.1 shows the status of all the devices that intervene in each converter, this mode is made up of five stages, (S_{1U}, S_{2U}, S_{3U}, S_{4U}, S_{5U}). Although adaptation to the branch forces each converter to have different auxiliary components, the operation of the Z-source in step-up mode is the same in the two converters. Fig. 2.2(c) shows the switching technique and the operation in this mode. The switching technique is very simple (only transistor S_e is switched); if the Z-source is properly designed, the converter executes the entire switching process autonomously, this process being the one that gives it the boost capacity. When the inverter is working in steady state, capacitors C_1 and C_2 start the cycle with a voltage value V_{0C}. The Z-source is symmetric, so that the inductances and the capacitances respectively meet $L_1=L_2=L$, $C_1=C_2=C$.

Stage-$S_{1U}[t_0\text{-}t_1]$: It starts with the connection of S_e, the capacitors C_1 and C_2 charged to the initial voltage $V_C=V_{0C}$, discharge their energy through L_1 and L_2 respectively (energizing the inductors), leaving the capacitors $V_C=V_S/2$ at the end of the stage at t_1. Due to L_1 and L_2, at t_0 $I_{Se}=0$, then the connection of S_e is smooth.

Stage-$S_{2U}[t_1\text{-}t_2]$: When $V_C=V_S/2$, at t_1 S_{ce} or D_e start to drive (depends on the type of converter), L_1 and L_2 continue to be powered in series from the source throughout the stage, also complies, $V_C=V_S/2$ and $V_{Se}=0$, where $V_{in}=Vs$.

Stage-$S_{3U}[t_2\text{-}t_3]$: In t_2 S_e disconnects, this disconnection occurs with a value of V_{Se} between $V_S/2$ and V_S . In t_2, $V_{C2}=V_{C1}=V_S/2$ also is satisfied. Throughout the stage, $I_{L1}=I_{C1}$ and $I_{L2}=I_{C2}$ are verified. When S_e is disconnected, C_1 and C_2 are recharged with energy from the coils and the source. At t_3 the capacitors acquire a charge value $V_{C2}=V_{C1}=V_{0C}$, which is kept until the moment t_0 of the following cycle.

It is also observed that I_{Sce} or I_{De} increase sharply after t_2, see Fig 2.2(c). This occurs by reconfiguring the Z-source circuit after disconnecting S_e. Depending on the type of converter, it is true throughout the stage that $I_{Sce}=I_{L1}+I_{L2}$ or $I_{De}=I_{L1}+I_{L2}$. V_{Se} rises from a value close to zero at t_2, to a value somewhat higher than V_H en t_3, see Fig 2.2(c).

Stage-$S_{4U}[t_3\text{-}t_4]$: At t_3 V_{Se} is slightly rising greater than V_H. Then, D_d or S_{e1} start driving. Then current flows from the source and coils L_1 and L_2 to the capacitor C_a and therefore to the DC link, this energy being distributed to the load throughout the period. In this stage $I_{C1}=I_{C2}=0$ is fulfilled, then the capacitors help in raising the voltage V_{Se} but do not provide energy to the DC link.

Stage-$S_{5U}[t_4\text{-}t_0]$: In t_4 L_1 and L_2 have been completely de-energized, $I_{L1}=I_{L2}=0$, $V_{in}=V_{Se}=V_{C1}=V_{C2}=V_{0C}$ is also fulfilled, this situation remains until the beginning of the next cycle in t_0. Z-source does not circulate current in any of its components. The maximum boost duty cycle allowed is $D_{max}=0.85T$, but for safety $D_{max}=0.8T$ has been used.

- Step-down mode. This mode only occurs in the bidirectional converter working as a buck, in this case it only works in discontinuous conduction (DC). The same variables

have been preserved in the two modes, but have different meanings in both modes. Fig. 2.2(d) shows the graph of the most significant variables in this mode. Input voltage at the impedance source V_{Se}, output voltage from the impedance source V_{in}, converter output voltage $V_{CS}=V_S$, I_{L4} current in L_4. In the inductors $I_{L1}=I_{L2}$ is met but only I_{L1} has been represented. G_{SrD} is the gate signal of the transistor S_{rD}, this is the only one that switches according to the reductive duty cycle D_r, the transistors S_{cr1} y S_{cr2} are integration transistors, they are connected whenever this mode is active, both in the stage S_{1D} and in S_{2D}.

Stage- $S_{1D}[t_0\text{-}t_1]$: S_{rD} is connected between t_0 and t_1. At this time D_r*T, the capacitors and inductors of the Z-source absorb energy from the DC link.

Stage- $S_{2D}[t_1\text{-}t_2]$: in t_1 S_{rD} is disconnected, which remains disconnected until t_0 of the following period, at this time DC link power is not supplied to the Z-Source. Inductors L_1, L_2 and L_4 close their circuit through D_3 and L_3. The energy stored in the Z-source and in L_4, during the previous stage S_{1D}, is delivered to the capacitor C_S in this stage, the current I_{Scr1} flows from the Z-source to C_S. Then throughout the period C_S contributes energy to the DC source (battery).

2.4 ANALYSIS OF THE MODES OF OPERATION OF THE CONVERTER AND GAIN OF VOLTAGE.

The necessary analysis (based on the switching and operation) is presented, obtaining only the key formulas that allow designing the converters to be integrated in the branch.

2.4.1. Analysis of operating modes

- Step-up mode. consisting of 5 stages, occurs in Uc connected and the Bc boost, the equations planned in this way are obtained from the circuit of Fig. 2.2 (a).

Stage S_{1U}: In the Uc the devices are: (S_{ce}=1, S_e=1 D_d=0, D_a=0); in the Bc they are in: (D_e=0, S_{e1}=1, S_{e2}=1, S_e=1, D_a=0)**.** The most significant variables in this way are shown in Fig. 2.2(c), in this stage, observing the input mesh is fulfilled:

$$V_{in}(t) = V_C(t) + V_L(t) \tag{1}$$

$$V_C(t) = V_L(t) \tag{2}$$

The current equation in the Z-source is:

$$\left(V_{0C} - \frac{1}{C}\int I_L dt\right) + L\frac{dI_L}{dt} + R_{LC}I_L = 0 \tag{3}$$

The Z-source capacitor voltage equation (4) obtained from (3) taking into account that

$$V_c(t) = \left(V_{0C} - \frac{1}{C}\int I_L dt\right),$$

is:

$$V_c + LC\frac{d^2V_c}{dt^2} + R_{LC}C\frac{dV_c}{dt} = 0 \tag{4}$$

By solving (4) and applying approximations, the voltage function of the capacitors in the Z-source obtained at this stage is:

$$V_c(t) = V_{0C}\left(1 - \frac{t^2}{2LC}\right) / \quad \forall t \in [t_0, t_1] \tag{5}$$

The current function on the Z-source coils has been obtained by solving (3).

$$I_L(t) = \frac{2\sqrt{C}V_{0C}\sin\left(\frac{t\sqrt{4L-CR^2}}{2\sqrt{C}L}\right)e^{-\frac{Rt}{2L}}}{\sqrt{4L-CR^2}} / \quad \forall t \in [t_0, t_1] \tag{6}$$

Developing (6) in Taylor series and evaluation in (t_1) we obtain (7), which is one of the key values that we need for the design of the converter, being the current in the inductors at time t_1.

$$I_L(t_1) = \sqrt{\frac{C}{L}\left(\frac{V_H^2}{4} + \frac{V_H V_S}{2}\right)} \tag{7}$$

Stage S_{2U}: the device positions are the same as in the previous stage. This stage begins at t_1, when the capacitors C_1 and C_2 have lowered their voltage value to $V_s/2$, being fulfilled throughout the stage.

$$V_s = V_C(t) + V_L(t) \tag{8}$$

$$V_S = 2V_L \tag{9}$$

and

$$I(\mathrm{t}) = I_L(t_1) + \frac{V_S}{2L}\int_{t_1}^{t} dt \quad \forall t \in [t_1 - t_2] \tag{10}$$

Obtaining the current function in the Z-source inductors of (10), as a function of the boost duty cycle D_e, this is shown in (11).

$$I_L(t) = I_L(t_1) + \frac{V_{Sn}}{2L}D_e T \quad \forall D_e \in [0 - 0.8] \tag{11}$$

Stage S_{3U}: at t_2 S_e is disconnected, leaving the devices in Uc at: (S_{ce}=1, D_e=0 D_d=0, D_a=0); and in the Bc in (D_e=1, S_{e1}=1, S_{e2}=1, S_e=0, D_a=0). The energy stored in the coils, charges the capacitors C_1 and C_2 again, being fulfilled in the input mesh of the Z-source, $V_S + V_L(t) = V_C(t) + V_{R_{LC}}(t)$ and in the output mesh $V_{Se}(t) = V_C(t) + V_L(t)$ for $V_{Se}(t) < V_H \ \forall t \in [t_2, t_3)$, being the equations of discharge current of the coils and of charge of the capacitors in the Z-source, (12) and (13) respectively.

$$-L\frac{dI_L}{dt} = I_L R_{LC} + \frac{1}{C}\int_{t_3}^{t_2} I_L dt \tag{12}$$

$$V_C(t) = \frac{V_S}{2} + \frac{1}{C}\int_{t_2}^{t_3} I_L(t)dt \tag{13}$$

$$V_C(t_3) = \frac{(V_H + V_S)}{2} = V_{0C} \tag{14}$$

Solving (12) and (13), and studying the function at point t_3, the equation (14) is obtained, which shows the voltage value at which the capacitors V_{C1} y V_{C2} are left at point t_3, which is a value key to the design of the converter, this value is retained in the capacitors for the next two stages until the start of the next cycle.

Stage S_{4U}: at t_3 when V_{Se} is a little larger than V_H, the energy transmission from inductors L_1 and L_2 to the capacitor C_a occurs, then the energy is transmitted to the load throughout the period, leaving L_1 and L_2 totally de-energized.

Stage S_{5U}: at t_4 The Z-source inductors have been completely de-energized and the transfer of energy from the inductors (L_1, L_2) to C_a ends. This stage is necessary, if the cycle exceeds 0.85, this stage disappears, then a current circulation within the Z-source occurs, which causes the converter to increase the losses within the Z-source without producing any benefits.

- **Step-down mode.** occurs in the Bc buck, this mode consists of two stages, in our case the converters with this mode take power from the DC link and store it in batteries.

Stage S_{1D}: This stage starts at t_0 to t_1, it is the time that L_4 and the Z-source are energizing, (15) and (16) are verified in it. The value of V_{Se} in this mode, can be expressed with (17).

$$V_{Se}(t) = V_C(t) + V_L(t) \tag{15}$$

$$V_{in}(t) = V_C(t) - V_L(t) \tag{16}$$

$$V_{Se}(t) = V_H - V_{L_4}(t) \tag{17}$$

The current equation is shown in (18), which has been obtained from the Fig. 2.2(b) buck, integrating (18) the current in the limiting inductor L_4 is obtained, the solution is approximated by (19). Fulfilling $I_{L1}=I_{L2}=I_L=I_{L4}/2$, this current is a significant data for the design of L_4 and the transistor S_{rD}.

$$L_4\frac{dI_{L_4}}{dt}+L\frac{d\left(I_{L_4}/2\right)}{dt}+V_S+\frac{1}{C}\int_0^D\frac{I_{L_4}}{2}dt+RI_{L_4}=V_H \tag{18}$$

$$I_{L_4}=\frac{2\left(V_{Hn}-V_S\right)t}{L+2L_4}\quad \forall t\in[0,DrT] \tag{19}$$

Stage S_{2D}: This stage starts at t_1 to t_0, the energy stored in L_4 and in the Z-source in the previous stage, is transferred to the battery.

2.4.2. Voltage gain in both modes

The Z-source has lifting and reducing gain, but when you want to give it the double application (reducing and lifting), the design of the Z-source must be done for the lifting function, then with L4 the reducing function is adjusted. The energy transmitted from Z-source to the DC-link can be evaluated very closely with the values of ILt1 and ILt2, therefore taking into account (7) and evaluating (11) at time t_2, it is verified (20) that it represents the energy transferred from the Z-source to the load (with current I_{Load}) in any of the converters that work in boost mode.

$$V_{Hn}I_{Load}T=L(I^2(t_2)-I^2(t_1)) \tag{20}$$

With (7) (11) and (20) is obtained (21), this allows calculating the boost voltage gain, that has been studied in all its generality, having application throughout the work cycle.

$$V_{Hn}=\frac{D_e^2C\sqrt{L}V_{Sn}^3-2D_e^2\sqrt{C}\sqrt{V_{Sn}^5}(\sqrt{M})+D_e^2I_{Load}\sqrt{LT}V_{Sn}^2}{4I_{Load}^2\sqrt{L^3}-D_e^2C\sqrt{L}V_{Sn}^2} \tag{21}$$

con

$$M = \frac{V_S D_e^2 T^2}{16} + \frac{I_{Load} LT}{2} + \frac{CLV_{Sn}}{4}$$

To facilitate the control of the proposed system, the contributions of all the terms have been studied, neglecting those with the lowest contribution. This make their contribution to the general expression for low values of the duty cycle, non-linear zone (where the system does not work), obtaining the linear function (22) that can be set as indicated in (23), with application range obtained with (24).

$$V_{Hn} = \frac{-C^{\frac{1}{2}} V_S T D_e + 2 I_{Load} L^{\frac{1}{2}} T}{-2C L^{\frac{1}{2}}} \tag{22}$$

$$V_{Hn} = \alpha D_e - \beta I_{load} \quad con \;\; \alpha = \frac{V_S T}{2C^{\frac{1}{2}} L^{\frac{1}{2}}}; \;\; \beta = \frac{T}{C} \tag{23}$$

$$\left((2 * I_{load} \sqrt{L}) / \sqrt{C} V_S \right) < D_e < 0.8D \tag{24}$$

In buck mode there are two alternate states within the cycle, which are represented by equations (25), the states are differentiated with subscripts 1 and 2.

$$V_{1Se}(t) = 2V_{1L}(t) + V_{1S}(t) \;\; ; \;\; V_{2Se}(t) = -2V_{2L}(t) + V_{2S}(t) \tag{25}$$

If the second volts (V/s) in the entire period are calculated, taking into account that in the inductors the V/s are zero, it is obtained that in average value in the whole cycle $\overline{V}_{Se} = \overline{V}_S$.

In L_4 (26) is fulfilled, taking into account that from (26) the reduction voltage gain is obtained with (27).

$$\overline{V}_{L_4} = L_4 \frac{dI_{L_4}}{dt} = 0 \Rightarrow \int_0^{DrT} (V_H - V_{Se}) dt - \int_{DrT}^{T} V_{Se} dt = 0 \tag{26}$$

$$V_S = V_{Hn} \cdot D_r \tag{27}$$

2.5 DESIGN OF THE CONVERTERS TO BE INTEGRATED IN THE BRANCH

For the design of the converters, the quantity and type of sources that are integrated in the branch must be defined. The power of each source as well as its output voltage must be known, and the number of independent accumulators per branch. The value of the DC bus voltage will determine the maximum number of sources connected in the branch. In addition, the number of minimum sources or batteries that can cover the demand and the maximum power demanded.

The design of the Z-source converter, starts with the boost mode (in case of being a unidirectional converter it only has this mode), then the reducer mode is designed. The inductance and capacitance values of the Z-source satisfy that $L_1=L_2=L$ y $C_1=C_2=C$.

-**Step-up mode.** it is contained in the Uc and Bc. The converter must be designed taking into account the maximum power generated by the source E_{max}. The maximum energy supplied by the source to the load by the converter in each cycle is obtained with (28).

$$E_{\max} = P_s T D_{\max} = L(I_{Lt_2}^2 - I_{Lt_1}^2) \tag{28}$$

$$(V_{0C})_{t'_2} = \frac{(V_{Hn} + V_{Sn})}{2} \tag{29}$$

At time t_3 of the switching process, see Fig. 2.2(c), the capacitors C_1 and C_2 are charged to the voltage V_{0C} (where V_{Hn} y V_{Sn} denote the source voltage and output voltage of the n_{th} converter respectively) whose value is shown in (29), obtained from (14), but adapted to the branch. This voltage remains in the capacitors until the beginning of the next period at t_0. Between t_0 and t_1 capacitors C_1 and C_2 discharge from V_{0C} to $V_{Sn}/2$. In t_1 the current appears in the Z-source. This is a key piece of information to obtain the right converter design for each situation. The value of I_{Lt1} is obtained with (30), obtained from (7), but adapted to the branch.

$$(\mathrm{I}_L)_{t_1} = \sqrt{\frac{C}{L}\frac{\left(V_{Hn}^2 + 2V_{Hn}V_{Sn}\right)}{4}} \tag{30}$$

When the converter works with the maximum lift cycle D_{max}, the maximum current value $(I_{L\max})_{t_2}$ flowing through L_1 and L_2 shown (31) is obtained, an expression obtained from (11). This current is necessary for the choice of devices S_{ce}, S_e, D_e and the section of the copper wire of the inductors L_1 and L_2.

$$(I_{\mathrm{L}\max})_{t_2} = I_{Lt_1} + \frac{V_{Sn}}{2L}D_{\mathrm{e}\max}T \tag{31}$$

With (28), (30) and (31), is obtained (32), to calculate the maximum power P_s that the converter can transport between source and network. This must be equal to or slightly greater than that generated by the source, which is intended to be connected by the converter in the branch.

$$P_s = (2I_{Lt_1} + \frac{V_{Sn}}{2L}D_{\mathrm{e}\max}T)\frac{V_{Sn}}{2}D_{\mathrm{e}\max} \tag{32}$$

The parameters that determine the maximum energy that the converter can transport are the inductance and the capacitance of the Z-source, since P_s, V_{sn} and D_{max} are imposed, clearing L from (32), the inductance can be obtained with (30). Solving for C from (30) we obtain (34), which allows obtaining the capacity of the Z-source.

$$L = \frac{V_{Sn}^2 D_{\max}^2 T}{4(P_s - I_{Lt_1}D_{\max}V_{Sn})} \tag{33}$$

$$C = \frac{4\mathrm{L}(\mathrm{I}_L^2)_{t_1}}{\left(V_{Hn}^2 + 2V_{Hn}V_{Sn}\right)} \tag{34}$$

If, for example, it is intended to design a converter for a renewable source with a range of source voltages RV_S=(8-15) V with a mean value of V_{Sn}=10V, which suplies the branch a mean voltage value V_{Hn}=100V, the maximum step-up duty cycle that the converter supports is $D_{e\text{-}max}$=0.8. The switching frequency (in this case) is fixed at 10kHz. It is wanted to integrate into the branch a source that provides a power of P_s=600W at an

average voltage of 10V. The converter must be able to transfer all the power from the source.

Assuming constants V_{Sn} and V_{Hn} with the values indicated above, the power that the converter can transfer depends on (L, I_{Lt1}) and the variable I_{Lt1}, which depends on (L, C). As the converter is bi-directional, the choice of optimal values (C, L) must be able to transmit the expected power, with a value of L high enough for the source to help L_4 in the step-down mode.

In Fig(s). 2.3 (a and b) is represented (32). In these figures it can be seen that to achieve a high power transmission, a high I_{Lt1} current and a low inductance L are required. To get the optimal choice, in Fig. 2.3(b), the values of L and I_{Lt1} must be chosen as a function of P_s. Observing Fig. 2.3(b), by drawing a horizontal line, the optimum point is taken as the cut-off point with the red line with the highest current value, to transmit 600W the approximate values of I_{Lt1}=60 A and L=14µH can be taken. Inductance values should be chosen that can be found on the market or that can be constructed.

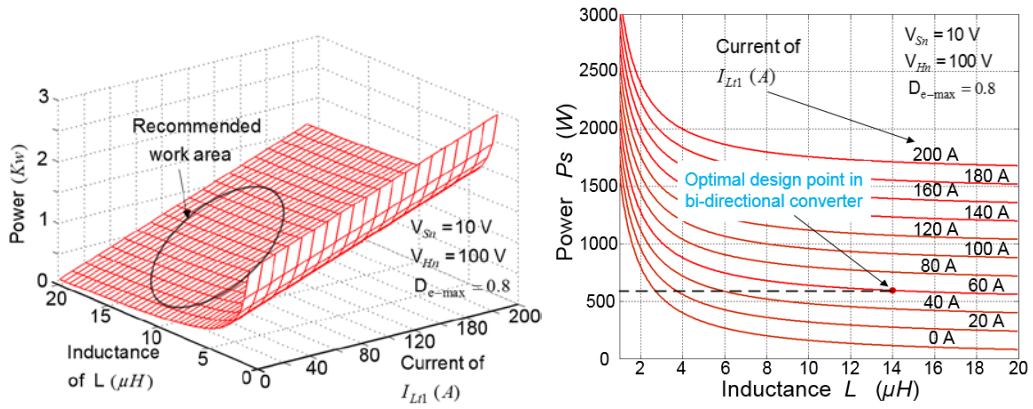

(a) Converter working area.

(b) Power abacus.

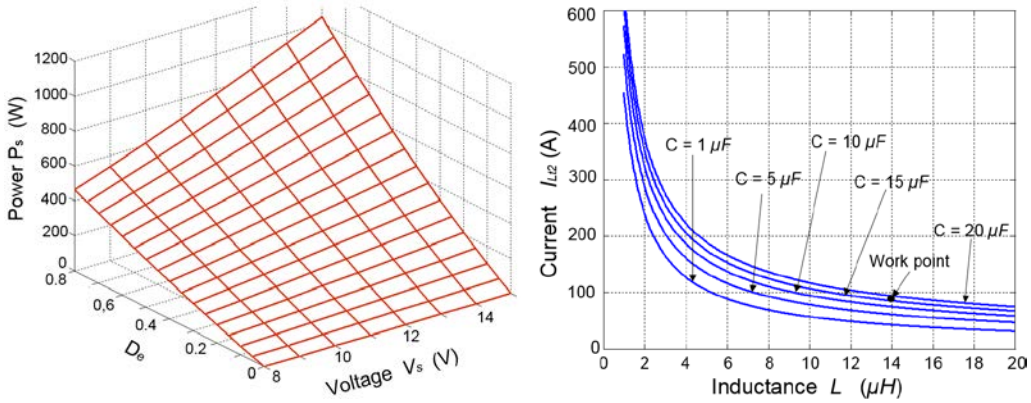

(c) Power converter by converter.

(d) I_{LT2} based on Z-source.

Fig. 2.3.converter working area, power abacus, power converter by converter and I_{LT2} based on Z-source.

Then, the chosen values for I_{Lt1} and L are replaced in (34) and C=16.8 µH is obtained. With this pair of values (L, C), the Z-source can transmit the desired power. But due to commercial availability, two inductors and two capacitors will be used (L=14 µH and C=18µF), these are close to the optimal values.

With (30), the value of I_{Lt1}=62.1A is recalculated.

Obtained L and C from the Z-source and taking into account (31), the value of I_{Lt2} = 90.57A is determined. This is the highest theoretical current that exists in the Z-source. With the calculated values C=18, L=14, the voltage ranges RV_S = (8-15) and the cycle D_e = (0-0.8); the equation (31) has been represented in Fig. 2.3(d). It can be seen that the value of I_{Lt2} becomes larger as the value of the capacities increases and the value of the inductances of the Z-source decreases. The converter working point has been shown in this graph, it can be observed that the I_{Lt2} value is in the low current zone, this is due to the choice of (L, C) close to the optimum.

The graph of (32) has been represented in Fig. 2.3(c), where the ideal power range can be seen, which is (0-1,002)W. Also, using for a cycle 0.8 and a source voltage of 10 V is obtained P_s=611W, which is similar to the power of the proposed source.

If, with the chosen values (*C*, *L*), the results were not as expected, and the Z-source needed to be adjusted, it is possible to increase power, increasing the value of *C*, reducing *L* or doing both. To reduce power can be achieved by doing the opposite.

- **Step-down mode.** is contained in the Bc. This has more capacity to transmit power (energy is transmitted from a high voltage level to a lower one), once the Z-source values for the step-up mode have been obtained, it is necessary to design the value of L_4, to this is used the expression (35). Being the maximum power transmitted by the converter in step-down mode (P_r), obtained with (36), (35) and (36) has been obtained from (19).

$$I_{L_4} = \frac{2\left(V_H - V_{Sn}\right) D_{r\max} T}{L + 2L_4} \tag{35}$$

$$\mathrm{Pr} = V_{Hn} * \frac{\left(V_H - V_{Sn}\right) D_r^2 T}{L + 2L_4} \tag{36}$$

It must always be borne in mind that the side with the lowest voltage level is where the highest currents occur, this forces limiting the duty cycle in buck mode. Expression (35)has been represented in Fig. 2.4(a). In it, it can be seen how the value of I_{L4} decreases when the L_4 inductance value increases. The green line corresponds to an inductance value of 50µH. If the value of D_r increases, it is observed that I_{L4} increases. D_r has been limited to 0.1 to avoid excessively high currents.

As shown in Fig. 2.4(b), the green curve represents the transmitted power as a function of the cycle with an inductance value of L_4=50µH, as we decrease the inductance values in L_4 more power can be transmitted but at cost of increasing the robustness of some components. If the following values are substituted in (35) (L_4=50 μH, D_r=0.1, V_{Sn}=10V, V_{Hn}=100V, L=14μH y L_4=50μH), we obtain a value of I_{L4}=86A, this being the maximum peak value of I_{L4}. This value will be taken into account for the design of L_4 and the choice of S_{rD} and S_{cr2}.

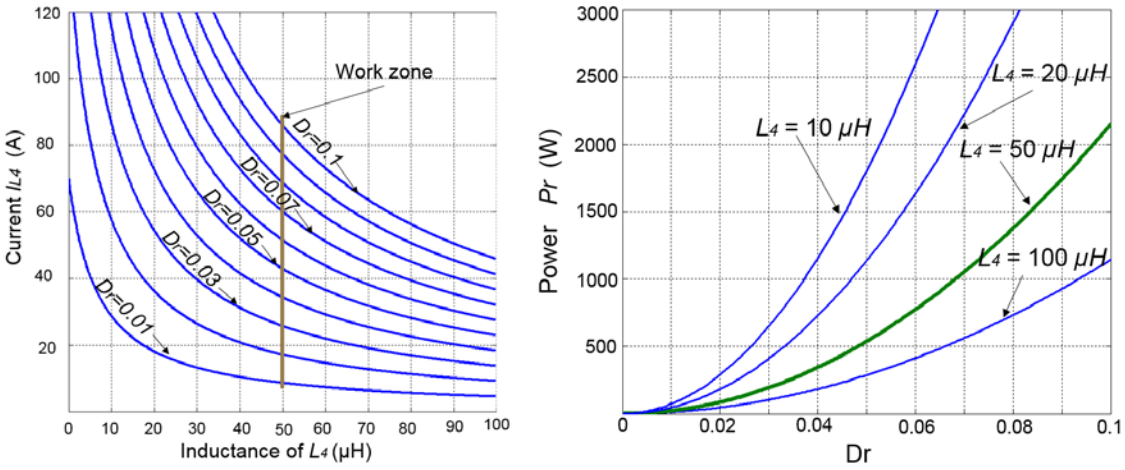

(a) Current.

(b) Transmitted power.

Fig. 2.4. Current and transmitted power.

For the dimensioning of the semiconductors the operation of the converter has been taken into account, obtaining the expressions from (37) to (41), with which the maximum average current supported by each one of the semiconductors that intervene in the converter is calculated. These currents are a function of the critical currents $(I_L)_{t1}$, $(I_L)_{t2}$, I_{L4} and the maximum powers converted in the step-down and step-up modes.

$$\overline{I}_{Se} = \frac{(I_L)_{t_1} + (I_L)_{t_2}}{2} * 0.85 \tag{37}$$

$$\overline{I}_{Sce} = \overline{I}_{De} = \frac{(I_L)_{t_1} + (I_L)_{t_2}}{2} \tag{38}$$

$$\overline{I}_{SrD} = 2 * \overline{I}_{D_3} = 2 * \overline{I}_{Scr2} = \frac{I_{L4}}{10} \tag{39}$$

$$\overline{I}_{Se1} = \overline{I}_{Se2} = \frac{P_{\max}\ converted\ (mode\ step-up)}{V_{Hn}} \tag{40}$$

$$\overline{I}_{Scr1} = \frac{P_{\max}\ converted\ (mode\ step-down)}{V_s} \tag{41}$$

2.6 CONTROL STRATEGY.

The system admits various control techniques according to the objectives, in this case, the converters in step-up mode have a linear response in most of the cycle, with the work zone (0.1<D<0.8) contained in the linear zone, this is a great advantage of this converter. In our case, the dynamic model has been studied, which has been linearized for D=0.8, to obtain the transfer function the average value of the parameters of all the converters of the branch has been obtained (V_s=22 V, C=3µF, L=18µH, C_a=250µF, R=0.002Ω, R_{Load}=75 Ω), substituting these in the dynamic model, (42) has been obtained, this is possible because the converters have very similar and linear responses for most of the cycle.

$$G(s) = \frac{38*10^3 s^2 + 2.249*10^8 s - 0.0002508}{s^3 + 142.2 s^2 + 2.643*10^7 s + 1.043*10^9} \quad (42)$$

$$C(s) = \frac{175(s+20)(s+40)}{s(s+70)} \quad (43)$$

If the transfer function is analyzed with the place of the roots, see Fig. 2.5 (a), its poles and zeros are in the left half plane, it has an infinite gain margin and a phase margin of 87.5º, then the plant is stable. Using Matlab, a PID controller has been designed (which acts on the duty cycle of all the converters in step-up mode), shown in (43), composed of an integrator, a pole at -70 and two zeros at -20 and -40, the response of the open and closed loop system is presented in Fig. 2.5 (b), where through the step response, it is observed that the plant has been controlled with the proposed controller, with constants K_p=121.4, T_i=0.06 and T_d=0.0063.

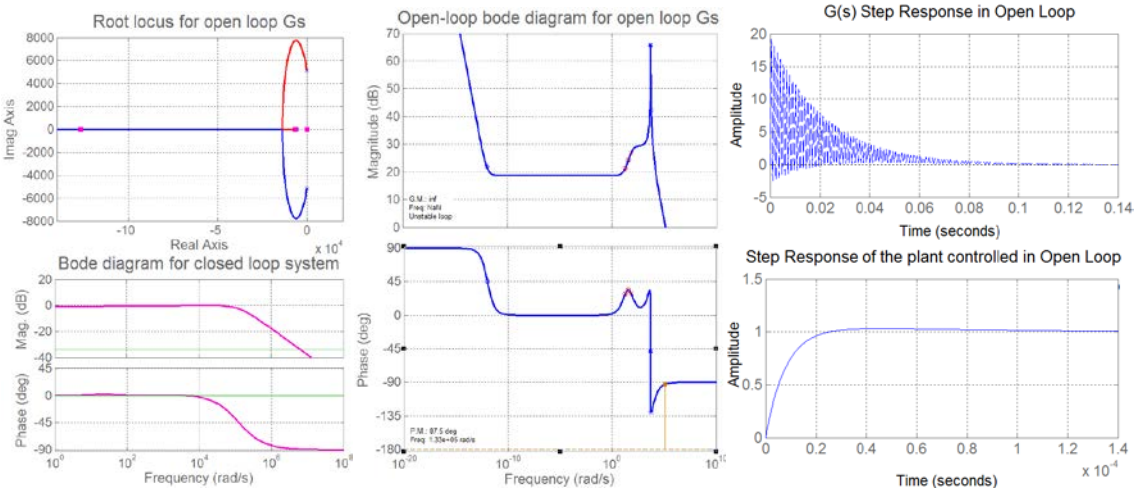

(a) Root locus for open-loop and Bode diagrams.

(b) Uncontrolled (open loop) and controlled (closed loop) G(s) step responses of plant.

Fig. 2.5. Root locus for open-loop and Bode diagrams, uncontrolled (open loop) and controlled (closed loop) G(s) step responses of plant.

2.7 EXPERIMENTAL RESULTS

2.7.1. Design considerations

The experimental network where the proposed system has been tested is a laboratory network consisting of five sources. A Nexa®1200 fuel cell, with a nominal power of 1,200W at 25ºC, with a range of voltages at its output of (20-36 V_{DC}). A Bornay 600W three-phase wind turbine without regulator, with full bridge rectifier and filter at the output, its voltage being dependent on the wind speed (5-26V), the nominal power is obtained at 11m/s, producing automatic braking at 13m/s. 8 solar panels, with a maximum nominal power of 415W per plate, which in working conditions can provide 308W with an irradiance of 800W/m^2 and an output voltage under maximum power conditions of 35.9 V.

Two groups of 600Ah and 12V batteries. For these sources, the energy management branch has been implemented. The converters for the integration of the sources in the

branch have been designed using the proposed method, this method can also be applied for higher powers and voltages, taking the precaution of adapting the semiconductors to the stress voltage of the converters.

Tables 2.2. Design data for Uc and Bc boost and parameters obtained for design, Uc and Bc boost

Table 2.2.1. Design data form Uc and Bc boost.

Source	Rated power of source	Design voltage (V_{Sn})	Design power	D_{max}
Fuel cell	1200W	28V	1600W	0.8
Solar panels	2434W	35.9V	2600W	0.8
Wind turbine	600W	16V	800W	0.8
Battery	600Ah	12V	1100W	0.8

Table 2.2.2. Parameters obtained for design, Uc and Bc boost.

$L_1, L_2\ \mu H$	$C1,\ C2\ \mu F$	Peak currents of I_{Lt1}, I_{Lt2}	P_{max} converted
18	2	46A, 108A	1729W
18	3	57.8A, 137A	2808W
10	0.7	35A, 99A	859W
9	5	97A, 150A	1192W

The DC link voltage is 500V, since two batteries are available, it is expected that both can support the system if necessary (if the rest of the sources cannot provide anything) and a design value of V_{Hn}=250V is assigned. The data calculated for the design of the converter components, necessary to integrate the different sources into the branch, are shown in Tables 2.2.

Table 2.3. Design parameters obtained for the redactor Bc.

Step-down circuit, for battery converter				
$L_4\ \mu H$	$L_3\ \mu H$	Peak current I_{L4} (A)	Dr_{max}	P_{max} converted
50	2	89A	0.1T	2238W

For the choice of diodes and transistors of the different converters, equations (37) to (41) have been used, the values of critical currents and converted powers are shown in tables 2.2 and 2.3. Each of the five converters that make up the branch, adapts the energy from a renewable source or storage system, to be able to integrate it with the other sources so that the energy produced by the sources can be used regardless of their randomness.

To justify its operation, tests have been forced to demonstrate the robustness of the system, against variations in load, as well as in generation. System management has been implemented with two S7-1500 controllers, CPU 1516F-3 PN/DP, one of them with four AI 8xU/I/RTD/TC ST analog modules, which is used only for signal capture and monitoring of the entire system. The other controller is intended for system management (not studied in this paper) with a DI 32x24VDC HF module, another DQ 32x24VDC/ 0.5A ST and two AQ 4xU/I ST analog output modules. This management system can keep track of all monitored signals. These signals have been sent to Simulink by an OPC connection executed with KEPServerEX. The samples have been taken with a maximum duty cycle of 10ms, and a minimum of 1ms. In Fig. 2.9(a), the management system is shown. In boost mode (source to load), the control consists of a single PID that sends the duty cycle signal to all drives. In buck mode (contained in battery converters) the controller is integrated into the converter's DSP. In Fig. 2.6 shows the results of a forced operation to see the behavior of the designed converters that make up the branch, also the converter waveforms in both modes are shown in Fig. 2.8.

2.7.2. Branch results.

Stage (AB), in A the connection of the converters to the sources is made, this is done without load, the current rise seen in the Fig. 2.6(b) is due to the energization of the coils and capacitors of the converters. Then, a load of 700Ω is connected and in B another of 150Ω in parallel with the previous one.

The stage (BC) extends from the connection to the disconnection of the 150Ω resistance, in it there are two sudden variations in the load (rise and fall). The values of the voltage and current in the load are V_{DC}=500V and I_{DC}=5A. If observed (Fig. 2.6(e)) the current pulses of the load are shown in a change of the load, measured in the AG, y the variation of V_{DC}, the voltage V_{DC} in the changes varies only 0.03%. Also due to the decrease in wind speed, the voltage and power produced by the wind turbine are decreasing, but this is offset by the rest of the connected sources, which increase their supplied power to meet demand. If the output voltages of the converters are observed in Fig. 2.6(c), that of the wind turbine Vo_{AG} decreases, but it is compensated by the other sources, being complied with at all times (44).

$$Vcc = Vo_{AG} + Vo_{FC} + Vo_{PV} + Vo_{B1} + Vo_{B2} = 500V \pm 1\% \quad (44)$$

In stage (CD), the wind input continues to decrease until the system disconnects the wind turbine at D. Also, before D there is a sudden rise in V_{sPV}, which lasts during stage (DF), this is accompanied by an increase in I_{sPV}. This supposes an increase in power supplied by this source, while decreasing the power supplied by the other connected sources.

In stage (GH), a sudden disconnection of the solar panels occurs, this being compensated proportionally by the other sources, the system preserving the stability of voltage and intensity in the load.

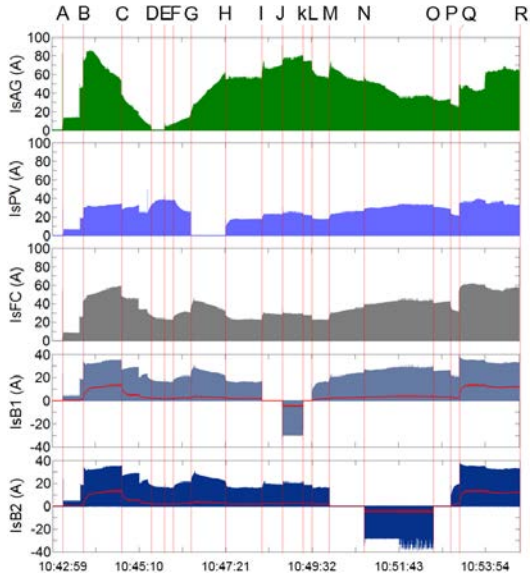

(a) Source voltages.

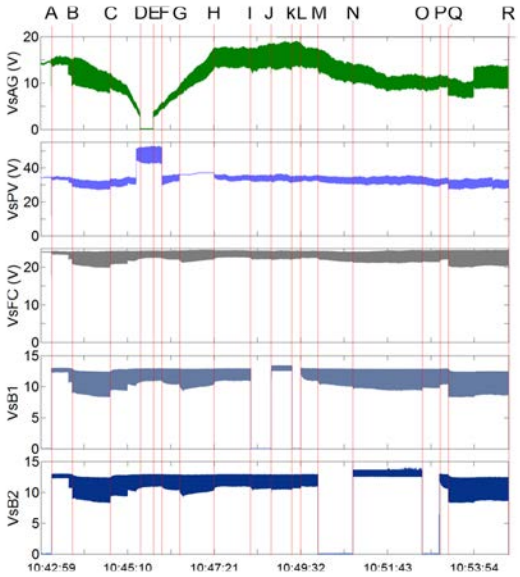

(b) Currents at the converter inputs.

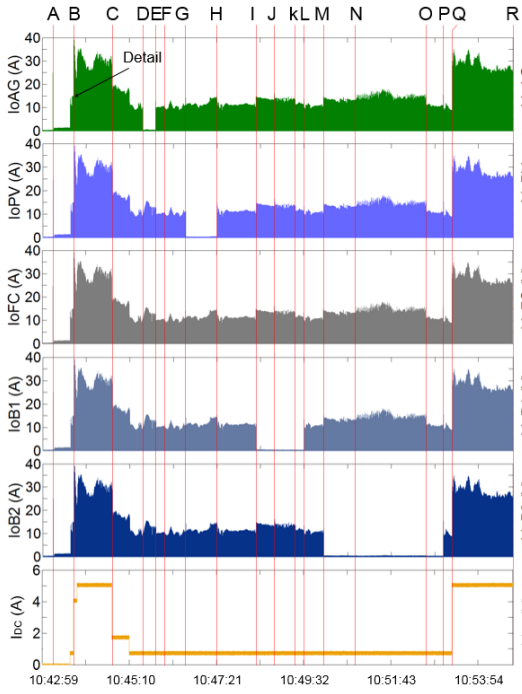

(c) Voltages at the converters output and $V_{DC\ bus.}$

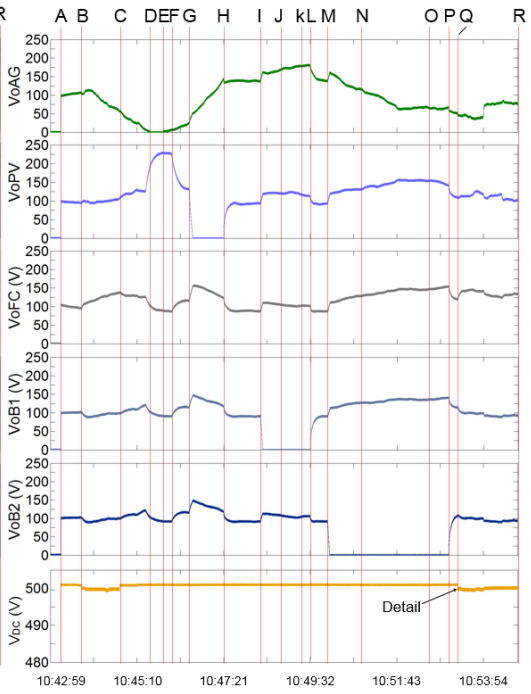

(d) Currents at the converters output and $I_{DC\ bus.}$

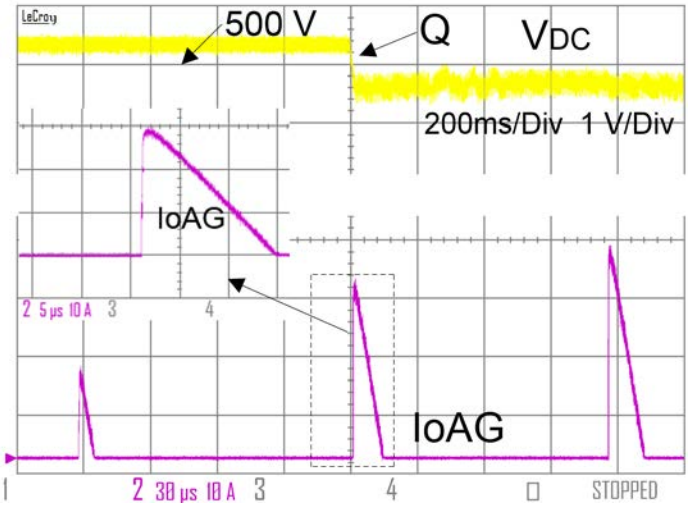

(e) Oscilloscope details.

Fig. 2.6. Experimental results.

In stage (IL) battery B_1 has been disconnected from the branch, and in stage (JK) the system is charging battery B_1, taking power from the rest of the sources, maintaining demand on the load without alterations. In Fig. 2.6(b), it can be seen how the current at the I_{sB1} has changed the direction. The same operation of disconnecting and charging the battery has been carried out on the B_2 battery in stages (MP) and (NO). Finally, the B_2 battery has been reconnected in P time and the 150Ω resistor in Q time.

As shown Fig. 2.6(a), abrupt variations (forced disconnection of converters) or natural variations (wind turbine voltage variation) have occurred at the input of the converters, but these variations are attenuated at the output of the converters. In Fig. 2.6(c), when any of the sources stops supplying or forces the disconnection of its converter, then the converters of the active sources increase their voltage, covering the deficiency of the absent source. So, the V_{DC} bus voltage is always conserved, which is indicated in the reference of the controller that manages the duty cycle of the converters, in this case 500V. This can be seen in Fig. 2.6(c). The current pulses supplied by each converter to its output capacitor C_a are the same, see Fig. 2.6(d), but the power that each converter provides to its C_a capacitor is different, since each capacitor is at a different voltage. This current becomes zero in those sources that are not providing energy to the

load, then the load current is provided by the converters of the active sources, the power supplied at each moment by each source is proportional to the output voltage of the source converter (Fig. 2.6(c)).

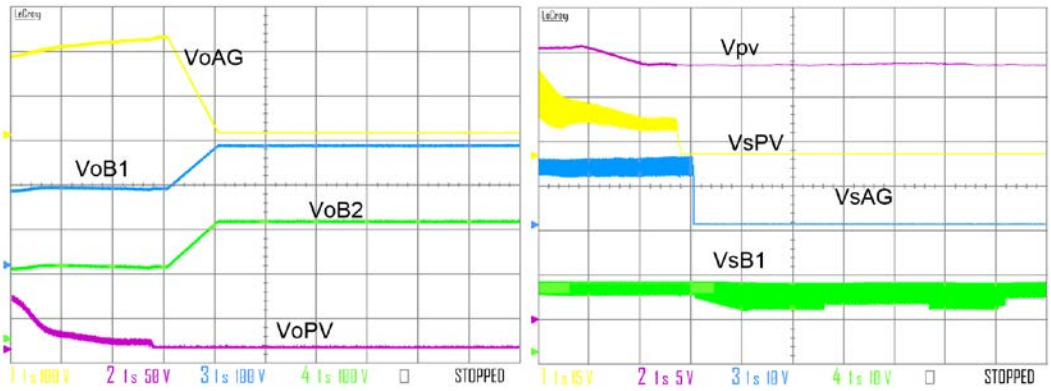

(a) Voltages at the converter inputs.

(b) Voltages at the converters outputs.

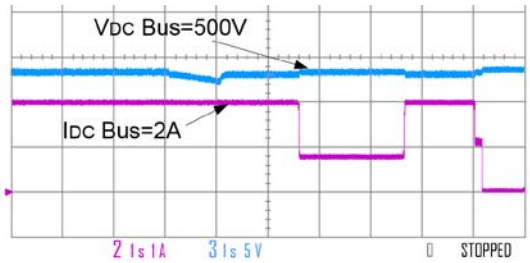

(c) Voltage and current in DC bus.

Fig. 2.7.Experimental results with elimination of sources.

In Fig. 2.7, the experimental results of the performance of the system are presented when some of its sources are eliminated (the experiment has been done with enough air but with little solar radiation), the system is initially powered with the two batteries, the wind turbine and the solar panels, being the voltages of the sources at the input of the converter respectively, V_{sB1}, V_{sB2} (in Fig. 2.7 (a), only V_{sB1} is shown), V_{sAG} and V_{sPV}.

To carry out the tests, the solar panels were first shaded and then covered. V_{sPV} is the voltage at the input of the PV converter, which depends on the charge of the capacitor C_s, placed at the input of each converter. See Fig. 2.7 (a), Due to the shading, V_{pv} (voltage at

the solar panel terminals), undergoes a variation of approximately 2.5V, so that it produces less and less current, for this reason the decrease in V_{sPV} begins, until that the disconnection of the solar panel is made and V_{sPV}=0.

If the voltage at the output of the V_{oPV} converter is observed (see Fig. 2.7 (b)), it begins to decrease (the power supplied by the PVs is decreasing, until it becomes zero), the voltage of the rest of the source is rising as V_{oPV} drops (the rest of the sources are covering the demand). Afterwards, the wind turbine is abruptly disconnected, and it is observed how the two batteries remain powered by the load, each providing approximately 250V.

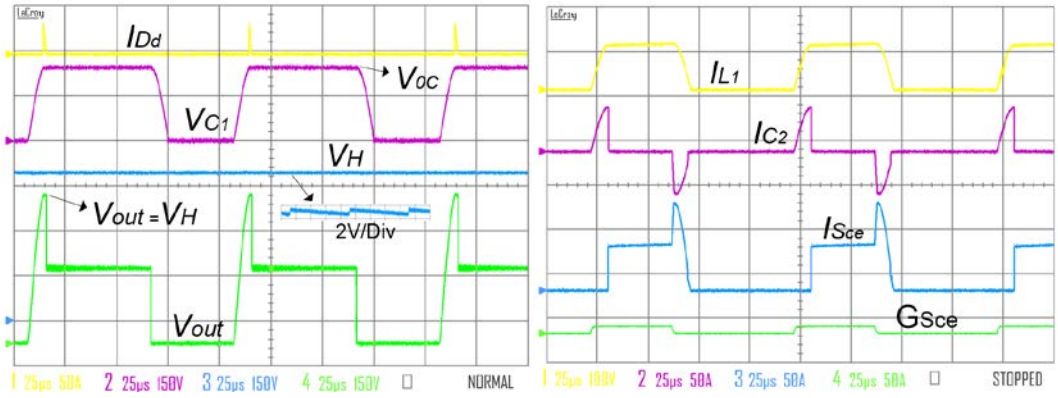

(a) Step up mode.

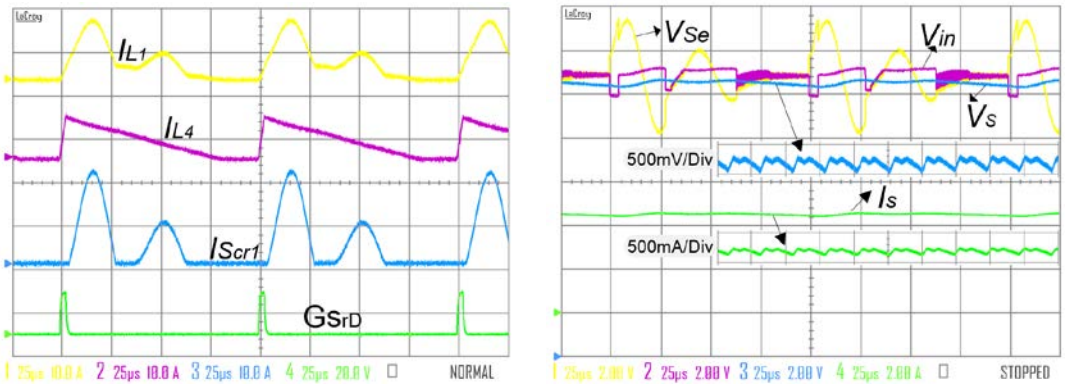

(b) Step down mode.

Fig. 2.8. Waveform in step up and step down modes.

In Fig. 2.7 (c), the value of the $V_{DC\ bus}$ voltage is shown, with a scale of 5V/Div, and it can be seen that it undergoes very few variations, there have also been sudden changes in the load (maximum power 1000W), see Fig. 2.7 (c), these affect very little V_{DC} bus, all these changes have been supported without problems by the two batteries, then in an extreme situation (where one or all the generators of the system fail), the demand can be supported by accumulators, it is also shown that sudden changes at the input of the converters are attenuated at the output of these, without affecting the load.

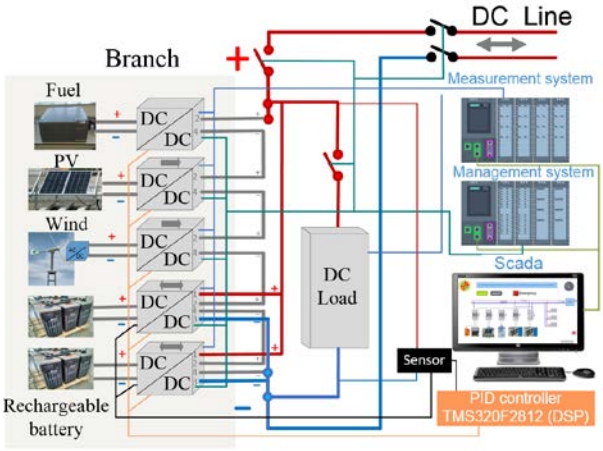

(a) Management, measurement and control system.

(b) Laboratory system.

Fig. 2.9. Management, measurement, control system and laboratory system.

2.7.3. Advantages of the proposed system compared to conventional solutions.

The advantages that the proposed converter stand out over the conventional ones are:

Its easy switching and its step-up mode gain that is linear throughout the work zone, this greatly facilitates the control of converters placed in series, these characteristics are not found in conventional converters [19].

The proposed system allows coupling sources in series by adding their voltages to the output of the converters, this means that for the same power, the currents at the input of the converters are smaller than in a traditional system, lowering costs in converters. As it is modular, it allows the DC bus voltage to be raised without the converters suffering from voltage stress problems, this is not possible in a traditional system. It also allows to couple several small sources and obtain a high output voltage and high power, with a simple control system.

The proposed system responds very well to the randomness of renewable energy resources, since the sources are in series, the voltage and power deficiencies of one or more sources can be covered by other sources or by energy storage systems. If the system is designed properly, with few accumulators we can cover the temporary deficiencies with a simple control.

2.8 CONCLUSIONS

This paper presents an innovative method of connecting power sources by using source-Z converters. This method allows you to connect several sources and accumulators in series, so that they all provide power to the same DC bus. The system eliminates the problems that arise from the randomness of renewable sources, being able to maintain the

needs of the demand without alterations. Furthermore, this can be done with a very simple control system, in this case a single PID has been used to control the five sources.

The most significant innovation is the integration of the converters in the branch (which achieves a great reduction in the control system of the converters), and the design method presented to calculate the necessary elements of each converter, depending on the conditions of the branch, the sources to be integrated and the needs of the demand. The system provides the possibility of coupling renewable and non-renewable DC sources, with different voltage and power levels, so that the system always takes the energy from the source that has it, and if any of the sources does not have capacity to provide energy, the rest cover the demand, without affecting the load. The system also allows the storage of surplus energy in batteries by means of the designed converters.

2.9 REFERENCES

[1]S.B. Siad, A. Malkawi, G. Damm, L. Lopes, L.G. Dol, Nonlinear control of a DC MicroGrid for the integration of distributed generation based on different time scales, Int. J. Electr. Power Energy Syst. 111 (2019) 93–100. https://doi.org/10.1016/j.ijepes.2019.03.073.

[2]M.V. Ortega, F. Jurado, M. Ortega, D. Vera, Current control in high-efficiency unidirectional converter for fuel cell, Int. J. Electron. 106 (2019) 1101–1112. https://doi.org/10.1080/00207217.2019.1582708.

[3]E.S. Roudbari, M.T.H. Beheshti, S.M. Rakhtala, Voltage and frequency regulation in an islanded microgrid with PEM fuel cell based on a fuzzy logic voltage control and adaptive droop control, IET Power Electron. 13 (2020) 78–85. https://doi.org/10.1049/iet-pel.2019.0592.

[4]Y. Zhang, C. Fu, M. Sumner, P. Wang, A Wide Input-Voltage Range Quasi-Z-Source Boost DC-DC Converter with High-Voltage Gain for Fuel Cell Vehicles, IEEE Trans. Ind. Electron. 65 (2018) 5201–5212. https://doi.org/10.1109/TIE.2017.2745449.

[5]S.K. Kuncham, K. Annamalai, S. Nallamothu, Single-Phase Two-Stage Seven-Level Power Conditioner for Photovoltaic Power Generation System, IEEE J. Emerg. Sel. Top. Power Electron. 8 (2020) 794–804. https://doi.org/10.1109/JESTPE.2019.2913216.

[6]D. Sun, B. Ge, D. Bi, F.Z. Peng, Analysis and control of quasi-Z source inverter with battery for grid-connected PV system, Int. J. Electr. Power Energy Syst. 46 (2013) 234–240. https://doi.org/10.1016/j.ijepes.2012.10.008.

[7]R. Soares, N. Djekanovic, O. Wallmark, P.C. Loh, Integration of Magnified Alternating Current in Battery Fast Chargers Based on DC-DC Converters Using Transformerless Resonant Filter Design, IEEE Trans. Transp. Electrif. 5 (2019) 925–933. https://doi.org/10.1109/TTE.2019.2920328.

[8]C. Bai, B. Han, B.H. Kwon, M. Kim, Highly Efficient Bidirectional Series-Resonant DC/DC Converter over Wide Range of Battery Voltages, IEEE Trans. Power Electron. 35 (2020) 3636–3650. https://doi.org/10.1109/TPEL.2019.2933408.

[9]F. Shi, D. Song, A novel high-efficiency double-input bidirectional DC/DC converter for battery cell-voltage equalizer with flyback transformer, Electron. 8 (2019). https://doi.org/10.3390/electronics8121426.

[10] J. Ke, Z. Zhengxuan, Z. Qijuan, Y. Zhe, B. Tianshu, Islanding detection method of multi-port photovoltaic DC micro grid based on harmonic impedance measurement, IET Renew. Power Gener. 13 (2019) 2604–2611. https://doi.org/10.1049/iet-rpg.2019.0271.

[11] M. Ortega, F. Jurado, M. Valverde, Novel topology for DC/DC unidirectional converter for fuel cell, IET Power Electron. 7 (2014) 681–691. https://doi.org/10.1049/iet-pel.2013.0142.

[12] M. Ortega, M.V. Ortega, F. Jurado, J. Carpio, D. Vera, Bidirectional DC–DC converter with high gain based on impedance source, IET Power Electron. 12 (2019) 2069–2078. https://doi.org/10.1049/iet-pel.2018.5385.

[13] Q. Wu, Q. Wang, J. Xu, H. Li, L. Xiao, A high-efficiency step-up current-fed push-pull quasi-resonant converter with fewer components for fuel cell application, IEEE Trans. Ind. Electron. 64 (2017) 6639–6648. https://doi.org/10.1109/TIE.2016.2638800.

[14] J. Kan, S. Xie, Y. Tang, Y. Wu, Voltage-Fed Dual Active Bridge Bidirectional, IEEE Trans. Power Electron. 29 (2014) 3582–3590.

[15] M. Nymand, M.A.E. Andersen, High-Efficiency Isolated Boost DC – DC Converter for, Ieee Trans. Ind. Electron. 57 (2010) 505–514.

[16] A.A. Abduallah, M. Meraj, M. Al-Hitmi, A. Iqbal, Space vector pulse width modulation control techniques for a five-phase quasi-impedance source inverter, IET Electr. Power Appl. 12 (2018) 379–387. https://doi.org/10.1049/iet-epa.2017.0340.

[17] T. Liang, S. Member, J. Lee, Novel High-Conversion-Ratio High-Efficiency Isolated Bidirectional DC – DC Converter, IEEE Trans. Ind. Electron. 62 (2015) 4492–4503.

[18] F.Z. Peng, S. Member, Z-Source Inverter, IEEE Trans. Ind. Appl. 39 (2003) 504–510.

[19] W.R. Evs, Q. Liu, J. Li, M. Sumner, S. Member, A.Z. Abstract, A Common Ground Switched-Quasi- Z -Source Bidirectional DC – DC Converter With, IEEE Trans. Ind. Electron. 65 (2018) 5188–5200.

[20] X. Zhu, B. Zhang, D. Qiu, Enhanced boost quasi-Z-source inverters with active switched-inductor boost network, IET Power Electron. 11 (2018) 1–14. https://doi.org/10.1049/iet-pel.2017.0844.

[21] S. Sonar, T. Maity, M. Minu, Single phase transformerless wide range ac boost voltage regulator based on z-source network, Int. J. Electr. Power Energy Syst. 47 (2013) 193–197. https://doi.org/10.1016/j.ijepes.2012.10.065.

[22] A.R. Dehghanzadeh, V. Behjat, M.R. Banaei, Double input Z-source inverter applicable in dual-star PMSG based wind turbine, Int. J. Electr. Power Energy Syst. 82 (2016) 49–57. https://doi.org/10.1016/j.ijepes.2016.02.017.

[23] C.N. Papadimitriou, E.I. Zountouridou, N.D. Hatziargyriou, Review of hierarchical control in DC microgrids, Electr. Power Syst. Res. 122 (2015) 159–167. https://doi.org/10.1016/j.epsr.2015.01.006.

[24] A. Frances, R. Asensi, O. Garcia, R. Prieto, J. Uceda, Modeling electronic power converters in smart dc microgrids - An overview, IEEE Trans. Smart Grid. 9 (2018) 6274–6287. https://doi.org/10.1109/TSG.2017.2707345.

[25] Y. Liu, H. Abu-Rub, B. Ge, Front-End Isolated Quasi-Z-Source DC-DC Converter Modules in Series for High-Power Photovoltaic Systems-Part I: Configuration, Operation, and Evaluation, IEEE Trans. Ind. Electron. 64 (2017) 347–358. https://doi.org/10.1109/TIE.2016.2598673.

CAPÍTULO III. Design of an energy management system applied to an electric power plant based on a biomass gasifier

(Publicado en Renewable Energy, Volumen 216, Noviembre de 2023, DOI:10.1016/j.renene.2023.119116)

ÍNDICE CAPÍTULO III:

CAPÍTULO III. Design of an energy management system applied to an electric power plant based on a biomass gasifier 93

3.1. INTRODUCTION 99

3.2. PROBLEM STATEMENT, PROPOSED SOLUTION AND BUILDING OF THE MANAGEMENT SYSTEM 103

3.2.1. Converters operations Problem statement and proposed solution .. 103

3.2.2. Environmental and economic benefits of the system 106

3.2.3. Choosing the right type of converter 106

3.3. The converters 107

3.3.1 Converter requirements 107

3.3.2 Converters Operations 108

3.3.3 Criteria for energy management and system operation 112

3.3.4 Constraints and design considerations for converters 114

3.4. Experimental applications and results 119

3.4.1 Measurements of used syngas 119

3.4.2 Results of the proposed management system 121

3.4.3 System response to disturbances 124

3.5. CONCLUSIONS 128

3.6. ACKNOWLEDGEMENTS 129

3.7. REFERENCES 130

TABLA DE FIGURAS CAPÍTULO III:

Fig. 3.1.(a) Schematic of the gasification plant and its components. 104
Fig. 3.2. Classic GEG system coupled to an AC grid, GEG system proposed to work isolated and connected to a weak DC grid. 106
Fig. 3.3. Power circuit of the converters. 110
Fig. 3.4. Switching and operations in all modes..... 111
Fig. 3.5. Process flowcharts..... 114
Fig. 3.6. Power charts for design. 118
Fig. 3.7. Gasification plant installed in IFAPA oil mill and Product gas composition in test number 3. 121
Fig. 3.8. Response due to increased load, supply with batteries, load increase detail and load decrease..... 125
Fig. 3.9. Management, measurement, control system and laboratory system. 128

TABLA DE TABLAS CAPÍTULO III:

Table 3.1. Components status in the converters. 112
Table 3.2. Voltage ranges and operating modes of the converters..... 115
Table 3.3. Product gas composition and efficiency parameters of the gasification plant. 120
Table 3.4. Design data for converters..... 122

Design of an energy management system applied to an electric power plant based on a biomass gasifier

Abstract: Biomass gasification plants for electricity generation are an environmentally friendly technology. One of their main problems is their poor responsiveness to load variations when the plant operates off-grid. For this reason, they are usually grid-connected systems.

Therefore, as a solution, an energy management system that allows the plant to operate off-grid is proposed. The system has been obtained through the optimal design of unidirectional and bidirectional Z-source converters and their coupling with their series outputs. This approach has been applied to a biomass gasification power plant.

To validate the system, the results of an experimental 10kW gasification plant are presented. With the plant working off-grid, there is a sudden load increase of 2.5kW, and due to the proposed system performance, there is only an output voltage oscillation of less than 1%, preserving a stable power supply.

This proposed system allows the plant to work isolated or coupled to a weak micro-grid of renewable energies. Obtaining a permanent supply of quality and also improving its efficiency. Thus, the gasification technology can be used for electricity generation in isolated areas of many developing countries, where the electrical grid is not totally developed, but there are available biomass sources.

Keywords: Energy management, Biomass gasification, Z-source converter, Renewable energy sources, DC/DC converter.

Nomenclature

Bc	DC Bidirectional converter
C	Capacitance of each z-source capacitor
$C_1=C_2=C$	Capacitance of the Z-source capacitors.
D	Duty cycle
DC	Direct current
D_e	Step-up duty cycle
d1 y d2	Directions of converters operation one and two
D_{eB}	Step-up duty cycle of the battery converters
D_{eG}	Step-up duty cycle of the EG converter
D_r	Step-down duty cycle
D_{rG}	Step-down duty cycle of the EG converter
D_{r1}	Step-down duty cycle in directions one
EG	Engine-generator
EMS	Energy management system
f_c	Switching frequency
GEG	Gasifier-engine-generator
$I_{L(t1)}$	Current through inductors L_1 and L_2 at time t_1
$(I_{Lmax})_{t_2}$	Maximum current through inductors L_1 and L_2 at time t_2
L	Inductance of each z-source inductor
$L_1=L_2=L$	Inductance of the Z-source inductors.
LHV	Lower heating value

Uc	DC Unidirectional converter
V_B	Battery voltage
V_{CC}	DC bus voltage
$V_{CC\text{-}ref}$	Reference voltage of DC bus voltage
V_{Hn}	Output voltage of the nth converter at the coupling
V_{out}	Converter output voltage
V_{outB}	Battery converter output voltage
V_{outG}	EG converter output voltage
V_{ref}	Reference voltage of V_{outG}
V_s	Converter input voltages working at d1

3.1. INTRODUCTION

Biomass gasification has recently increased attention to foster the circular economy concept by closing the loop of many agri-food industries (e.g. olive oil production) through combined heat and power (CHP) generation in a decentralized manner. On a large scale, it could replace coal-fired power plants [1]. Gasification is slightly less efficient than combustion, since it can achieve conversion efficiencies up to 85%; however, it has a greater potential since it allows the use of biomass sources with relative high ash and moisture content (e.g. up to 60% and 25%, respectively, in updraft reactors). In addition, this thermochemical process has lower CO_2, particles matter and NOx emissions [2], due to the reaction temperature is lower than the combustion temperature [3].

Gasification is a thermo-chemical conversion process where a solid fuel is transformed into a gaseous fuel composed mainly of H_2, CO, CH_4, H_2O, N_2 and CO_2 called product gas or synthesis gas (syngas). This renewable gas can be used for both electric and thermal energy production. Most of the works in the literature review about biomass gasification plants are focused on the production of electrical and thermal energy or biofuels such as ammonia [4], also cogeneration systems consisting of a gasifier and a Rankine organic cycle generator [5].

-Biomass gasification for decentralized power generation:

The use of air as gasification agent is usually preferred over oxygen or steam. Even though gasification with pure oxygen avoids nitrogen dilution, which allows obtaining a synthesis gas with a higher energy density [3], an air separation unit is typically not considered for small-scale CHP plants, because the excessively high capital and operational costs do not compensate for any improvement achieved [3]. After a cleaning and cooling phase, the producer gas, can be used as a suitable fuel for decentralised electricity and/or heat production using internal combustion engines, gas turbines or even fuel cells [6]. However, internal combustion engines are nowadays the most usual option for small-scale biomass gasification CHP plants, due to their numerous advantages, such as low capital

cost, modularity, efficiency [7]. Among the existing designs for gasification reactors, downdraft gasifiers are possibly the best choice for small-scale distributed generation systems (< $1MW_{th}$) CHP plants [8]. The downdraft reactors are characterized by a relatively simple construction, low investment costs, reliable operation and applicability to numerous biomass feedstocks with sufficient carbon conversion efficiency [9]. The producer gas from in air-blown downdraft reactors has a relatively low energy density (LHV=4–6 MJ/Nm^3) as a result of the nitrogen dilution effect [10].

-Biomass gasification for off-grid electrification:

Concerning the application of biomass gasification technology in decentralized power generation, some authors studied its potential benefits and implications for off-grid power supply systems in remote areas. An evaluation of off-grid gasification power supply for eastern Nigeria was carried out in [11], the gasifier was fuelled with rice husk. The gasification system was designed and sized based on the mass flow rate of producer gas required to feed the gas engine at full load; however, it was not experimentally tested. In [12] the authors compare different renewable energy generation solutions for rural electrification of isolated communities in the Amazon region, including run-of-the-river and hydrokynetic, biomass (direct combustion or gasification), bio-fuels, vegetable oils and also hybrid (solar-wind-diesel). The gasifier was fed with the açaí (an Amazonian fruit) kernel, In addition, this work also included the implementation of a 12 km mini-grid. The demonstration plant had an output of 80kW. In all scenarios, gasification proved to be a more convenient option than direct burning of the waste. Waste gasification based off-grid electricity generation in developing countries like Pakistan was investigated in [13], utilizing mixed biomass composts. Although the estimated electricity price was higher in all studied scenarios as compared to average governmental electricity tariff, a large potential of gasification for off-grid electricity generation was reported. In [14] conducted an economic analysis on utilization of rice residues for decentralized electricity generation in Ghana. They found that husk gasification mini-grids can be a suitable electrification

solution, as their cost was lower than the average cost for grid extension of diesel mini-grids and off-grid solar systems in remote communities of Ghana. Finally [15] presented a financial viability model for biomass gasifier power projects to improve access to electricity in India and other developing countries. They concluded that large-scale deployment of rural electrification requires minimisation of maintenance requirements for biomass gasification systems, especially with regard to gas cleaning y capability of multi-fuel use of the gasification system without compromising gas quality. The few studies presented in the literature on off-grid electrification using gasification technology show a lack in the state of the art focusing on system operation under variable load changes. A quality electricity supply needs to track the load well therefore, this is a constraint that the gasification plant needs to cover during its continuous operation.

It is important to highlight the most of the works presented in the literature are focused on grid-connected systems. However, the state of the art based on gasification plants in off-grid applications is still in an incipient stage. Here, the main focus of the studies presented are based on economic studies [14] and grid-connected gasification plant with other renewable energy sources [12]. In parallel, some works have been carried out on gasification plants for autonomous electricity supply, such as the sizing of batteries integrated with a biomass gasifier [2]. Due to the inertia of the chemical reactions involved in the gasification process, the response of the gasifier-engine-generator (GEG) group to load variations is slow.

-Power converters and renewable energies:

Renewable energy sources are being used more and more frequently throughout the world. Many of them produce direct current (DC) [16], but a direct coupling with alternating current (AC) grids is not possible, as is the case with photovoltaic systems [17], where multilevel inverters are used for their AC grid coupling [18] o fuel cells [19], which require converters with high voltage gain [20]. When there

is surplus DC power, it can be stored in batteries or supercapacitors for later use [21], for which voltage equalisation circuits can be used [22]. DC power management needs DC converters [23]. Unidirectional DC converters (Uc) converts power in one direction only [24] in step-up and step-down modes [20], soft switching techniques are used to achieve high efficiencies [25]. If is necessary to transfer energy in two directions, then bidirectional DC converters (Bc) are used [26]. There are many converter topologies that can be employed, among them are: current-fed DC converters [27], voltage-fed DC converters [28], which usually use high frequency transformer [29]. Moreover, both techniques have been integrated into a unidirectional DC converter improving its efficiency [30], In addition, high efficiency has been achieved by interleaving the primary and secondary windings of the high-frequency transformer [25]. Another remarkable topology is the quasi-Z-source derived from the Z-source, both converters are similar although each one has its peculiarities, nonetheless their switching techniques are also compatible with most of the inverters [31], where Z-source adjusts the voltage level on the DC link of the inverter [32]. Among their most significant characteristics, it is worth mentioning that they are converters with a very fast response. But in addition, the Z-source presents an almost linear response in most of its duty cycle. This feature greatly facilitates its control [33] and due to its dynamic behaviour improves the coupling of renewable energy sources [34].

Taking into account the situation of biomass gasification for off-grid electrification, the aim of this article is the study and implementation of an energy management system (EMS) based on Z-source converters, this system allows the GEG to work in stand-alone mode or in other occasions coupled to the grid. Thus, the GEG can withstand wide load variations while preserving a quality supply without significant disturbances, taking advantage of all the energy generated. It also prevents disturbances due to gas quality from reaching the load.

3.2. PROBLEM STATEMENT, PROPOSED SOLUTION AND BUILDING OF THE MANAGEMENT SYSTEM

3.2.1. Converters operations Problem statement and proposed solution

The GEG plant used consists of a downdraft-type fixed-bed reactor, a product gas cooling and cleaning system, as well as a gas engine-based power generation unit. Fig. 3.1(a) shows a general scheme of the plant and its component elements. The gasification process is represented by the equation(1).

$$CH_aO_bN_cS_d\ ashes + wH_2O + \dot{m}(O_2 + 3.76N_2) \rightarrow y_1H_2 + y_2CO + y_3CH_4 + y_4CO_2 + y_5N_2 + y_6H_2O + coal + ashes + impurities(dust, tar) \quad (1)$$

The first term has to do with the biomass chemical formula based on elemental analysis (CHNS); the second and third terms represent the biomass moisture content and the air introduced into gasification process, respectively; a, b, c and d are the numbers of the hydrogen, oxygen, nitrogen and sulphur atoms; the values (y1-y6) show the composition of product gas, which depends on the used fuel (moisture, ash, LVH and particle size).

The product gas contains impurities (particles, dust, etc.) and tar (liquid particles of compounds C_xH_y). Under these conditions, this gas is not suitable for use in internal combustion engines, therefore it must be cooled and cleaned. Finally, the gas obtained is poor and the process has a high chemical inertia. This fact causes drawbacks in the electrical supply.

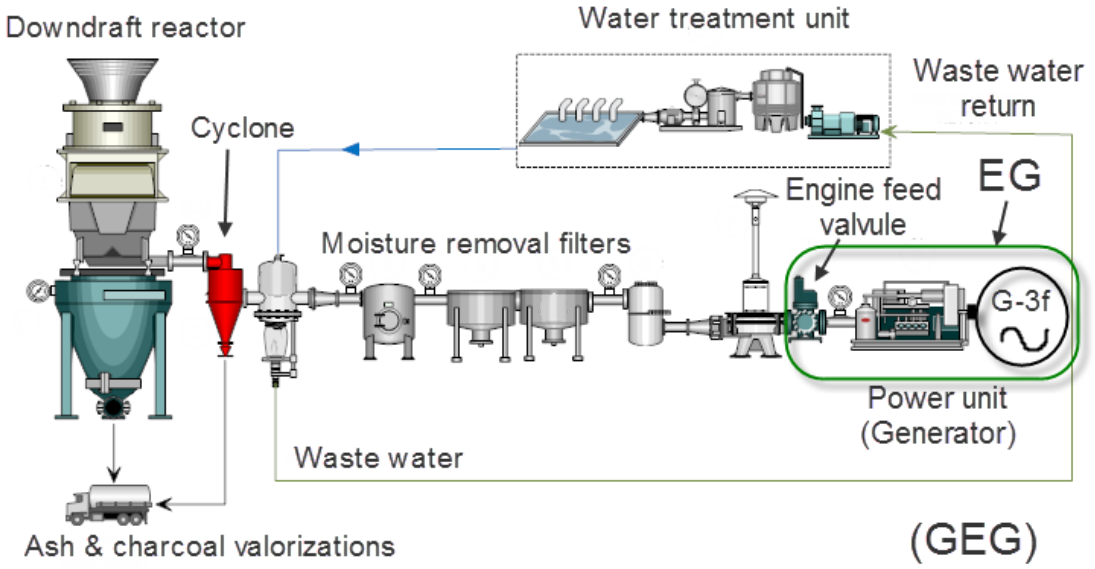

Fig. 3.1.(a) Schematic of the gasification plant and its components.

The engine-generator (EG) group is fed by synthesis gas, in our case, from the gasification of exhausted olive pomace pellets. The gas composition is shown in table 3.3. Since it is a gas with lower LHV, the inherent drawbacks to these systems occurs due to the high inertia of the gasification reactions. Consequently, the majority of these power plants are grid-connected systems, as shown in Fig. 3.2(a). However, if these systems are used in isolation, the following problems may occur: the GEG cannot adapt to changes in the demanded load quickly enough and neither can it supply loads of approximately less than 30% of the rated power of the GEG.

The GEG generates AC current and when is coupled to a powerful power grid, it has no problem, since the load variations are supported by the power grid. But if the GEG is coupled to a weak power grid, such as a small renewable energy grid, then the load variations have to be shared between the grid and the GEG. Therefore, this can cause a poor supply and these problems are further aggravated when the GEG is operating in isolation. Then it needs help from outside to maintain a quality supply when load variations occur. The problem is aggravated if there is a sudden elevation, especially when the GEG is intended for off-grid operation.

In this work, an energy management system based on Z-source converters and batteries is proposed, which allows the GEG group to operate off-grid or coupled to an isolated DC renewable energy grid, getting a quality supply even with sudden load increases, see Fig. 3.2(b). The solution to this problem requires designing the appropriate converters as well as their integration with the GEG, in order to properly assist it.

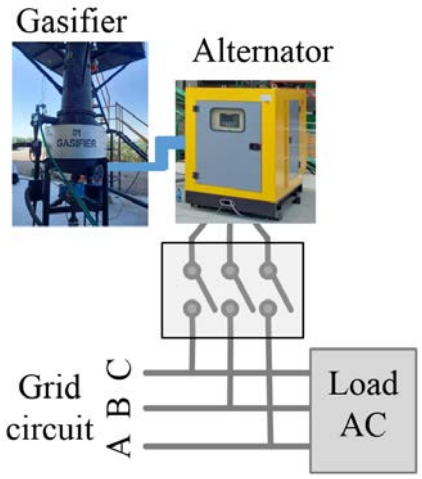

(a) Classic GEG system coupled to an AC grid.

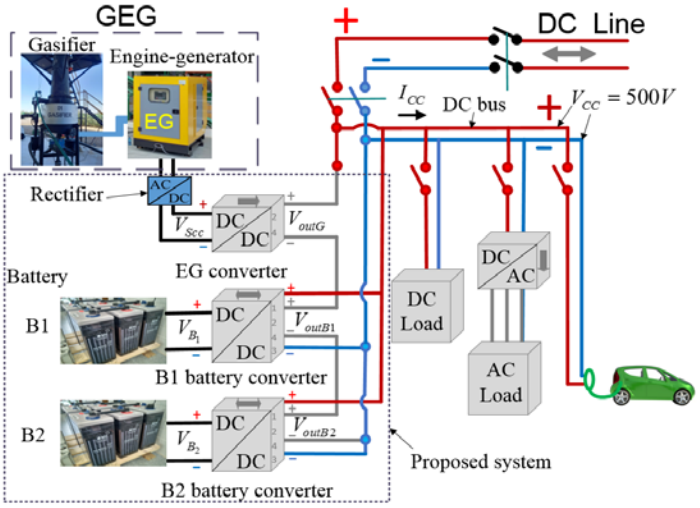

(b). GEG system proposed to work isolated and connected to a weak DC grid.

Fig. 3.2. Classic GEG system coupled to an AC grid, GEG system proposed to work isolated and connected to a weak DC grid.

3.2.2. Environmental and economic benefits of the system

The biomass gasification technology generates several environmental and economic benefits, especially in the agri-food sectors. It reduces sulphur and other particulate emissions, reduces CO, HC and NO_X emissions and does not contribute to the greenhouse effect, as it has a CO_2 neutral cycle. The use of agricultural and forestry residues for gasification avoids burning them and reduces the risk of fires. In terms of economic benefits, electric energy is produced with own resources that can be decoupled from the price fluctuation of imported fuels, as well as turning biomass into a source of employment, especially in rural areas [3] .

An example of the environmental impact study of the biomass gasification technology is presented in [35]. This study presented a gasification plant for the generation of renewable electricity and heat and fuelled with olive residues (taking the kg of olive oil as the functional unit). In terms of functional unit (1kg of olive oil produced), the plant generates 0.88kWh of renewable electricity per kg of olive oil and enough heat for the agri-food industry necessities. As a result, the gasification plant contributes to reducing the normalized environmental impact of olive oil production by 8.25%.

In terms of the climate change indicator (CO_2 emissions), the environmental impact of the functional unit is reduced from 2.21 to 1.74kg CO_2 eq. (-21%).

3.2.3. Choosing the right type of converter

The correct choice and design of a converter type is essential to achieve the pursued objectives, further the converters must be integrated into the proposed system. There are several different topologies of DC/DC converters. Among the classic ones, the following

topologies stand out: voltage source converters would not be suitable, due to the wide regulation range required for this application, current source converters are more limited than other topologies in voltage gain and converted power. Moreover, the interleaved buck-boost converter improves the power density but its output voltage is inverted, this property is not compatible with the desired solution. In addition, the cuk-derived and zeta-derived converters are not bidirectional [36]. The Z-source and qZ-source converters offer high voltage gain, they support a wide output voltage regulation and can be built as bidirectional using few components. Both would be good candidates. Their most significant differences are: the voltage stress suffered by the Z-source converter components is twice that suffered by the qZ-source ones [26], the voltage gain of the Z-source converter, which is somewhat higher than that of the qZ-source one. However, the Z-source converter presents a nearly linear voltage response against duty cycle variations (this greatly simplifies the control), besides it has a more symmetrical structure that facilitates the integration of the converters in the system. All the converters used have to be expressly designed for the desired objective.

3.3. The converters

3.3.1 Converter requirements

The design of each converter must take into account the restrictions to which it is subjected, as well as the coupling with the rest of the system elements, the most severe restrictions are imposed by the battery converters, which have to be bi-directional.

The **Unidirectional converter (Uc),** used for engine-generator**,** with step-up and step-down modes is shown in Fig. 3.3(a) and both operation modes are in one direction only. This converter is designed to convert power from V_{Scc} to V_{outG}, see Figs. 3.2(b) and 3.3(a). V_{outG} will be set by its reference value V_{ref}, V_{outG} can be higher or lower than V_{Scc}.

In additions, with this converter, the ripple of V_{outG} is much lower than that of V_{Scc}, so that the ripple reaches the DC bus very attenuated.

Owing to load variations or gasifier mismatches (type of fuel, fuel humidity, etc.), V_{Scc} may change. The following situations are possible: $V_{Scc} < V_{CC}$ or $V_{Scc} > V_{CC}$. This fact restricts the type of converter to be used. Moreover, the condition $V_{outG} = V_{CC}$ is verified in steady state. Considering this restrictions and the working values of V_{CC} and V_{Scc}, the EG converter must be designed with step-up and step-down modes, but with small gains, since the differences between V_{CC} and V_{Scc} cannot be very large.

The **bidirectional converter (Bc),** used for batteries**,** with step-up and step-down modes is shown in Fig. 3.3(b). The converter has three modes of operation and can converts power in two directions. In our configuration, two converters of this type are used (one in each battery). When the EG cannot keep V_{CC} close to $V_{CC\text{-}ref}$, then these converters (using power from their corresponding batteries) achieve that $V_{CC} = V_{CC\text{-}red}$.

Furthermore, these converters charging their batteries with EG energy, and when the demanded power is small, they can supply the load by themselves, keeping V_{CC} close to $V_{CC\text{-}ref}$. In order to meet the requirements, the converters are forced to have the following characteristics: high step-up gain and output voltages V_{outB} need to have a wide variation range starting from zero volts.

3.3.2 Converters Operations

The converters used that meet the imposed restrictions are shown in Fig. 3.3. The Z-source is composed of two inductors and two capacitors that satisfy $L_1 = L_2 = L$ and $C_1 = C_2 = C$.

-**The EG group** requires an Uc (EG converter). This converter is designed to allows the coupling between the EG and the EMS, as it is shown in Fig. 3.3(a), only an operation direction is used, direction one (d1), that converts power from V_{Scc} to V_{outG} and has been designed with step-up and step-down modes, both with moderate gain values. When $V_{Scc}<V_{CC}$ the step-up mode is applied, but if $V_{Scc}>V_{CC}$ the step-down mode is used.

The *Step-up mode* is achieved by acting on the components (see table 3.1), S_{ce} is active throughout the switching period (T), the step-up duty cycle D_{eG} acts on S_e. Subsequently the Z-source starts an automatic process shown in Fig. 3.4(a), based on the indicated switching, this process obtains $V_{outG}>V_{Scc}$ at the converter output terminals.

The *Step-Down* mode is used when $V_{Scc}>V_{CC}$. In this mode, the components operate as shown in table 3.1, S_e is switched off throughout the whole period and the step-down duty cycle D_{rG} acts on S_{ce}. Then the Z-source operates as shown Fig. 3.4(b). The voltage V_{outG} can change between zero and its maximum value V_{Scc}.

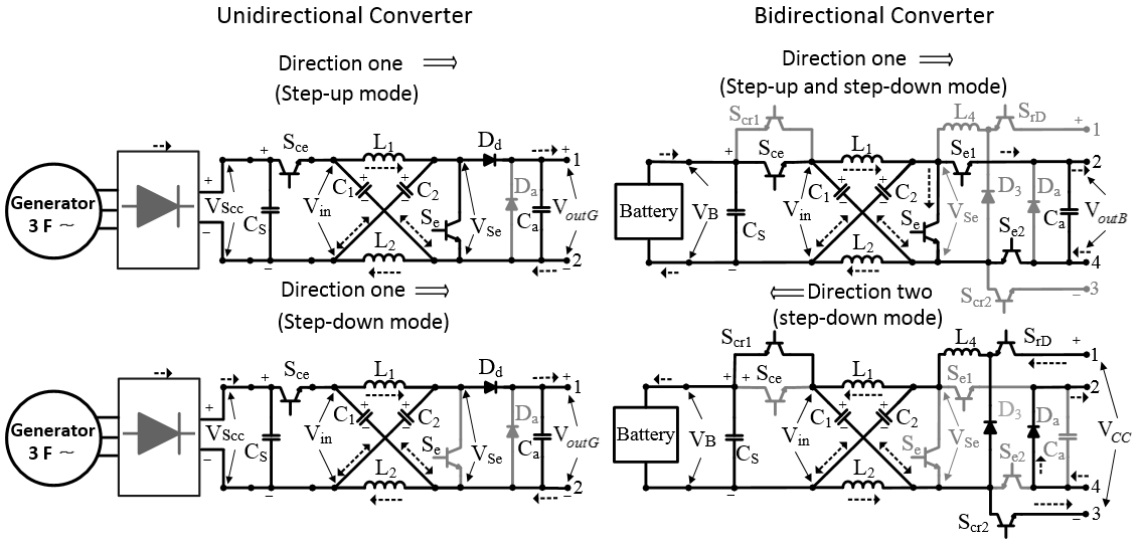

(a). Unidirectional converter.

(b). Bidirectional converter.

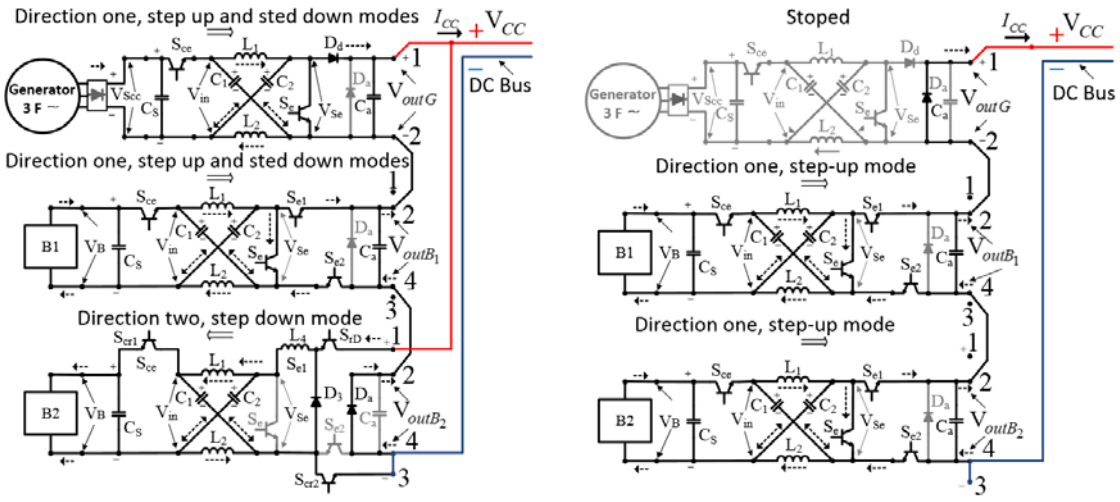

(c). B1 helping and B2 charging.

(d). B1 and B2 powering the load.

Fig. 3.3. Power circuit of the converters.

-**The batteries** need a Bc with two operating directions (battery converter), see Figs. 3.3(b). In d1, it converts energy from the batteries to the DC bus. This process occurs if the EG needs help from the batteries to power the load. The battery conveters works in direction two (d2) when there is surplus energy in EG and it is stored in the batteries. Table 3.1 shows the components status of the whole process.

-*The direction one* has two operation modes, the step-down is used when V_{CC_ref} -V_{outG} <V_B is verified. Therefore, the converter contribution to V_{cc} is lower than V_B (battery voltage). This situation arises with a small load increase. In this directions, the switching and operation of the Z-source is similar to that of the EG converter shown in Fig. 3.4(b). The Step-up mode is necessary when V_{CC_ref} -V_{outG} ≥ V_B and its voltage contribution is higher than V_B. Consequetly, in d1 the converters are designed with a large step-up duty cycle D_{eB} and a wide regulation range. Fig. 3.4 (c) shows the switching and operation of the battery converters in this mode.

-*The direction two* has only one working mode, which charges the batteries with surplus energy from the EG. This mode must be designed with a great step-down gain,

since the anergy conversion is made between two very different voltage levels (V_{cc} and V_B). In this mode and direction the Z- source operation is shown in Fig 3.4(d).

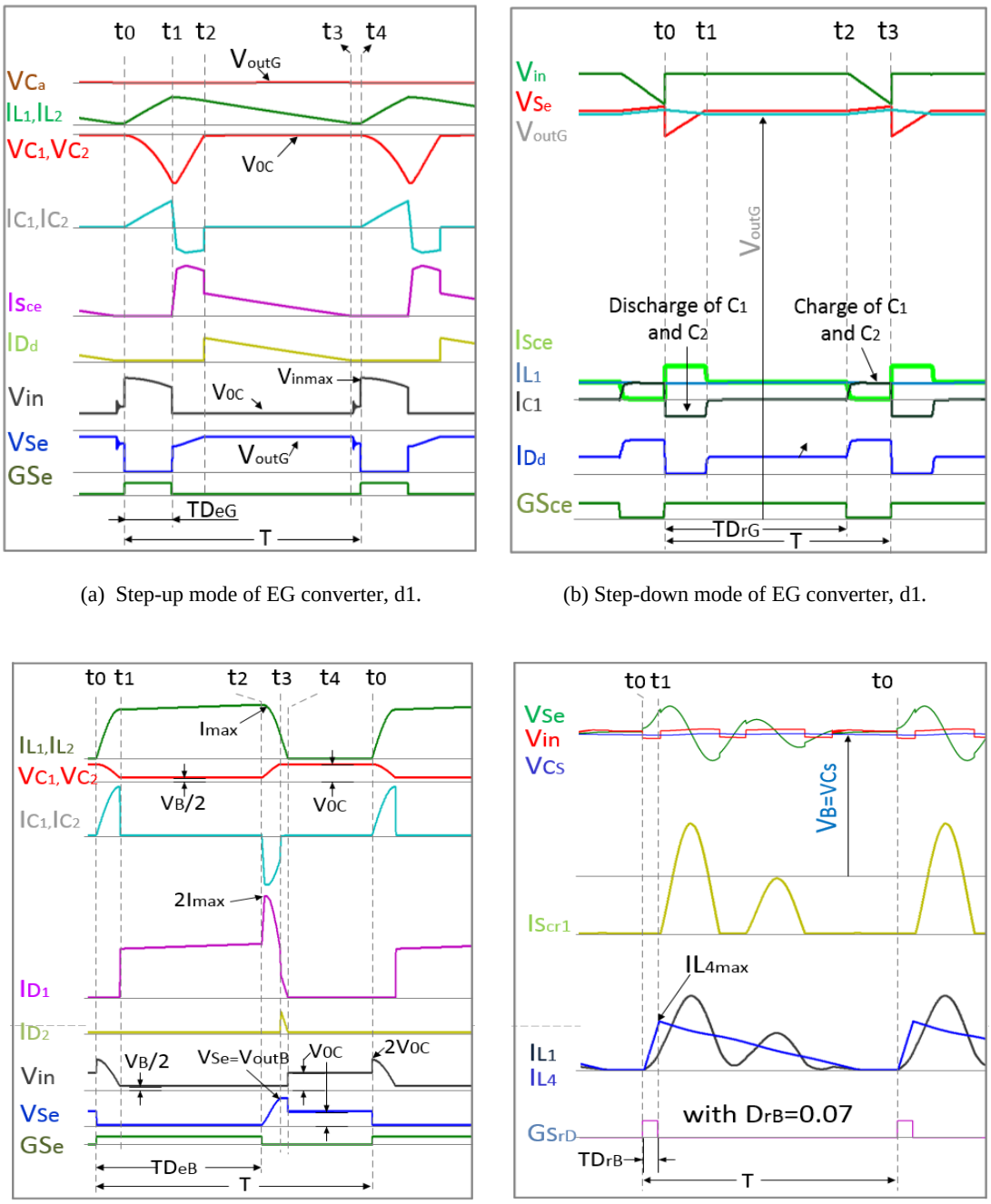

(a) Step-up mode of EG converter, d1.

(b) Step-down mode of EG converter, d1.

(c) Step-up mode of battery converter, d1.

(d) Step-down mode of battery converter, d2

Fig. 3.4. Switching and operations in all modes.

Table 3.1. Components status in the converters.

Unidirectional converter (Uc), used for EG, d1									
Components	S_{ce}	S_e	D_d	D_a	Dr				
Step-up	T	TD_e	(1-D)T	(1-D)T	0				
Step-down	TD	0	0	T	0				
Disconnected	0	0	0	0	T				
Bidirectional converter (Bc),used for battery									
Components	S_{cr1}	S_{cr2}	S_{rD}	D_3	S_{ce}	S_{e1}	S_{e2}	S_e	D_r
Direction one									
Step-up	5	0	0	0	T	T	T	TD_e	0
Step-down	0	0	0	0	TD_{r1}	1	1	0	0
Direction two									
Step-down	T	T	DT	$(1-D_{rB})T$	0	0	0	0	T
Disconnected	0	0	0	0	0	0	0	0	T

3.3.3 Criteria for energy management and system operation

The proposed system is shown in Fig. 3.2(b), The EG uses a three-phase full bridge rectifier and its output voltage V_{scc} is a DC voltage. This feeds the input of a Z-source

converter shown in Fig. 3.3 (a). This converter is expressly designed to couple the EG to the EMS, it allows the power generated by the EG to be adapted to the demand, but at the speed imposed by the gasifier. To improve the system and achieve a fast response, two more converters connected to two batteries are used, see Fig. 3.3(b). The converters are expressly designed to obtain at their output a series dynamic coupling between their output voltages, so that at all times (2) is fulfilled.

$$V_{cc} = V_{outG} + V_{outB1} + V_{outB2} \quad (2)$$

When the EG is stable, this supplies all the power demanded by the load and the condition $V_{CC}=V_{outG}$ is verified, so the batteries do not help the EG and now $V_{outB1}=V_{outB2}=0V$. When there is a sudden increase in the load, the EG cannot assume the load increase quickly and a decrease of V_{outG} happens (then EG still produces the same power), so that $V_{outG}<V_{CC}$, but a battery converter acts helping the EG. This situation covers both voltage and energy deficiency occurring at the EG converter output and (2) is met at all time, keeping V_{cc} almost constant during the EG stabilisation process, when it is finished then $V_{CC}=V_{outG}$ is obtained again. The Fig. 3.3(c) shows B1 battery converter assisting the EG and that of B2 ready to store surplus energy.

The EG can regulate the generated power slowly between approximately 30% and 100%. When the demanded load is less than 30% of the EG rated power, then the EG is regulated up to 30% of its rated power and the surplus power generated is stored in batteries, see Fig. 3.3(c).

If the batteries have enough charge and the demanded load is small, then the batteries supply the load as shown in Fig. 3.3(d). Therefore, the batteries and their converters have two key functions; they help to keep the system stable in all transient states (load variations or gassing problems) and to store all surplus energy. Flowcharts is shown in Fig. 3.5.

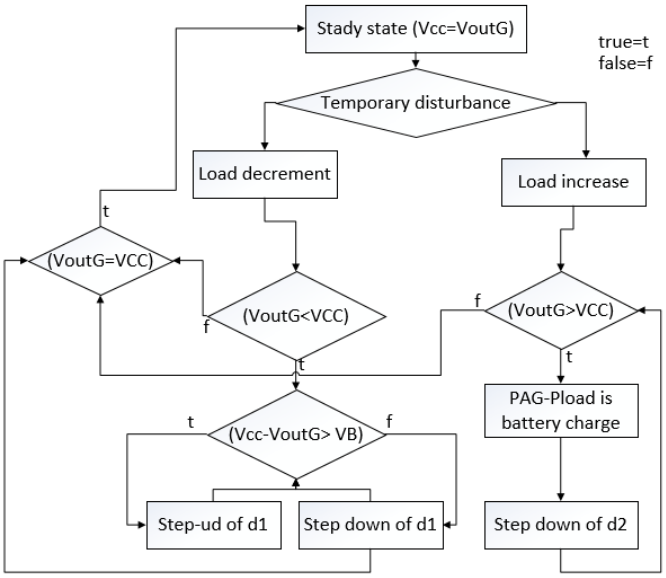

Fig. 3.5. Process flowcharts.

3.3.4 Constraints and design considerations for converters

- Constraints.

For the design of each converter, the maximum converted power and the connected voltages are considered. The working modes and functionality of each converter in the system are defined according to the system needs.

The EG converter converts energy between V_{Scc} and V_{CC}, in our case $400V<V_{Scc}<600V$ and $V_{cc} \simeq 500V$. As V_{Scc} can be both higher and lower than 500V, the step-up and step-down modes are necessary, but the two modes cannot work at the same time.

The battery converters help V_{outG} when $V_{outG}<V_{CC}$, so that (2) is always satisfied. This is achieved by working on d1. The step-down and step-up modes are used when $V_{CC}-V_{outG}<V_B$ and $V_{CC}-V_{outG} \geq V_B$, respectively. Furthermore, if the demand power is small,

then the batteries supply the load with (V_B=24V and V_{CC}=500V), therefore each battery converter needs a maximum voltage gain (M_{ve}=11.25) to get V_{outB}>270.

When the EG generates surplus energy, it is stored in the batteries and the battery converters use d2. As V_{CC}=500V and V_B=24V, in d2, these converters are designed with a maximum step-down gain $20 < M_{vr} < 25$.

Like the EG slowly tracks the load changes, then the system is configured with two batteries. The higher charge battery helps the EG to supply power to the load during transient states (when there is an increase of demand). When a load decrease occurs, the lower charge battery is used to store the excess energy from the EG group.

Table 3.2. Voltage ranges and operating modes of the converters.

<table>
<tr><td colspan="4">Battery converters</td><td colspan="3">EG converter</td></tr>
<tr><td colspan="4">Direction one (d1), Voltage regulation</td><td colspan="3">Only (d1) and Voltage regulation</td></tr>
<tr><td>V_B</td><td>V_{cc}-V_{outG}</td><td>Range of V_{outB}</td><td>mode</td><td>V_{Scc}</td><td>V_{outG}</td><td>mode</td></tr>
<tr><td>24V</td><td>V_{cc}-V_{outG}>V_B</td><td>(24-270) V</td><td>Step-Up</td><td>≥500V</td><td>(300-550) V</td><td>Step-Down</td></tr>
<tr><td>24V</td><td>V_{cc}-V_{outG}≤V_B</td><td>(0-24)V</td><td>Step-Down</td><td><500V</td><td>(300-550)V</td><td>Step-Up</td></tr>
<tr><td colspan="4">Direction two (d2), Current Regulation</td><td colspan="3" rowspan="3">Note: Strong variations in V_{Scc}, which depend on the type of biomass, reactor inertia and the load power</td></tr>
<tr><td>V_B</td><td>V_{cc}</td><td>M_V</td><td>mode</td></tr>
<tr><td>24 V</td><td>500V</td><td>(20-22)</td><td>Step-Down</td></tr>
</table>

- Converters design.

The Z-source design must be performed to meet all the restrictions imposed by the system. The calculation starts with step-up mode of d1 (since its constraints are more difficult to fulfil).

Step-up mode of d1. This mode is required for battery and EG converters, the maximum converted energy is obtained with (3). The maximum converted power P_{max} is a key design data. In our case, the EG converter has P_{max}=10kW. For battery converters, their maximum power is estimated about 30% of the EG nominal power.

$$E_{\max} = P_{\max} T f_c D_{\max} = L(I_{Lt_2}^2 - I_{Lt_1}^2) \quad (3)$$

$$(V_{0C})_{t_3} = \frac{(V_{out} + V_S)}{2} \quad (4)$$

V_{oc} is the capacitors voltage C1 and C2 when each switching cycle starts, it is obtained with (4), where V_{out} and V_s are the output and input voltages of the converter at d1. In the switching processes of this mode, shown in Figs. 3.4 (a) and (c), V_{oc} is obtained at t2 and t3 respectively, this voltage is reached in C1 and C2 before L1 and L2 are discharged on its output capacitor Ca. The Z-source of the EG converter has been designed with small step-up gain and that of the battery converters with large step-up gain, although its power circuits are the same, they have different performances. C_1 and C_2 discharge part of their energy through inductors L_1 and L_2 (between t_0 and t_1). This discharge produces a current $I_{L(t1)}$ through L_1 and L_2 which is obtained by (5).

$$(I_L)_{t_1} = \sqrt{\frac{C}{L}\frac{(V_{out}^2 + 2V_{out}V_S)}{4}} \quad (5)$$

$I_{L(t1)}$ is the maximum current through L_1 and L_2 in the EG converter, and $(I_{Lmax})_{t_2}$ is the same but in the battery converters. Both currents are obtained when maximum duty cycle $D_{e\max}$ is used. $I_{L(t1)}$ and $(I_{Lmax})_{t_2}$ are necessary for the choice of devices S_{ce}, S_e and the cooper wire section of the inductors L_1 and L_2, $(I_{L\max})_{t_2}$ is obtained with (6).

$$(I_{\mathrm{L\,max}})_{t_2} = I_{Lt_1} + \frac{V_S}{2L} D_{e\max} T \tag{6}$$

In d1, the maximum power converted by the battery converters (in watts), is obtained with (7).

$$P_s = (2I_{Lt_1} + \frac{V_S}{2L} D_{e\max} T) \frac{V_S}{2} D_{e\max} \tag{7}$$

The power converted by each converter depends on its Z-source (combination of L y C values). The value of L is obtained with (8) and that of C with (9)

$$L = \frac{V_S^2 D_{e\max}^2 T}{4(P_s - I_{Lt_1} D_{e\max}^2 V_S)} \tag{8}$$

$$C = \frac{4L(I_L^2)_{t_1}}{\left(V_{out}^2 + 2V_{out} V_S\right)} \tag{9}$$

The design process begins with d1. The abacus of Fig. 3.6(a) has been obtained with (5) and (7). The optimal point is found by iterating within the recommended area. For battery converters working in d1 and with maximum duty cycle $D_{e\text{-}max}$=0.8, a maximum converted power of 3000Watts or slightly higher is sought (with input voltages V_s=V_{in}=24V and output voltage V_{out}=270V). The values obtained for the design are: L=14μH, C=10μF, I_{t1}=123.8 A and I_{t2}=192.3 A, the maximum power converted with these values will be 3035W, close to the chosen power.

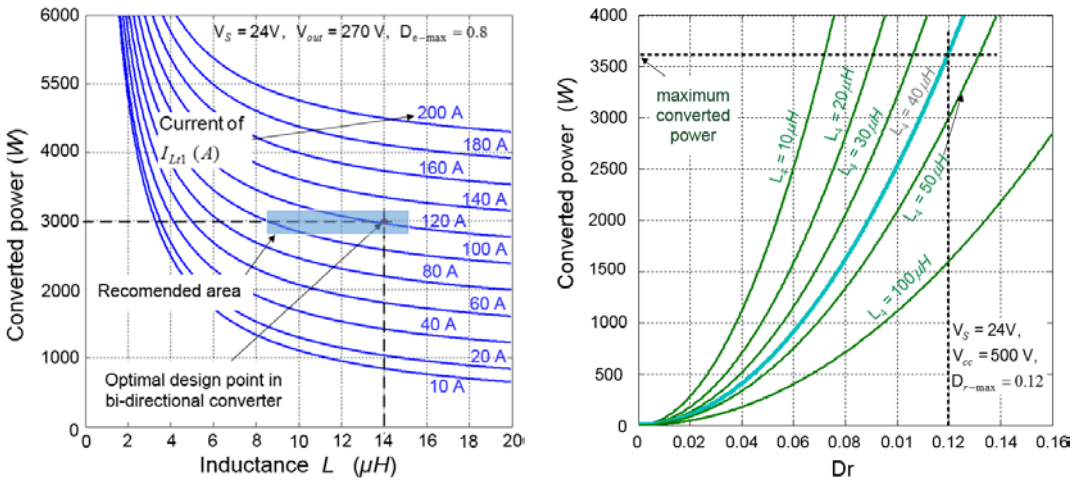

(a) Step Up mode, d1.

(b) Step Down mode, d2.

Fig. 3.6. Power charts for design.

Step-down mode in directions d1 and d2. In d1, this mode is required when $0 \leq V_{outB} \leq V_B$, it is used in the battery converters to help the EG converter if V_{CC}-V_{outG} <V_B. This mode is defined by the Z-source parameters already calculated for the step-up mode.

In d2, the step-down mode is necessary to charge the batteries $(V_B = 24V)$ from the DC bus $(V_{cc} = 500V)$. After knowing the L and C values of the Z-source, the value of L_4 is calculated using (10) and with (11) the maximum converted power is obtained.

$$I_{L_4} = \frac{2(V_{cc} - V_B) D_{r\max} T}{L + 2L_4} \tag{10}$$

$$Pr_{\max} = V_{Hn} * \frac{(V_{cc} - V_B) D_{r\max}^2 T}{L + 2L_4} \tag{11}$$

In d2, as the step-down voltage gain is very high, current stress on the semiconductors is avoided with L_4 and by limiting the duty cycle. In addition, the L_4 inductance provides a nearly linear Z-source response and a wider duty cycle range (both in this mode only), which facilitate control. The Fig. 3.6(b) has been obtained with (10) and (11). So, it shows a design abacus for the step-down mode. Starting from designed Z-source and taking as

an example a value of $L_4 = 40\mu H$, a power greater than 3500W can be converted from a voltage $V_{cc} = 500V$ to one of $V_B = 24V$, limiting D_r in the range (0-0.12T).

To size the semiconductors, the converters operation has been taken into account and the expressions from (12) to (16) have been obtained. With these expressions, the maximum average current through each device can be calculated.

$$\overline{I}_{Se} = \frac{(I_L)_{t_1} + (I_L)_{t_2}}{2} * 0.85 \tag{12}$$

$$\overline{I}_{Sce} = \overline{I}_{De} = \frac{(I_L)_{t_1} + (I_L)_{t_2}}{2} \tag{13}$$

$$\overline{I}_{SrD} = 2 * \overline{I}_{D_3} = 2 * \overline{I}_{Scr2} = \frac{I_{L4}}{10} \tag{14}$$

$$\overline{I}_{Se1} = \overline{I}_{Se2} = \frac{P_{\max}\ converted\ (mode\ step - up)}{V_{Hn}} \tag{15}$$

$$\overline{I}_{Scr1} = \frac{P_{\max}\ converted\ (mode\ step - down)}{V_s} \tag{16}$$

3.4. Experimental applications and results

3.4.1 Measurements of used syngas

The experimental system has been tested in a pilot plant (see Fig. 3.7(a)). The biomass source has been exhausted olive pomace pellets. The obtained gas chromatography results are: a high H_2 content (around 16-18% vol.), Methane content (2-3%) and CO (12-14%) are acceptable. According to table 3.3, the average producer gas LHV in three tests has been 4.7MJ/Nm^3.

Table 3.3. Product gas composition and efficiency parameters of the gasification plant.

Measured parameters	Unit	Test 1	Test 2	Test 3	Average
H_2	%	16.31	17.90	18.22	17.48
O_2	%	0.96	0.78	0.48	0.74
N_2	%	54.50	51.66	52.00	52.72
CH_4	%	3.10	2.24	2.77	2.70
CO	%	12. 1	14.60	12.94	13.77
CO_2	%	13.10	12.64	13.57	13.10
Calorific power	MJ/Nm^3	4.53	4.72	4.75	4.67
Pomace pellets consumption	kg/h	14.52	15.12	14.95	14.86
Product gas flow	m^3/h	40.85	38.20	39.50	39.52
Gasification performance	%	73.67%	68.93%	72.54%	71.72%

(a) Gasification plant installed in IFAPA oil mill (Venta del Llano, Mengíbar, Spain).

The measured biomass consumption ranged between 14-15 kg/h. Fig. 3.7(b) shows the chromatography of the product gas during test number 3.

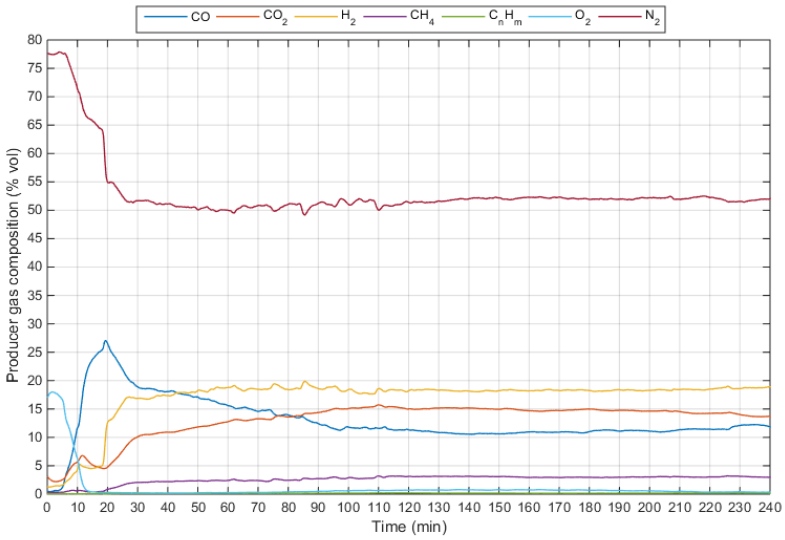

(b) Product gas composition in test number 3 (duration 4 hours).

Fig. 3.7. Gasification plant installed in IFAPA oil mill and Product gas composition in test number 3.

3.4.2 Results of the proposed management system

3.4.2.1 Implemented experimental system

This work has been implemented with two controllers Cs1 and Cs2, both Siemens S7-1500, CPU1516F-3 PN/DP, see Fig. 3.9, which have been used to manage the system converters. The samples are taken with a minimum cycle of 10 ms and a maximum of 40 ms. An OPC connection has been executed using KEPServerEX and the signals captured with Cs1 have been sent to Simulink.

Moreover, five PIDs have been programmed: one of them regulates the duty cycle of the EG converter and other two regulate the duty cycles of the battery converters working in d1 and step-up and step-down modes (to stabilize V_{cc}). The remaining two regulate the charge of the B1 and B2 batteries independently.

The electrical system consists of a 10kVA three-phase alternator with terminal voltage between 400 and 460V and automatic voltage regulation, prepared for the grid connection. To work off-grid, a three-phase full-bridge rectifier has been installed at the alternator output. Its output voltage V_{scc} is converted to V_{outG} through the EG converter. This regulates the value of V_{outG}.

For transient damping (due to load changes or fuel deficiencies), two batteries of 600Ah and 24V have been used, composed by two groups of 12V each. Every battery is connected to the EG through a Bc of fast response. Those two converters add their output voltage with V_{outG}, see Fig. 3.3 (c,d). When there is a decrease in V_{outG} (due to problems in the gasifier or increased load), it is compensated with the voltage and energy contributions from one of the batteries through its converter.

3.4.2.2 Converters design parameters obtained

The parameters calculated to design the converters components with the proposed method are shown in tables 3.4.

Table 3.4. Design data for converters.

Source	Rated power of source	Design voltages	Design powers	D_{emax}
Step-Up mode, Uc and Bc, (d1)				

EG	10000VA	V_s= 400V, V_{out}=560V	10000W	0.8
Battery	600Ah	V_s=24V V_{out}= 270	3000W	0.8
Step-Down mode, Bc (d2)				Dr_{max}
Battery	600Ah	V_{cc}=500V V_B=24V	3500W	0.16

Table 3.4. Parameters obtained for converter design.

Source	$L_1, L_2\ \mu H$	$L_4\ \mu H$	$C_1, C_2\ \mu F$	Currents (A)	Converted P_{max}
Step Up mode, Uc and Bc, (d1)					
EG	350	_	0.5	I_{L1}=16.3, I_{L2} =62	12525W
Battery	14	_	10	I_{L1}=124, I_{L2}=192,	3036W
Step Down mode, Bc (d2)					
Battery	-	70	_	I_{L4}=99	3956 W

For the choice of the power converters devices (transistors, diodes, etc.) expressions (12) to (16) have been used. As shown in Figs. 3.2(b) and 3.3(c-d), the converters are coupled in series through their outputs (V_{outG}, V_{outB1} and V_{outB2}), so that any disturbances occurring in the EG group are compensated by the battery converters. To justify its good operation, several tests are carried out to demonstrate the system's robustness against load variations, allowing the EG to operate off-grid mode or connected to a DC grid.

3.4.3 System response to disturbances

To test the efficiency of the system, several graphs representing the system response to sudden variations in load. A load sudden increase of 2500W (25% of GEG rated power) are shown, see Fig. 3.8(c), the response begins at coordinate A, with an increase in I_{CC} of (5A). To prevent the GEG from disturbances, only a small part of power increase is compensated by the speed decrease of the EG generator rotor; the rest is compensated by the battery B1 (in this case). After load increase, the EG converter regulates its V_{outG} voltage and drops to values lower than 400V (the power supplied by the EG changes very little). Most of the power increase demanded by the load is supplied by the B1 battery converter, which provides the voltage V_{outB1} ($V_{outB1max}$>100V), with $V_{outG}+V_{outB1}=V_{cc}$ throughout the transient (B2 does not intervene). In the V_{cc} graph of Fig. 3.8(c), the voltage oscillations (shown in detail) are due to the B1 battery converter switching, especially those of coordinates B and C, which occur in the switching changes between step-up and step-down modes. But the voltage fluctuation (in a limit situation like the one presented) is less than 5V which is equivalent to ± 1%. This transitory process lasts until the GEG adjusts its mass flow to a new load point (in this case, the elapsed time between coordinates A and D is 1.75 minutes). After the transient, the EG can supply the new demanded power alone, keeping V_{cc} almost constant.

Fig. 3.8 (a) shows how the battery converters can help the EG, that is working with a power greater than 6500W. There are two successive load increases: the first of 500W and 1A (shown between coordinates A and B), the second of 900W and 1.8A (shown between C and D). Battery B1 compensates the first increment and B2 compensates the second one (the battery with the higher charge level always compensates), so that V_{cc} remains almost constant. Both transients last approximately 0.43 and 0.83 minutes respectively.

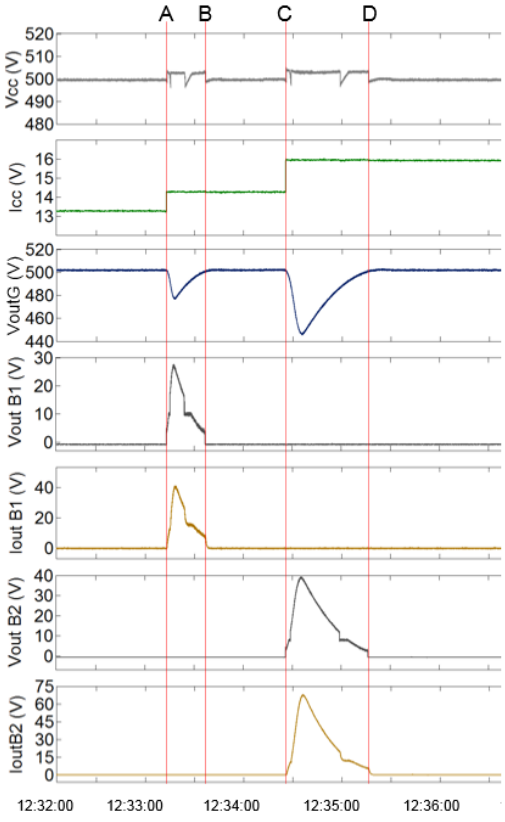

(a) Response due to increased load.

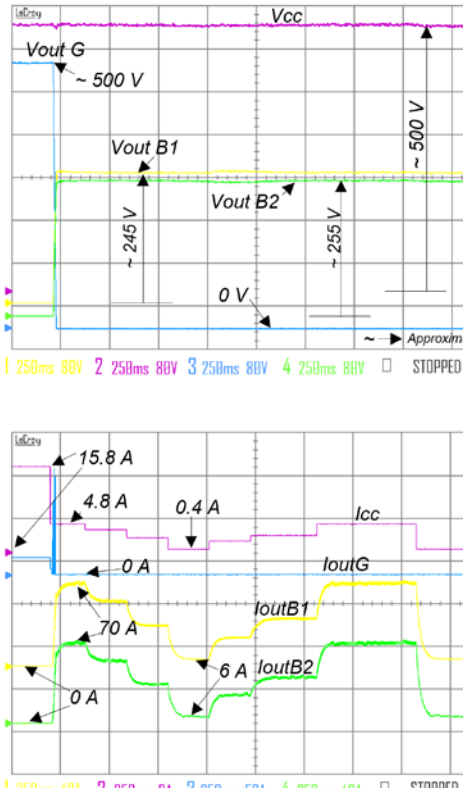

(b) Supply with batteries.

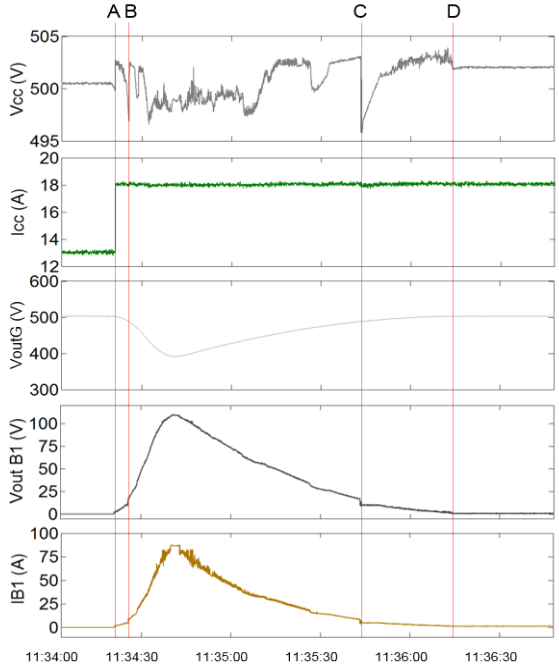

(c) Load increase detail.

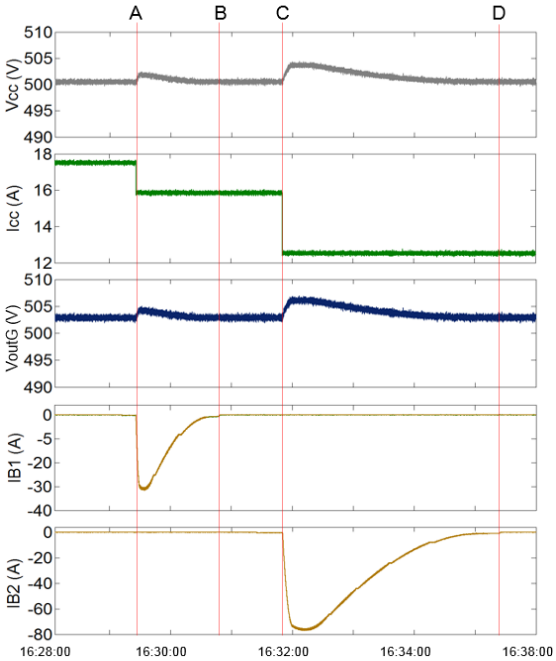

(d) Load decrease.

Fig. 3.8. Response due to increased load, supply with batteries, load increase detail and load decrease.

When a load decreases occurs, until the gasifier adapts to the new load situation, the difference between the generated and consumed energy is stored in one of the batteries (the least charged one). Fig. 3.8(d) shows the results about two load decrements: in the first, I_{cc} decreases 1.66A or 830W, in the second, I_{cc} decreases 3.57A or 1780W, equivalent to 8.3% and 17.8% of the rated power of the EG, respectively. The excess energy from the first decrease is stored in B1 and that from the second one in B2. The storage times last until the gasifier reaches a new working point (approximately 1.2 and 2.6 minutes respectively). The decision-making is done so that the battery that helps the EG (when load increase occurs) is the more charged at that time, and the other one absorbs the excess energy when load decreases occur. If the load drops below 30% of the rated power of the EG, then EG generate 30% of its rated power (minimum allowed), with this power, the load is powered and the excess energy is stored in the batteries. If the batteries exceed 95% of their charge and the load connected to the EG is less than 30% of the rated power of the EG, then the load is powered only by batteries. Also, when the batteries charge level is less than 70%, the gasifier needs to work again. Fig. 3.8(b) shows the system behaviour during a limit test. After a load decrease of 5.5kW (the demanded load power is less than 30%), then EG is abruptly disconnected from system, leaving the load powered only by the batteries and their converters, Figs. 3.8(b1 and b2) in channels 1 and 4 (V_{outB1}, I_{outB1}, V_{outB2} and I_{outB2}) show the rapid response of battery converters when an EG sudden disconnection occurs. Next, three disconnections and three load connections are forced, with the loads being powered by the batteries at all times, fulfilling that $V_{outB1}+V_{outB2} \simeq V_{CC}$ and keeping V_{cc} close to 500V, see Fig. 3.8(b1) channel 2. In channel 2 of Fig. 3.8(b2) it can be seen that I_{cc} (demanded load) has had several changes in a very short time, but the system can maintain the demand at all times with almost constant V_{cc}. All the presented tests have been carried out with off-grid gasification plant (which is the most extreme situation), these tests justify a perfect operation of the off-grid plant. In all the load increase tests, it can be observed that the voltage V_{outG} suffers important variations, although, due to the performance of the proposed system, these do not affect

the DC bus voltage V_{cc}, which is always kept close to 500V. Moreover, when load decreases occur, the surplus energy is stored in the batteries, improving the efficiency.

The presented system focuses on the converters design and their integration with GEG, so that the GEG can operate off-grid or even coupled in weak renewable energy micro-grids. This technique grandly expands the GEG possibilities and it can be applied where there is no electrical grid and biomass is available, such as in many developing countries (Africa, Latin America, etc.). Also, the proposed system allows the GEG to be integrated with other renewable energies (air, sun, etc.), to help power the load when there is a lack of these energies. Thus, a permanent and good quality energy supply can be obtained. Furthermore, another great advantage is that the residue from the gasifier (biochar) can be used as fertiliser. This technology is environmentally friendly and meets the circular economy criteria.

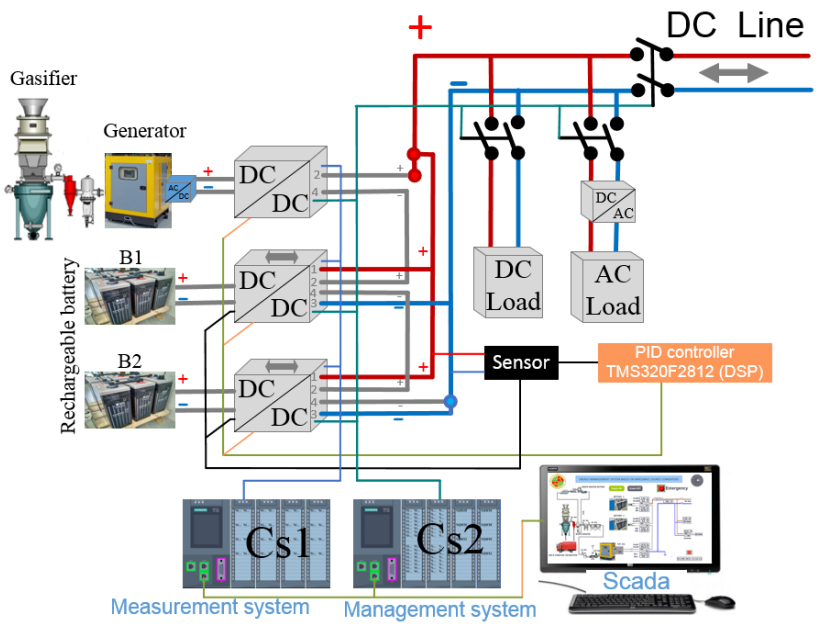

(a) Management, measurement and control system.

(b) Laboratory system.

Fig. 3.9. Management, measurement, control system and laboratory system.

3.5. CONCLUSIONS

Electric power generation from biomass gasification plants present a high chemical inertia. For this reason, they have problems feeding the load when it undergoes sudden changes. Therefore, these systems do not offer a quality supply if they work in off-grid systems. This work presents an innovative system based on the optimal design of impedance source converters, both unidirectional (for EG) and bidirectional (for batteries), to be coupled according to the different operating modes studied. The main contributions are: the converters coupling structure and its design method with the operating modes used. By means of their coupling, it has been possible to integrate an EG and two batteries, obtaining a system that helps the EG to track the load changes without any supply disturbance; this tracking is achieved even if there are changes in the gas quality.

This study presents an experimental approach applied for a 10 kW gasification plant operating in off-grid connection. This system can work in isolation with a high quality supply feeding the load continuously, or even if there are disturbances in the load and in the syngas. For its verification, sudden changes of load increase and decrease have been forced and the management system has achieved the plant maintains an undisturbed supply.

This research can help to improve renewable energy micro-grids, considering that the fuel for gasification can be stored, electricity generation with GEG can be done at any time, then the integration of GEG plants with renewable generation from the sun and air, can help to achieve more stable micro-grids and less dependent on the randomness of the air and the sun.

This work can be extended by advancing on the coupling of GEG with other renewable energies, it is also recommended to investigate on optimal management operations of these systems, using artificial intelligence techniques such as reinforcement learning.

3.6. ACKNOWLEDGEMENTS

This work was supported in part by the project entitled “Renewable energies for Africa: Effective valorisation of agri-food wastes (REFFECT AFRICA)". This project has received funding from the European Union's Horizon 2020 Research and Innovation programme under the Grant Agreement number 101036900".

3.7. REFERENCES

[1]H.A.M. Knoef, Handbook Biomass Gasification Second Edition. Biomass Technology Group (BTG), 2012.

[2]A.K.S. Parihar, V. Sethi, R. Banerjee, Sizing of biomass based distributed hybrid power generation systems in India, Renew. Energy. 134 (2019) 1400–1422. https://doi.org/10.1016/j.renene.2018.09.002.

[3]P. Basu, Biomass Gasification, Pyrolysis and Torrefaction: Practical Design and Theory, 2013. https://doi.org/10.1016/C2011-0-07564-6.

[4]S. Mazhkoo, H. Dadfar, M.S. HajiHashemi, O. Pourali, A comprehensive experimental and modeling investigation of walnut shell gasification process in a pilot-scale downdraft gasifier integrated with an internal combustion engine, Energy Convers. Manag. 231 (2021) 113836. https://doi.org/10.1016/j.enconman.2021.113836.

[5]B. de Mena, D. Vera, F. Jurado, M. Ortega, Updraft gasifier and ORC system for high ash content biomass: A modelling and simulation study, Fuel Process. Technol. 156 (2017) 394–406. https://doi.org/10.1016/j.fuproc.2016.09.031.

[6]L. V. Martínez, J.E. Rubiano, M. Figueredo, M.F. Gómez, Experimental study on the performance of gasification of corncobs in a downdraft fixed bed gasifier at various conditions, Renew. Energy. 148 (2020) 1216–1226. https://doi.org/10.1016/j.renene.2019.10.034.

[7]F.Y. Hagos, A.R.A. Aziz, S.A. Sulaiman, Trends of syngas as a fuel in internal combustion engines, Adv. Mech. Eng. 2014 (2014). https://doi.org/10.1155/2014/401587.

[8]J.D. Martínez, K. Mahkamov, R. V. Andrade, E.E. Silva Lora, Syngas production in downdraft biomass gasifiers and its application using internal combustion engines, Renew. Energy. 38 (2012) 1–9. https://doi.org/10.1016/j.renene.2011.07.035.

[9]A.A.P. Susastriawan, H. Saptoadi, Purnomo, Small-scale downdraft gasifiers for biomass gasification: A review, Renew. Sustain. Energy Rev. 76 (2017) 989–1003. https://doi.org/10.1016/j.rser.2017.03.112.

[10] P. Basu, Design of Biomass Gasifiers, First Edit, © 2010 Elsevier Inc., 2010. https://doi.org/10.1016/b978-0-12-374988-8.00006-4.

[11] O.S. Ejiofor, P.A. Okoro, U.C. Ogbuefi, C.V. Nnabuike, K.E. Okedu, Off-grid electricity generation in Nigeria based on rice husk gasification technology, Clean. Eng. Technol. 1 (2020). https://doi.org/10.1016/j.clet.2020.100009.

[12] A.S. Sánchez, E.A. Torres, R.A. Kalid, Renewable energy generation for the rural electrification of isolated communities in the Amazon Region, Renew. Sustain. Energy Rev. 49 (2015) 278–290. https://doi.org/10.1016/j.rser.2015.04.075.

[13] M. Naqvi, J. Yan, E. Dahlquist, S.R. Naqvi, Waste Biomass Gasification Based off-grid Electricity Generation: A Case Study in Pakistan, Energy Procedia. 103 (2016) 406–412. https://doi.org/10.1016/j.egypro.2016.11.307.

[14] P.V. Ramamurthi, M.C. Fernandes, P.S. Nielsen, C.P. Nunes, Utilisation of rice residues for decentralised electricity generation in Ghana: An economic analysis, Energy. 111 (2016) 620–629. https://doi.org/10.1016/j.energy.2016.05.116.

[15] D. Palit, R. Malhotra, A. Kumar, Sustainable model for financial viability of decentralized biomass gasifier based power projects, Energy Policy. 39 (2011) 4893–4901. https://doi.org/10.1016/j.enpol.2011.06.026.

[16] S.W. Lee, J. Kim, Small-signal modeling, integration, and hardware implementation for optimized DC distribution system based on hierarchical control master–slave structure, Electr. Power Syst. Res. 177 (2019) 105998. https://doi.org/10.1016/j.epsr.2019.105998.

[17] A. Goudarzian, A. Khosravi, H.A. Raeisi, Analysis of a step-up dc/dc converter with capability of right-half plane zero cancellation, Renew. Energy. 157 (2020) 1156–1170. https://doi.org/10.1016/j.renene.2020.05.088.

[18] S.K. Kuncham, K. Annamalai, S. Nallamothu, Single-Phase Two-Stage Seven-Level Power Conditioner for Photovoltaic Power Generation System, IEEE J. Emerg. Sel. Top. Power Electron. 8 (2020) 794–804. https://doi.org/10.1109/JESTPE.2019.2913216.

[19] M.V. Ortega, F. Jurado, M. Ortega, D. Vera, Current control in high-efficiency unidirectional converter for fuel cell, Int. J. Electron. 106 (2019) 1101–1112. https://doi.org/10.1080/00207217.2019.1582708.

[20] Y. Zhang, C. Fu, M. Sumner, P. Wang, A Wide Input-Voltage Range Quasi-Z-Source Boost DC-DC Converter with High-Voltage Gain for Fuel Cell Vehicles, IEEE Trans. Ind. Electron. 65 (2018) 5201–5212. https://doi.org/10.1109/TIE.2017.2745449.

[21] C. Bai, B. Han, B.H. Kwon, M. Kim, Highly Efficient Bidirectional Series-Resonant DC/DC Converter over Wide Range of Battery Voltages, IEEE Trans. Power Electron. 35 (2020) 3636–3650. https://doi.org/10.1109/TPEL.2019.2933408.

[22] F. Shi, D. Song, A novel high-efficiency double-input bidirectional DC/DC converter for battery cell-voltage equalizer with flyback transformer, Electron. 8 (2019). https://doi.org/10.3390/electronics8121426.

[23] J. Ke, Z. Zhengxuan, Z. Qijuan, Y. Zhe, B. Tianshu, Islanding detection method of multi-port photovoltaic DC micro grid based on harmonic impedance measurement, IET Renew. Power Gener. 13 (2019) 2604–2611. https://doi.org/10.1049/iet-rpg.2019.0271.

[24] F. Wang, A novel quadratic Boost converter with low current and voltage stress on power switch for fuel-cell system applications, Renew. Energy. 115 (2018) 836–845. https://doi.org/10.1016/j.renene.2017.08.032.

[25] M. Ortega, F. Jurado, M. Valverde, Novel topology for DC/DC unidirectional converter for fuel cell, IET Power Electron. 7 (2014) 681–691. https://doi.org/10.1049/iet-pel.2013.0142.

[26] M. Ortega, M.V. Ortega, F. Jurado, J. Carpio, D. Vera, Bidirectional DC–DC converter with high gain based on impedance source, IET Power Electron. 12 (2019) 2069–2078. https://doi.org/10.1049/iet-pel.2018.5385.

[27] Q. Wu, Q. Wang, J. Xu, H. Li, L. Xiao, A high-efficiency step-up current-fed push-pull quasi-resonant converter with fewer components for fuel cell application, IEEE Trans. Ind. Electron. 64 (2017) 6639–6648. https://doi.org/10.1109/TIE.2016.2638800.

[28] J. Kan, S. Xie, Y. Tang, Y. Wu, Voltage-Fed Dual Active Bridge Bidirectional, IEEE Trans. Power Electron. 29 (2014) 3582–3590.

[29] M. Nymand, M.A.E. Andersen, High-Efficiency Isolated Boost DC – DC Converter for, Ieee Trans. Ind. Electron. 57 (2010) 505–514.

[30] A.A. Abduallah, M. Meraj, M. Al-Hitmi, A. Iqbal, Space vector pulse width modulation control techniques for a five-phase quasi-impedance source inverter, IET Electr. Power Appl. 12 (2018) 379–387. https://doi.org/10.1049/iet-epa.2017.0340.

[31] X. Zhu, B. Zhang, D. Qiu, Enhanced boost quasi-Z-source inverters with active switched-inductor boost network, IET Power Electron. 11 (2018) 1–14. https://doi.org/10.1049/iet-pel.2017.0844.

[32] A. Ahmad, V.K. Bussa, R.K. Singh, R. Mahanty, Switched-boost-modified Z-source inverter topologies with improved voltage gain capability, IEEE J. Emerg. Sel. Top. Power Electron. 6 (2018) 2227–2244. https://doi.org/10.1109/JESTPE.2018.2823379.

[33] M. Ortega, E. Lanagrán, M.V. Ortega, F. Jurado, Design and integration of Z-source converters for energy management with series operation: Applied to DC microgrid, Int. J. Electr. Power Energy Syst. 128 (2021). https://doi.org/10.1016/j.ijepes.2021.106781.

[34] E. Lanagran, M.V. Ortega, M. Ortega, J.P. Roa, P. García-Triviño, Improvement of the Coupling of Renewable Sources through Z-Source Converters Based

on the Study of Their Dynamic Model, Electron. 11 (2022). https://doi.org/10.3390/electronics11132074.

[35] L. Fernández-Lobato, R. Aguado, F. Jurado, D. Vera, Biomass gasification as a key technology to reduce the environmental impact of virgin olive oil production: A Life Cycle Assessment approach, Biomass and Bioenergy. 165 (2022) 106585. https://doi.org/10.1016/j.biombioe.2022.106585.

[36] A. Amir, A. Amir, H.S. Che, A. Elkhateb, N.A. Rahim, Comparative analysis of high voltage gain DC-DC converter topologies for photovoltaic systems, Renew. Energy. 136 (2019) 1147–1163. https://doi.org/10.1016/j.renene.2018.09.089.

CAPÍTULO IV: Improvement of the coupling of renewable sources through Z-source converters based on the study of their dynamic model

(Publicado en Electronics, Volumen 11, edición 13, Julio de 2022, DOI10.3390/electronics11132074)

ÍNDICE DEL CAPÍTULO IV:

4.1. INTRODUCTION 140

4.2. ARCHITECTURE AND OPERATION OF THE CONVERTER 142

4.2.1. Choice of converters 142

4.2.2. Step-up mode stages 143

4.3. CONVERTER ANALYSIS 146

4.4. DYNAMIC MODEL AND CONVERTER COUPLING CONTROL STRATEGY 153

4.5. RESULTS 155

4.5.1. Design considerations. 156

4.6. DISCUSSION 165

4.7. REFERENCES 167

TABLA DE FIGURAS CAPÍTULO IV:

Fig. 4.1. Circuits of the different stages of the converter. 144
Fig. 4.2. Waveforms: (a) step-up mode, (b) step-down mode. 146
Fig. 4.3 (a) Evolution de Me versus De with resistances of different loads. (b) Evolution de Me versus De with different Z-source resistances. (c) Evolution of Me varying De, with various values of C of the Z-source and different resistances of load. (d) Evolution of Me varying De, with various values of L of the Z-source and different resistances of load. (e) Converted power into a function of the parameters L and C of the Z-source. 152
Fig. 4.4. Root locus for open-loop and Bode diagrams, uncontrolled (open loop) and controlled (closed loop) G(s) step responses of plant. 155
Fig. 4.5. Source coupling: (a) Classical structure, (b) Proposed coupling scheme, (c) Simulink® model of the proposed coupling. 160
Fig. 4.6. Simulation model obtained results. (a) Voltages in the sources; (b) Currents in the converters inputs; (c) Voltages in the converters outputs and Vdc; (d) Currents in the converters outputs and Idc. 163

TABLA DE TABLAS CAPÍTULO IV:

Table 4.2.1. design data, for the step-up mode of the Uc and Bc converters. 158
Table 4.2.2. Parameters obtained for the step-up mode design of the Uc and Bc. 158
Table 4.2.3. Design parameters obtained for the step-down mode of the Bc. 159

Improvement of the coupling of renewable sources through Z-source converters based on the study of their dynamic model

Enrique Lanagran [1], María Victoria Ortega [1], Manuel Ortega [1], Juan Pedro Roa and Pablo García [2,*]

[1] Higher Technical School, University of Jaén; elvargas@ujaen.es; mvortega@ujaen.es; maortega@ujaen.es; jproa@ujaen.es
[2] Higher Technical School of Engineering of Algeciras, University of Cadiz; pablo.garcia@uca.es
* Correspondence: pablo.garcia@uca.es

Abstract: The classical coupling of renewable energy sources greatly limits the coupling power and the output voltage of the coupled sources. Moreover, it does not eliminate the randomness of the sources. In this work a renewable sources coupling with high randomness is obtained by series connection of the output terminals of Z-source converters. To achieve the coupling, the stationary and dynamic models of a Z-source based converter has been studied. With the results of the stationary model, the converter behaviour has been evaluated as a function of its parameters and a method for calculating the Z-network parameters has been implemented. Moreover, with the dynamic model a controller has been designed for all the converters. The main contributions of this work are the coupling of the sources, the stationary and dynamic models obtained and their analysis. The coupling achieves a stable supply avoiding that the sources randomness reaches the load. A system composed of a wind turbine, a set of photovoltaic panels and two groups of batteries has been modeled. To study the system behaviour and the supply quality, several aggressive tests have been forced.

Keywords: Z-source converters; Energy management; DC converters; DC microgrid; Energy renewable.)

4.1. INTRODUCTION

Renewable energy sources are increasingly being used around the world. Some of these are not directly compatible with the electricity grid, as is the case with fuel cells [1,2] and PV systems [3,4]. These sources produce energy in the form of DC that can be stored in batteries and be used later in AC form using inverters [5,6]. In DC, more and more often, voltage changes are necessary for which DC converters are required [7,8]. Special features are also created that need DC-DC and DC-AC multi-task converters [7]. In addition, coupling renewable energy sources of different types and with different characteristics is a necessity and this situation requires specific design of converters to cover specific objectives [9].

Among the DC-DC converters, there are several topologies and several types of techniques that can be distinguished and among them the classic ones stand out: voltage-fed DC-DC converters which usually need high frequency transformer [10-12], current-fed DC-DC converter with elevator and reducer modes [13]. There are many switching techniques, but the goal is to lose as little energy as possible in the switching of the active elements using a smooth switching technique [14]. A mixture of fed-current and fed-voltage topologies with smooth switching have been integrated into a single unidirectional converter [14]. Some topologies have also been proposed for high-voltage applications seeking to obtain a large voltage gain [15,16]. Impedance source-based converters is one of the most promising techniques. This topology was introduced in [17] and since then it has been used in inverters [18]. The Z-source can regulate the DC bus voltage in inverters, being its switching technique compatible with that of most techniques used for inverters [19,20]. Making modifications on the Z-source circuit, the qZ-source is obtained as can be seen in [21]. Both circuits are very similar but have some differences in their operation: the Z-source has a higher step-up voltage gain; the qZ-source converters suffer from a lower voltage stress on their components than those of Z-source. The qZ-source has also been used in inverters [22]. In [23] a family of DC-DC converters with high step-up gain is presented. Most works about renewable energy

management require converters and especially DC ones [24,25], converters are normally treated as ideal elements, not taking into account the behaviour of the converters integrated in the microgrid. This does not model the real behaviour of any converter and the actual results may be very different from those studied theoretically.

Renewable energy sources generate different voltages with associated random disturbances that are difficult to control. Nevertheless, electrical grid need a stable voltage that does not depend on the sources randomness. Currently, structures that eliminate this problem are in an incipient state, especially with small and medium power sources for residential use. In [26, 27] hierarchical control in DC microgrids and a review of power converters for microgrids with classical structures are presented.

The contribution of this paper focuses on a new configuration to improve the classical structures, where batteries and renewable energy sources are connected through converters with their outputs in series, as shown in Fig. 4.5b. The design of this structure is obtained from studies of the stationary and dynamic model of a Z-source converter. With the stationary model, the behaviour of the converter can be predicted as a function of its design parameters, optimizing the converters of each source or battery to be coupled in the branch.

With the dynamic model, the design of the converter controller is obtained.

The final objective is to improve the renewable sources coupling by synchronizing all the converters of the generating branch through a single controller, avoiding that the sources randomness reaches the load. Obtaining a stable and quality supply independent of the sources randomness. This requires a proper design of the controller and the converters.

With the results obtained, four converter models have been designed to couple two batteries, a wind turbine and a set of solar panels. The controller has also been designed to synchronize the four converters when they work in step-up mode.

4.2. ARCHITECTURE AND OPERATION OF THE CONVERTER

The converter power circuit on which the dynamic and stationary models have to be obtained, is shown in Fig. 4.1. All the stages of the switching process are high-lighted in black. Two levels of voltage are defined: V_{Lo} (low voltage level) and V_H (high voltage level). The circuit has two modes of operation: the step-up mode, which converts power from V_{Lo} to V_H, and the step-down mode which converts inversely from V_H to V_{Lo}. To carry out the study, it must be started by complying with the most demanding restrictions, which are given for the step-up mode. This mode contains a process with five stages.

The state of the active elements (transistors and diodes) is identified with 1 when they are active and 0 when they are not active. The Z-network is symmetric with $L_1=L_2=L$, $C_1=C_2=C$, and every times $I_{L1}=I_{L2}=I_L$, $I_{C1}=I_{C2}=I_C$, is verified. The entire switching process of the converter in step-up mode is shown in Fig. 4.2. In [7] the detailed switching process is shown.

4.2.1. Choice of converters

There are many topologies of DC-DC converters and many applications for them, the converter must be searched according to the application. Among the classic topologies, the following stand out. Voltage source converters, which would not be suitable in our application, because it needs a wide range of voltage regulation. Current source converters, which are more limited than other topologies in voltage gain and converted power. Converters based on high frequency transformers (HFT), could be suitable for our application, but with high voltage gains, they need a lot of copper wire and are more expensive, they are also more limited in converted power, in [12] a converter working as a battery equalizer is presented and in [13] a method of compensation of the leakage-inductor parameter based on converters (HFT) is proposed.

The Z-source has been used in inverters with very good results [18] looking for different applications such as motor control [24]. Making modifications on the Z-source is obtained the qZ-source [21]. Both techniques offer high voltage gain, support wide output voltage regulation and can be configured as bidirectional using few components. They are also good candidates for coupling. Their most significant differences are: the voltage stress of Z-source converters is twice that of qZ-source converters, the voltage gain of the Z-source converter is somewhat higher than that of the qZ-source converter. However, the Z-source converter was chosen because it has an almost linear voltage response versus duty cycle variations (which greatly simplifies control), as well as having a more symmetrical structure that facilitates the integration of the converters in the branch.

4.2.2. Step-up mode stages

Step-up mode is the only mode involved in the coupling and is found in both bidirectional (Bc) and unidirectional (Uc) converters. Fig. 4.1 shows the circuit stages of the used bidirectional converter. But to highlight the step-up mode circuit, the components S_3, S_4, L_3, L_4 and D_3 must be suppressed (in the Fig. 4.4. they have been drawn in gray) and consequently the step-down mode is eliminated from the converter. Fig 1 shows the circuits highlighted in black of the first four stages. The switching process takes place in the same order in which the stages occur. The stages of each converter in step-up mode are:

Stage-S1U, $[t_0\text{-}t_1]$: the following code indicates the status of the devices $S_1S_2S_3$=010, $D_1D_2D_3$=000, in the instant t_0 S_2 is turned on and the capacitors C_1 and C_2 are loaded with the voltage $V_C=V_{0C}$ (initial V_C of each duty cycle). At this stage, C_1 and C_2 discharge their energy through L_1 and L_2 respectively, the voltage of capacitors C_1 and C_2 varies from $V_C=V_{0C}$ to $V_C=V_{Lo}/2$. Then L_1 and L_2 are energized by the capacitors, in Fig. 4.2a,

all the variables of this stage can be observed between the coordinates t_0 and t_1. Similarly the variables of the remaining stages can be seen in their corresponding coordinates.

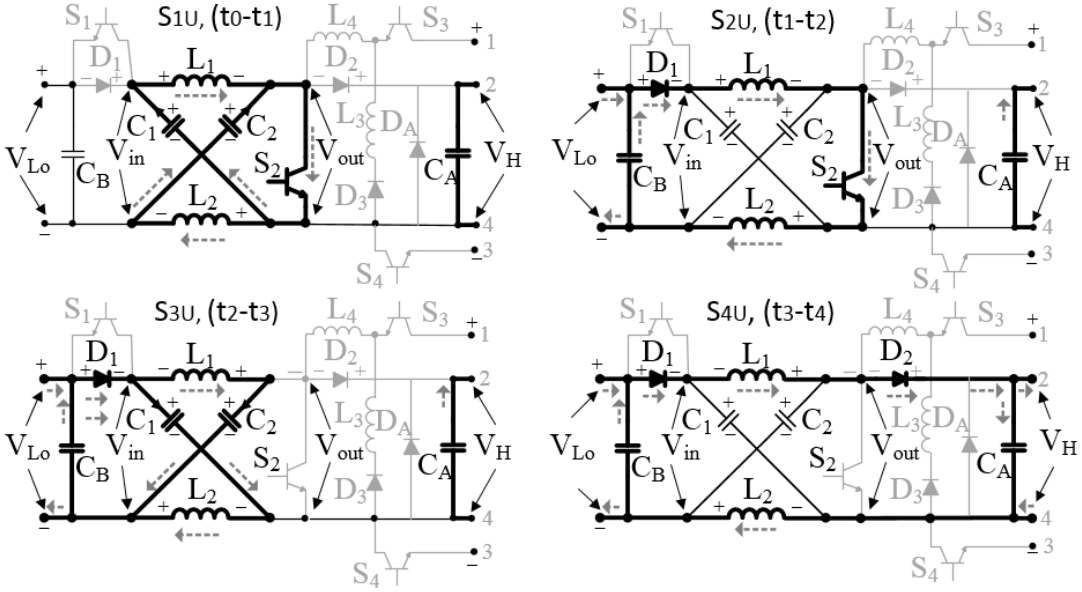

Fig. 4.1. Circuits of the different stages of the converter.

Stage-S2U, [t_1-t_2]: $S_1S_2S_3$=010, $D_1D_2D_3$=100. The inductors L_1 and L_2 are connected in series and are energized from the source through D_1, being satisfied in this stage $V_C=V_{Lo}/2$, $V_{out}=0$ and $V_{in}=V_{Lo}$. The energizing of L_1 and L_2 from the Z-source starts at t_1, and it starts with a high value of I_{L1} and I_{L2}. This value has been obtained by discharging C_1 and C_2 on L_1 and L_2 respectively (this is the key of the Z-source when it is working in step-up mode).

Stage-S3U, [t_2-t_3]: $S_1S_2S_3$=000, $D_1D_2D_3$=100, the disconnection of S_2 occurs in t_2, and $V_{out}=V_{Lo}/2=V_{C2}=V_{C1}$ is verified, see Fig. 4.2a. In the interval $t_2<t<t_3$, $I_{L1}=I_{C1}$ and $I_{L2}=I_{C2}$ are met, then the capacitors recharge happens from time t_2 to time t_3, when the condition $V_{C2}=V_{C1}=V_{0C}$ is verified, being the voltage V_{0C} maintained until the beginning of the next cycle. When S_2 is deactivated, two branches formed by L_1, C_2 and L_2, C_1 each branch are connected in parallel (seen from V_{in}), so that L_1 charges C_2 and L_2 charges C_1, see Fig. 4.1. Moreover, due to circuit configuration change at t_2, the current I_{D1}

experiences a strong increase fulfilling $I_{D1}=I_{L1}+I_{L2}$. Besides V_{out} raises its value from zero at t_2 to $V_{out}=V_{C1}+V_{L1}=V_{C2}+V_{L2}$ at time t_3.

Stage-S4U, [t_3-t_4]: $S_1S_2S_3$=000, $D_1D_2D_3$=110. V_{out} becomes slightly larger than V_H at t_3, consequently D_2 begins to conduct. Then, the energy is transferred from the battery and the inductors L_1 and L_2 to the capacitor C_A. After, this energy is supplied to the load throughout the whole period. At this stage, the conditions $V_{C1}=V_{C2}=V_{0C}$ and $I_{C1}=I_{C2}=0$ are verified, and then the contribution of energy to the load is made by L_1, L_2 and the battery, see Fig. 4.2a between times t_3 and t_4.

Stage-S5U, [t_4-t_0]: $S_1S_2S_3$=000, $D_1D_2D_3$=000. At t_4 the inductors have discharged all their energy on C_A and the current flow has been extinguished in D_1 and D_2. Moreover, is verified that $V_{in}=V_{out}=V_{C1}=V_{C2}=V_{0C}$. This situation is kept until the beginning of the next cycle. This converter have a discontinuous conduction mode thus this stage is necessary. Its duration depends on the value of the duty cycle D, during this period no current flows through any of its devices. This stage has not been represented in Fig1. During this stage current does not flows through any device, only the discharge of the C_a capacitor on the load is taking place.

The largest possible duty cycle is D=0.9T (T being the duty cycle). If D>0.9T then the converter can work in continuous conduction, circulating very high currents through the Z-network without ever extinguishing (the Z-network can be destroyed). For safety reasons the maximum duty cycle is limited to D_{max}<0.8T.

The step-down mode does not intervene in the coupling, it is only in the bidirectional converters and works in reverse of the step-up mode. The step-down mode only affects the battery converters when it has to store excess energy from the sources. Therefore, this subject is treated with less depth; its commutation is shown in Fig. 4.2b. The inductance L_4 has the mission to adapt the step-down gain, to convert the voltage of the DC bus ($V_{dc}=V_H$) to the voltage of the battery ($V_{Lo}=V_B$). The inductance L_4 is calculated after the design of all the step-up mode parameters.

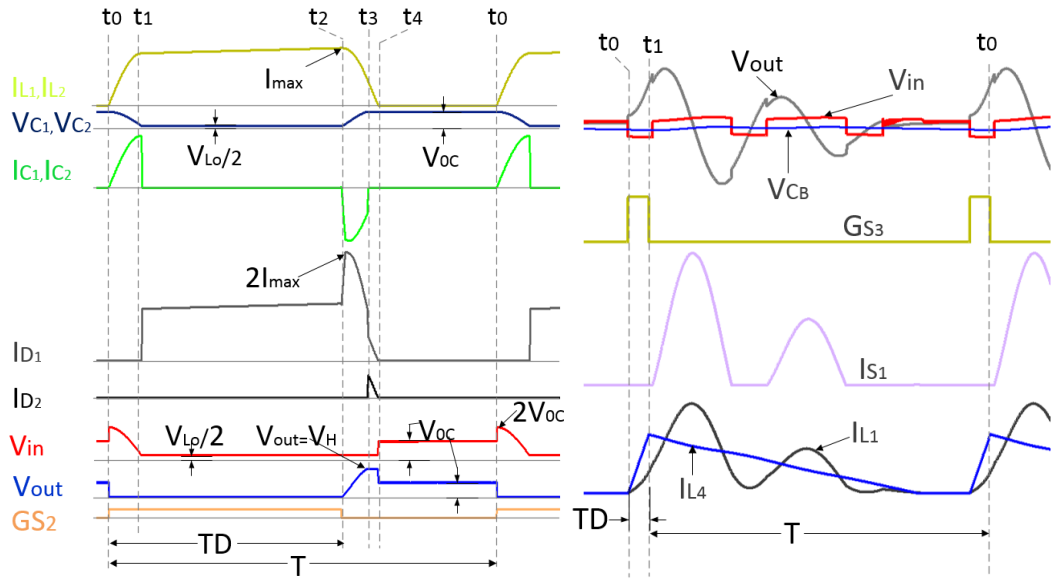

(a) (b)

Fig. 4.2. Waveforms: (a) step-up mode, (b) step-down mode.

4.3. CONVERTER ANALYSIS

Fig. 4.1 shows the four-stage circuits of the step-up mode. In the switching process five stages can be distinguished. Each of them is identified with a variable that represents the duration of the stage with respect to the total period T. All variables depend on the duty cycle D and the switching period T. Between these stages there are several relationships that have been taken from experimental tests and are shown in (1).

$$\text{Stage-S1U, } [t_0\text{-}t_1] \rightarrow \alpha = 0.13D*T; \qquad \text{Stage-S2U, } [t_1\text{-}t_2] \rightarrow \beta = 0.86D*T$$

$$\text{Stage-S3U, } [t_2\text{-}t_3] \rightarrow \gamma = 0.11D*T; \qquad \text{Stage-S3U, } [t_3\text{-}t_4] \rightarrow \delta = 0.05D*T \qquad (1)$$

$$\text{Stage-S5U, } [t_4\text{-}t_0] \rightarrow \lambda = (1-1.16D)*\mathrm{T} = (1-(1+\gamma+\delta)D)\mathrm{T}$$

Step up mode equations

In order to obtain the equations, the parameters that affect less to the final solution, such as the resistance of the capacitors, are not taken into account. In the study, transistors are considered ideal.

Stage-S1U, [t0-t1]: The converter circuit of this stage can be seen in Fig. 4.1. Only the operation of the Z-network has been highlighted. In equation (2), the current in the IL inductance of the Z-network is related to the voltage in the VC capacitors, in (3) the variation of the voltage in the Z-network is evaluated, For this reason the value of the converters output voltage VH has been taken into account, which in this stage is related to the capacitors voltage C1 and C2. In (4) the voltage variation in the output capacitor CA is valuated as a function of the load current, in the remaining stages this evaluation is also obtained.

$$L\frac{dI_L}{dt} = V_C - R_L I_L \tag{2}$$

$$C\frac{dV_C}{dt} = \frac{-V_H}{2*\alpha D}C \tag{3}$$

$$C_A\frac{dV_H}{dt} = -\frac{V_H}{R_{Load}} \tag{4}$$

Stage-S2U, [t1-t2]: D1 start driving and the circuit changes. The following equations can be proposed. In (5), the inductors current variation L1 and L2 is studied, they are fed from the battery with a voltage VLo/2, see Fig.4.1. The voltage variations on capacitors C1 and C2 are evaluated with (6), these are also evaluated in the remaining stages.

$$L\frac{dI_L}{dt} = \frac{V_{Lo}}{2} - R_L I_L \tag{5}$$

$$C\frac{dV_C}{dt} = 0 \tag{6}$$

$$C_A \frac{dV_H}{dt} = -\frac{V_H}{R_{Load}} \tag{7}$$

Stage-S3U, [t2-t3]: S2 is disconnected and the Z-network capacitors C1 and C2 starts a recharge process. The recharge energy is obtained from the source and the inductors. In (8) the IL1 and IL2 variations are evaluated according to all involved variables and in (9) the recharge process of C1 and C2 is modeled.

$$L \frac{dI_L}{dt} = -V_C - R_L I_L + V_{Lo} \tag{8}$$

$$C \frac{dV_C}{dt} = -I \tag{9}$$

$$C_A \frac{dV_H}{dt} = -\frac{V_H}{R_{Load}} \tag{10}$$

Stage-S4U, [t3-t4]: The voltage of the capacitors C1 and C2 after the recharging process has reached its maximum value, then the battery and the inductors L1 and L2 begin the process of transferring energy to the capacitor CA and the load. This situation can be modeled with the following equations.

$$L \frac{dI_L}{dt} = -R_L I_L - \frac{V_H - V_{Lo}}{2} \tag{11}$$

$$C \frac{dV_C}{dt} = 0 \tag{12}$$

$$C_A \frac{dV_H}{dt} = 2I_L - \frac{V_H}{R_{Load}} \tag{13}$$

Stage-S5U, [t4-t0]. During this stage all the variables within the Z-network remain constant and the only voltage that varies is that of the capacitor Ca (represented in 16), which feeds the load during the whole period. Equations (14) and (15) represent the

inductors current variations L1 and L2 and the capacitors voltage variations C1 and C2 respectively.

$$L\frac{dI_L}{dt}=0 \tag{14}$$

$$C\frac{dV_C}{dt}=0 \tag{15}$$

$$C_A\frac{dV_H}{dt}=-\frac{V_H}{R_{Load}} \tag{16}$$

The switching frequency used is 10 kHz or higher and then T=dt. In addition, by introducing a switching function satisfying (S_wD=D if S_w=1) and (1-S_w)D=D if S_w=0), this function activates each stage when necessary and the value of the state variables can be averaged over a switching period dt.

By introducing the switching function in the equations of the system (2)–(16), averaging throughout the whole period dt and simplifying the derivatives, the equations (17)–(19) are obtained.

$$\frac{dI_L}{dt}=\frac{RI_L}{L}(Sw(-\alpha-\beta+\gamma+\delta)+(-\gamma-\delta))+\frac{V_C}{L}(Sw(\alpha+\gamma)-\gamma)+\frac{V_H}{2L}\delta(Sw-1)+\frac{V_{Lo}}{L}\left(\mathrm{Sw}(\frac{\beta}{2}-\gamma-\frac{\delta}{2})+(\frac{\delta}{2}+\gamma)\right) \tag{17}$$

$$\frac{dV_C}{dt}=\frac{I_L}{C}(1-S_w)\gamma+\frac{V_H*S_W}{4D}\gamma \tag{18}$$

$$\frac{dV_H}{dt}=\frac{2I_L}{C_A}\delta(1-Sw)+\frac{V_H}{R_{load}C_A}(Sw(-\alpha-\beta+\gamma+\delta+\lambda)-(\gamma+\delta+\lambda)) \tag{19}$$

Taking into account that $(\alpha+\beta+\gamma+\delta+\lambda)\mathrm{D}=T$, eliminating the switching function S_w and reducing, the following expressions are obtained.

$$\frac{dI_L}{dt} = \frac{RI_L}{L}(-\alpha-\beta-\gamma-\delta)\,\mathrm{D} + \frac{\mathrm{V}_C}{L}(\alpha-\gamma)\,\mathrm{D} - \frac{V_H}{2L}\delta D + \frac{V_{Lo}}{L}\left((\frac{\beta}{2}+\gamma+\frac{\delta}{2})\right)D \tag{20}$$

$$\frac{dV_C}{dt} = -\frac{V_H}{2\alpha} - \frac{\mathrm{I}_L\,\gamma D}{C} \tag{21}$$

$$\frac{dV_H}{dt} = \frac{2I_L}{C_A}\delta D - \frac{V_H}{R_{load}C_A} \tag{22}$$

The steady state is obtained when the derivatives become zero, and taking into account that in the stage S1U, V_c varies from $(V_H + V_{Lo})/2$ in t_0 up to $V_{Lo}/2$ in t_1 and in the stage S3U, V_c varies from $V_{Lo}/2$ in en t_2 up to $(V_H + V_{Lo})/2$ in t_3. From the expressions (20)–(22) it is obtained (23) relating all the variables in a stationary model, with which the steady-state voltage gain can be analyzed in function of the component parameters of the converter.

$$\frac{V_H}{V_{Lo}} = \frac{2LR_{Load}\alpha^2 D + RR_{Load}\alpha\beta^2 D^2 + RR_{Load}\alpha^2\beta D^2 + 2LR_{Load}\alpha\beta D + 4LR_{Load}\alpha\gamma D}{2LR\alpha + LR_{load}\alpha^2 D + CLRR_{load}\beta + 3LR_{Load}\alpha\gamma D} \tag{23}$$

Substituting the values $\alpha = 0.13$, $\beta = 0.86$, $\gamma = 0.11$, and $\delta = 0.05$, expression (24) is obtained.

$$\frac{V_H}{V_{Lo}} = \frac{157300LR_{Load}D - 40807RR_{Load}D^2}{130000LR + 1300LR_{load}D + 430000CLRR_{load}} \tag{24}$$

With the expression (24) the behaviour of the converter can be evaluated at steady state. Consider that the model has been created in an average value, making 1/f=T=dt.

For example, if with (24) is studied the evolution of the gain in function of the duty cycle, assigning the values of the parameters $L = 1.5\mu H$, $C = 20\mu F$, $V_{Lo} = 12V$, $R_L = 0.002\ \Omega$ and taking three load resistors $R_{Load} = 75,\ 100\ and\ 150\ \Omega$, the three

graphs shown in Fig. 4.3a are obtained. In this figure it can be seen that the gain is higher as the loads become smaller.

If the study is performed by varying the internal resistance of the Z-network, with a load resistance of $R_{Load} = 85\Omega$, Fig. 4.3b is obtained. Where it can be observed that the gain decreases quite a lot with the increase of the internal resistance of the Z-network. Therefore, if large step-up gains are necessary, then the Z-network must have a low internal resistance and the inductors have few turns.

Figs. 3(c and d) show the study of the M_e evolution with respect to D_e, using different capacities and inductances respectively in the Z-network. It is obtained that the variation of the inductance values as of capacitance in the Z-network affect very little on the converter voltage gain. From the stationary model has been obtained (25). With this expression the converted power P_C can be found, shown in Fig. 4.4f, where it can be observed that the converted power increases as the capacitors capacity values increase and the inductors inductance values decrease.

$$P_C = Vs\left(\left(\sqrt{C\left(\frac{V_H^2}{4}+\frac{V_{Lo}V_H}{2}\right)\Big/L}\right)+\frac{TV_{Lo}D_{e\max}}{4L}\right)D_{e\max} \tag{25}$$

Consequently, the design of a Z-source converter requires a proper search of the parameters that make up the Z-network, the values of C_1, C_2, L_1 and L_2 as well as their internal resistances. This is made for obtaining the necessary gain, ensuring that the converters can convert the maximum power needed and limit the power in case of short circuit in the load. This search becomes more demanding when the converters must be coupled with their outputs in series.

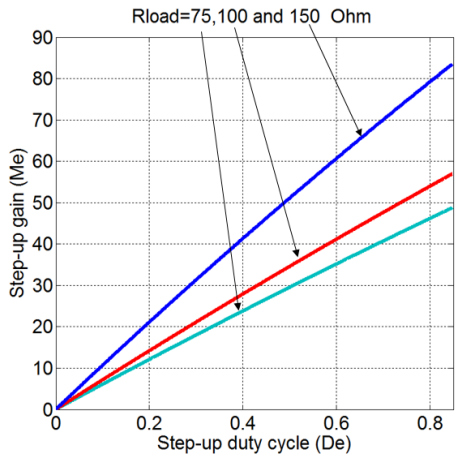

(a)

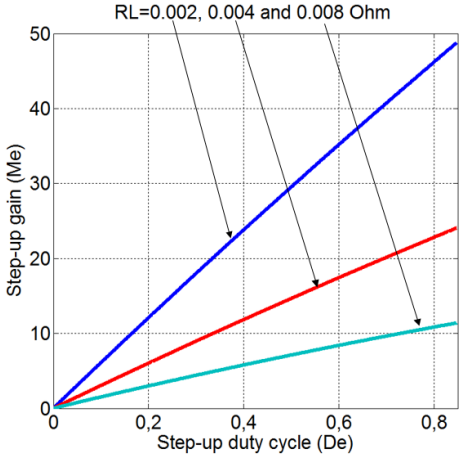

(b)

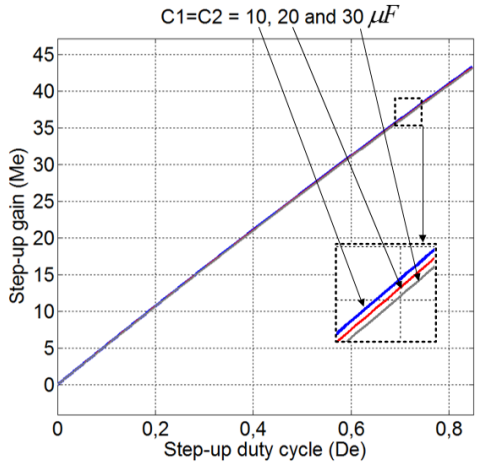

(c)

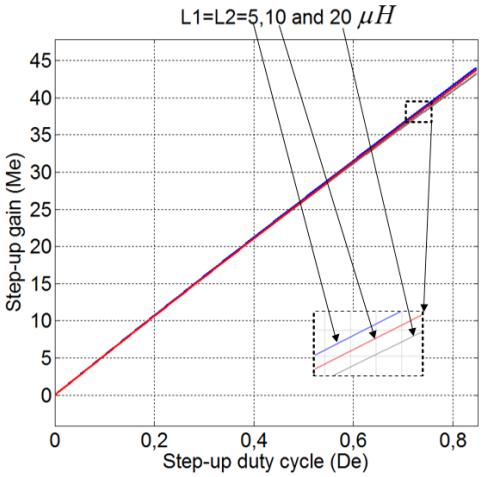

(d)

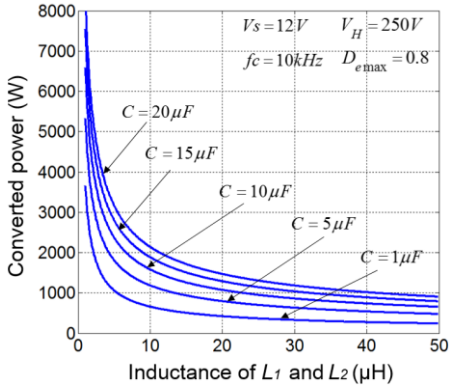

(e)

Fig. 4.3 (a) Evolution de Me versus De with resistances of different loads. (b) Evolution de Me versus De with different Z-source resistances. (c) Evolution of Me varying De, with various values of C of the Z-source and different

resistances of load. (d) Evolution of Me varying De, with various values of L of the Z-source and different resistances of load. (e) Converted power into a function of the parameters L and C of the Z-source.

4.4. DYNAMIC MODEL AND CONVERTER COUPLING CONTROL STRATEGY

Starting from the equations (20)–(22), the dynamic model of the system is obtained. This model permits to develop a driver for the converter. The following state variables are defined.

$$X_1 = I_L \quad X_2 = V_C \quad X_3 = V_H \quad \dot{X}_1 = \frac{dI_L}{dt} \quad \dot{X}_2 = \frac{dV_C}{dt} \quad \dot{X}_3 = \frac{dV_H}{dt} \quad u(\mathrm{t}) = D$$

The matrices of the dynamic model are:

$$A = \begin{pmatrix} -\frac{R}{L}(\alpha+\beta+\gamma+\delta)\bar{\mathrm{D}} & \frac{1}{L}(\alpha-\gamma)\bar{\mathrm{D}} & -\frac{1}{2L}\delta\bar{D} \\ -\frac{\gamma\bar{D}}{C} & 0 & -\frac{1}{4} \\ \frac{2}{C_A}\delta\bar{D} & 0 & -\frac{1}{R_{load}C_A} \end{pmatrix} \quad B = \begin{pmatrix} \frac{1}{L}\left(\left(\frac{\beta}{2}+\gamma+\frac{\delta}{2}\right)\right)V_{Lo} \\ -\frac{\mathrm{I}_L\gamma}{C} \\ \frac{2I_L}{C_A}\delta \end{pmatrix} \quad (26)$$

$$Y = \begin{pmatrix} 0 & 0 & 1 \end{pmatrix} * \begin{pmatrix} X_1 \\ X_2 \\ X_3 \end{pmatrix}$$

Starting from the dynamic model, the transfer function of the controller can be obtained. Since four converters whose outputs are connected in series and all four have the model shown in (26), must be controlled, each converter coupling a different source and then the converters have different parameters from each other. Therefore, to design the controller, we have worked with an average transfer function, averaging the parameters of the four converters.

Taking into account the four modeled converters, the average values of the converter parameters are: V_{Lo} = 22V (average power supply value of the source voltages), C=3µF,

L=18µH, C_A=250µF, R=0.002Ω, R_{Load}=75Ω (estimated average load resistance). Moreover the eigenvalues of the switching α=0.13, β=0.86, ϒ=0.11, δ=0.05, which are similar in the four converters. On the other hand, the most unfavorable working point must be taken into account with D=0.8, and a current in the inductors that in our case has been taken from I_L=95A. Substituting in (26), the transfer function of the converter plant of the average converter is obtained (27).

$$G(s) = \frac{38*10^3 s^2 + 2.249*10^8 s - 2508*10^{-4}}{s^3 + 142.2s^2 + 2.643*10^7 s + 1.043*10^9} \quad (27)$$

$$C(s) = \frac{175(s+20s)(1+0.40s)}{s(1+70s)} \quad (28)$$

In the representation of the place of the roots of (27), shown in Fig. 4.4, it can be seen that the system is stable, since it has all the poles and zeroes in the left half plane, and it presents a phase margin of 87.5 degrees and an infinite gain margin. Using MATLAB®, a PID controller has been designed (which acts in the step-up mode of the four converters varying its duty cycle) as shown in (28), composed of a pole at -70, two zeroes at -40 and -20 y an integrator. Fig. 4.4b shows the response of the system in open loop and in closed loop with the controller (28). Observing the step response, it can be verified that with the proposed controller the plant has been in fact controlled.

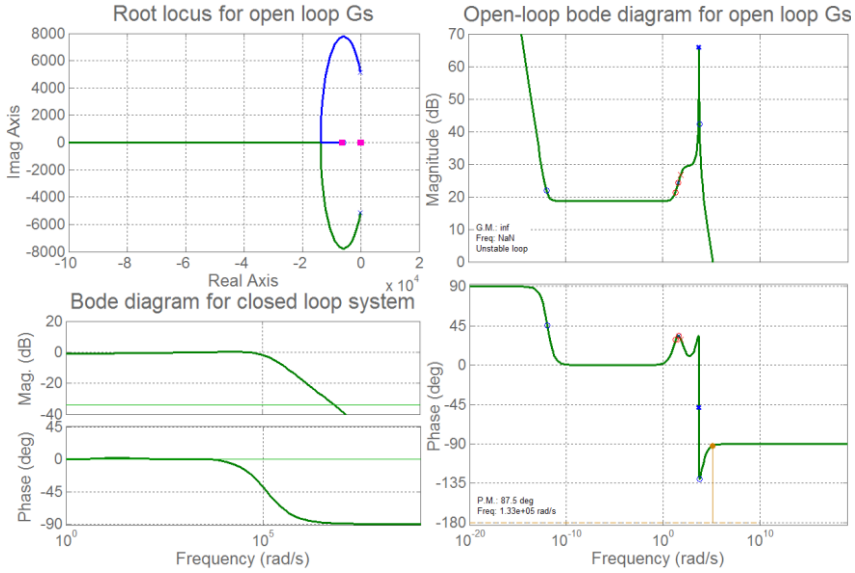

(a)

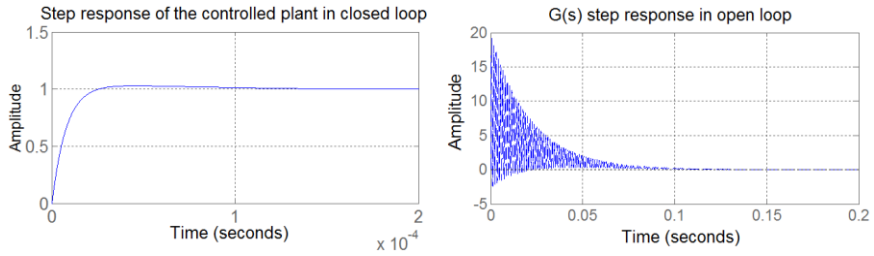

(b)

Fig. 4.4. Root locus for open-loop and Bode diagrams, uncontrolled (open loop) and controlled (closed loop) G(s) step responses of plant.

As it is indicated in (29), if the classical structure of a PID is compared with (28), then the constants are obtained with the values K_p=121.4, T_i=0.06 and T_d=0.0063.

As the controller is very fast and there is enough margin, the value of T_d can be disregarded and then the controller becomes a PI and its response is delayed a bit, but this situation is not significant. Likewise, the value of K_p can be reduced at the cost of increasing the establishment time, without a significant modification of the response.

$$Kp\left(1+\frac{1}{Ti*s}+Td*s\right)=\frac{175(s+20)(s+40)}{s(s+70)} \tag{29}$$

4.5. RESULTS

The difference between the classical coupling structure and the proposed coupling can be seen in Fig. 4.5a and 4.5b, respectively.

The proposed system has been tested with the coupling of the models of a wind turbine, some solar panels and two batteries, all of them coupled in series through the output terminals of the four Z-source converters, and a controller that regulates the duty

cycle of the four converters, see Fig. 4.5b. For the coupling of the sources and the batteries, unidirectional and bidirectional Z-source converters are utilized respectively.

The average dynamic model has been used for controller design. The designed converters have been tested by simulation working coupled as shown in Fig. 4.5c. The possibilities of management of the system for decision making are several (neural networks, fuzzy logic, etc.) but they are not contained in this work. The designed controller has the mission of maintaining stable V_{dc} by adapting the duty cycle of the four converters, in order to each source contributes proportionally to the power demanded by the load, having the system the capacity to work as if it were a single generation unit, taking advantage of all the energy generated. Fig. 4.6 presents the results of the system behaviour as well as its adaptive capabilities.

4.5.1. Design considerations.

In the coupling, a model of a three-phase wind turbine (WT) of 1000W without a regulator has been used, with a full bridge rectifier and a filter at the output. Its output voltage depends on the wind speed (5-26V). The nominal power is obtained at 12m/s, producing automatic braking at 14m/s. Another converter is placed in the model of 8 solar panels (PV), with maximum nominal power of 410W per panel, output voltage of 35.9V in conditions of maximum power. Two groups of 600Ah batteries of 18 and 12V have also been modelled. For the coupling of sources have been used the models of the four converters as indicated in Figs. 5(b and c). Consequently the four converters are coupled with their output terminals connected in series. Therefore the system (converters and controller) dampens the random variations that occur in the sources, the load is not affected at any time and always the tension in the DC bus V_{dc} remains substantially constant.

For the converters design that make the integration of the sources in the generating branch, the method exposed in [7] has been considered, which has been improved with

the results provided by the stationary model and the converted power expression (25). In the model, the reference voltage to obtain the voltage V_{cd} of the DC link, has been set at 500V. As two batteries are available, it is expected that both can support the system in case of need (if all other sources are unable to contribute). The design values assigned for the output voltage of the battery converters are: $V_{outB1}=V_{Hn}=270V$ and $V_{outB2}=V_{Hn}=450V$. The design data of the converters coupled to preserve the voltage $V_{dc,}$ close to 500V, are shown in Tables 4.2.

If a source with a generated voltage range (7-15)V is to be coupled to a generator branch, for the converter design the source power (e.g. 1000W) and average voltage value $V_{Sn}=12V$ must be considered. Likewise the average output voltage of the converter $V_{out}=250V$ must be defined (for this, the other sources and the most unfavorable coupling conditions must be taken into account), the maximum duty cycle, in this case is $D_{e\text{-}max}=$ 0.8 and the switching frequency, in this case it is set at 10kHz. Moreover, the converter must be able to convert a little more than 1000W, but not much more (even in case of short circuit) to protect the source.

The L and C values of the Z-network are obtained by substituting in (25) the previous data. In Fig. 4.3e the expression (25) has been represented with the indicated above values. To couple a source of 1000 W it can be seen that there are several L and C values that could be used. For example, if the L=18µH and C= 10µH is taken. Then with (24) the maximum gain obtained with these values is studied. For this objetive, a load resistance $R_{load}=62.5\Omega$ is taken (resistance that consumes 1000W fed with $V_H=250V$). The only missing parameter is the inductors resistance R. This parameter will be calculated so that the converter has the desired gain, in this case $M_e=20.86$ (250/12). The value obtained is R=71,236µΩ. To calculate the values of I_{t1} and I_{t2max} the expressions (31) and (32) are used respectively, obtaining $I_{t1}=97.89A$ and $It_{2max}=$ 126.78A, these values are necessary for the design of the components.

The coils will be designed for an average current value of I_{t1} and I_{t2max}, in this case with $I_{med}=112A$, inductance L=18µH and with internal resistance R lower than 71,236µΩ. For this purpose, as many parallel branches as they are necessary will be used.

The converters are designed with the above method and coupled as shown in Fig. 4.5b. They add up their energies from renewable sources, to obtain a quality supply. Therefore, even if the energy is produced with voltage and power disturbances, these do not reach the load. The Simulink® model is shown in Fig. 4.5c. The converters have been modeled with a high level of accuracy to obtain quality results. Different situations have been forced in the tests to show the capabilities of the coupling.

Table 4.2.1. design data, for the step-up mode of the Uc and Bc converters.

Source	Source rated power	Design voltage (V_{Sn})	Design power	D_{max}
P.V.	2400W	35V	2600W	0.8
W.T.	1000W	16V	1000W	0.8
B1	600Ah	18V	1650W	0.8
B2	600Ah	12V	1100W	0.8

Table 4.2.2. shows the parameters obtained for the modeling of the converters in step-up mode.

Table 4.2.2. Parameters obtained for the step-up mode design of the Uc and Bc.

Source	L_1, L_2 μH	C1, C2 μF	Currents I_{Lt1}, I_{Lt2}	Converted P_{max}
P.V.	18	6	58A, 135A	2808W
W.T	10	7	40A, 128A	1100W
B1	12	11	85A, 118A	1859W
B2	10	5	97A, 150A	1192W

Table 4.2.3. Design parameters obtained for the step-down mode of the Bc.

Step-down circuit for battery converter				
$L_4\ \mu H$	$L_3\ \mu H$	Peak current I_{L4} (A)	Dr_{max}	Converted P_{max}
50	2	88A	0.1T	2230W

If the output voltage of the wind turbine (Fig. 4.6a) is observed, it undergoes a large voltage oscillation that is proportional to the power generated. The coupling system allows the power generated with disturbances to reach the load without them. Observe the voltage of the bus DC V_{dc} in Fig.4.6c, where the V_{dc} voltage remains almost constant despite the power and voltage oscillations in the sources and changes in the demanded load.

Consequently the expression (30) is always verified.

$$V_{dc} = V_{outWT} + V_{outPV} + ... + V_{outB1} + V_{outB2} \tag{30}$$

$$(\mathrm{I_L})_{t1} = \sqrt{\frac{C}{L}\frac{V_H^2 + 2V_{Hn}V_{Sn}}{4}} \tag{31}$$

$$(\mathrm{I_{Lmax}})_{t_2} = I_{Lt1} + \frac{VSn}{2L} D_{e\max T} \tag{32}$$

There are two main sources PV and WT and two groups of batteries, with different voltages, both the sources and the batteries are coupled through the converters optimizing the energy generated and achieving a stable power supply. To show the operation of the system, tests have been forced on the model that demonstrate its robustness against variations in load as well as variations in energy production. To

better understand the results and the variables location in the circuit, figures F1 and F6 should be observed at the same time.

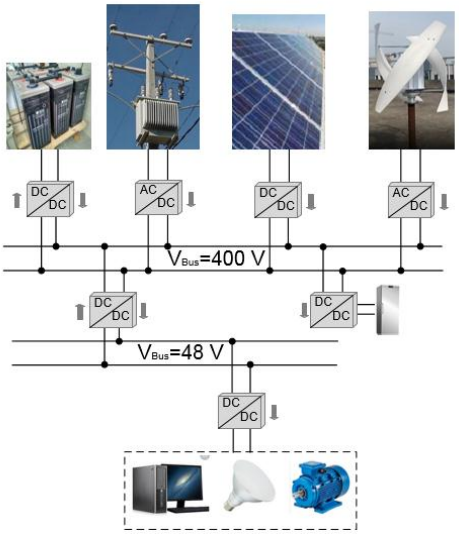

(a)

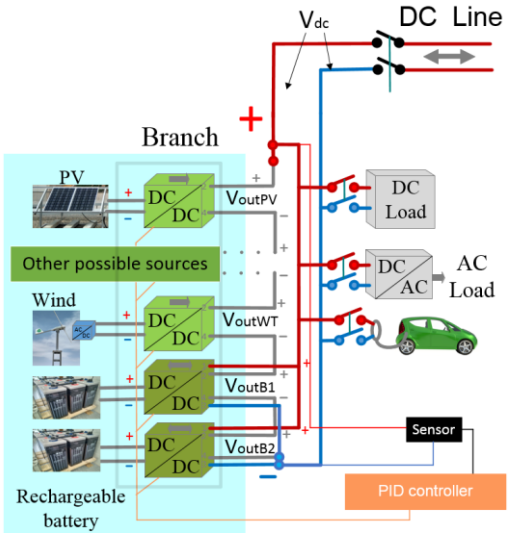

(b)

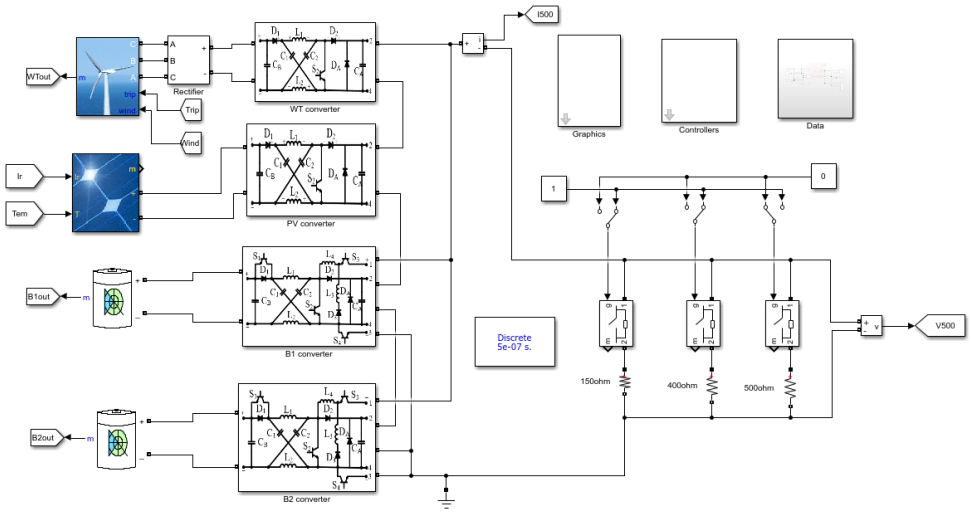

(c)

Fig. 4.5. Source coupling: (a) Classical structure, (b) Proposed coupling scheme, (c) Simulink® model of the proposed coupling.

In step-up mode, the control of all converters has been made with a single PID obtained in (28). In Fig(s) 6 the results of a forced operation are shown and can be seen the designed converters behaviour that integrate the coupling branch. Fig. 4.6b presents the currents between the C_B capacitors and the Z-source of each converter. In addition, in the battery converters the currents between the battery and the C_B capacitor are also represented in yellow (so that the battery charging process can be appreciated).

In the coordinates A, B and C three resistors of 500, 150 and 400Ω are connected successively, and can be seen how there is an currents increase in the capacitors output C_B of all the converters (see Fig. 4.6b). The contribution of power to the load is unequal in each source and depends on the design of the converter of each source and of the source itself. The system can supply energy to the load using the primary sources energy and when these do not cover the demand, some energy from the batteries is used.

Between the coordinates E and F_1 there are two zones to consider, (see Fig. 4.6a): when the voltage of the wind turbine becomes zero between the coordinates E and E_1 and when the total disconnection of the solar panels between F and F_1 occurs. As observed in Fig. 4.6b, in these zones the input currents to the wind turbine converter and the PVs converter become zero, each one in its corresponding zone and these sources do not provide power to the load.

Moreover, in Fig. 4.6c, it can be checked in the same coordinates (E, F_1 and F, F_1) that the output voltages of the PV and wind turbine converters are also zero, but the voltage in the DC bus V_{dc} is kept almost constant, being met at all times (30). In this case, the batteries are the ones that supply the energy demanded by the charge, when the sources do not cover the supply of the charge. Specifically in the coordinate E_1, the values of the voltages are approximately V_{outWT}=0V, V_{outPV}=0V, V_{outB1}=400V and V_{outB2}=100V, all adding up V_{dc}=500V.

After reconnecting the PVs at the coordinate F_1, battery B_1 at coordinate F_2 is disconnected. Due to this disconnection, in Figs, 6(b,c), there are sharp increases in both the input current to the PV converter and the V_{outPV} voltage, the power that was supplied by B_1 to the load is now supplied by PV. Then between the coordinates G and H the

battery B_1 has been put into charge storing energy from the primary sources. As seen in Fig. 4.6b, the input current to the battery converter B_1 is negative. Looking at Fig. 4.6c, can be seen that the battery that is being charged does not provide voltage to V_{dc}, being $V_{outB1}=0$ between the coordinates F_2 and I. The same procedure between the J and M coordinates has also been forced on the B_2 battery. If a battery is charging, it does not supply power to the branch, but it can store excess energy, while the other converters and their sources supply the load with a stable supply.

On the other hand, as seen in Fig. 4.6d, all the output currents of the converters are equal to each other, except during the time in which the sources do not produce energy or their converters have been disconnected. This is because the Z-networks of all active converters are connected in series while the switching of each active converter takes place. For example, in the E coordinate of Fig. 4.6d, I_{outWT} becomes zero (the wind turbine does not produce energy in that time), but the output currents of the other converters (I_{outPV}, I_{outB1} and I_{outB2}) are equal to each other and are those feeding the load. Each converter has an output capacitor labeled C_A. The currents I_{outWT}, I_{outPV}, I_{outB1} and I_{outB2} charge this capacitor in its corresponding converter. The shape of these currents are pulses shown in Fig. 4.6b.

Then, the bus current I_{dc} which feeds the load (shown in Fig. 4.6d), is continuous with very low oscillations, the output voltages V_{outWT}, V_{outPV}, V_{outB1} and V_{outB2} of each converter are measured at the terminals of the capacitors C_A of each converter, and the sum of them produces the bus voltage V_{dc} see Fig. 4.6c. Despite the large oscillations that occur in all the V_{out} voltages of the converters (due to the randomness of the load and the generation), the coupling system of the sources, by means of the Z-source converters, keeps the voltage value of the DC bar V_{dc} nearly constant (close to 500V) and provides a quality supply at the load. After the N coordinate there has been a sharp increase in the load. But despite this, a DC bus voltage oscillation of approximately 2V can be observed, see Fig 6c, which is less than 1% of the voltage V_{dc}.

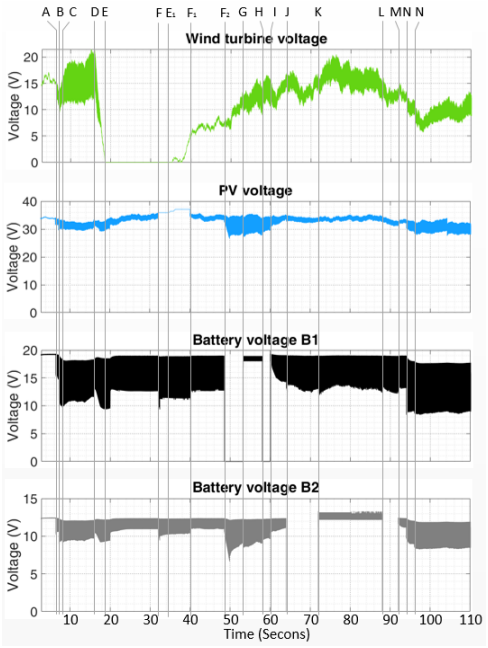

(a)

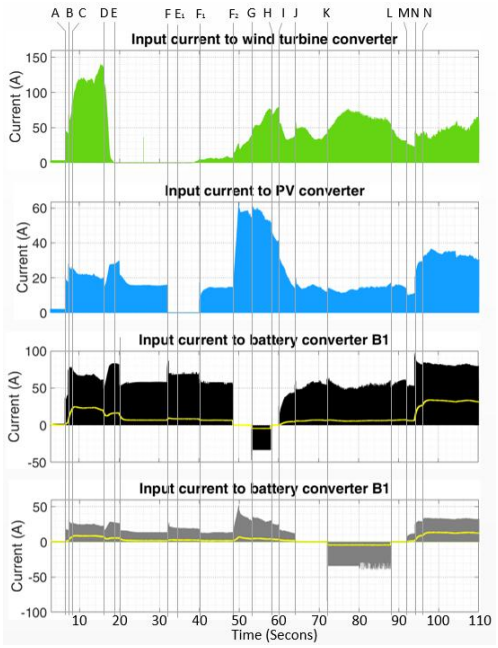

(b)

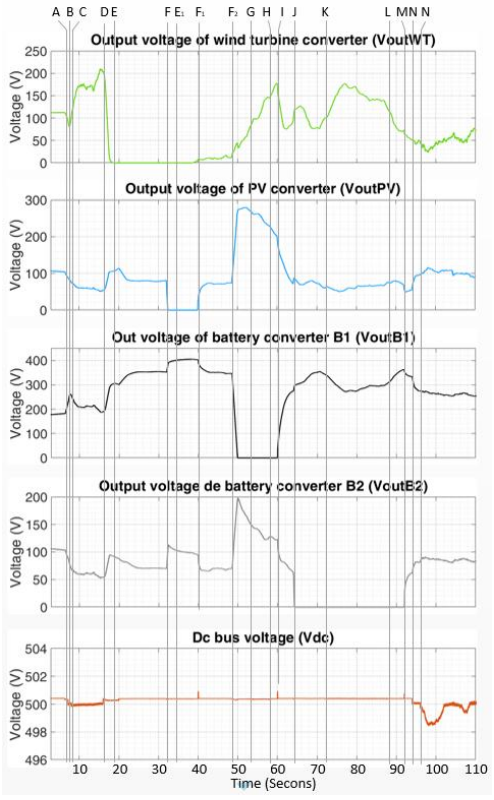

(c)

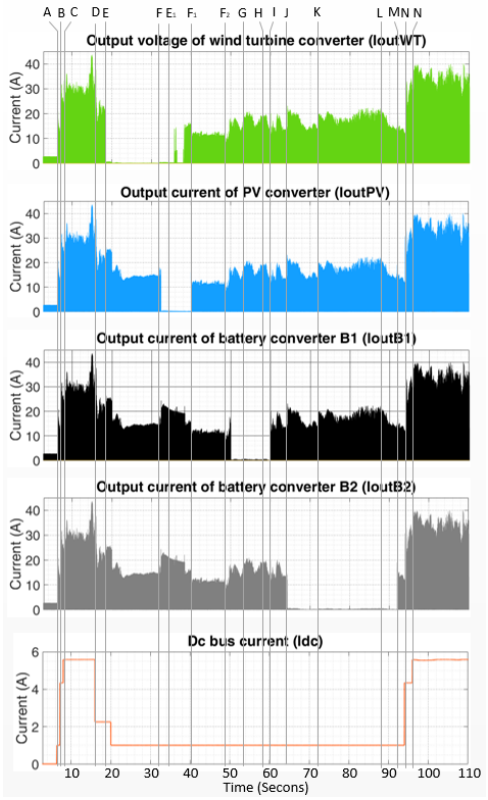

(d)

Fig. 4.6. Simulation model obtained results. (a) Voltages in the sources; (b) Currents in the converters inputs; (c) Voltages in the converters outputs and Vdc; (d) Currents in the converters outputs and Idc.

When the sources generates power with associated disturbances or a sudden disconnection of some source, battery or of its converters occurs and likewise when the generated power at the sources varies abruptly. The coupling ensures that these disturbances do not reach the load, maintaining a stable supply and the DC bus retains its voltage V_{dc} almost constant. In this case, the voltage V_{dc} is very close to 500V. The system also makes possible to take advantage of surplus energy from primary renewable sources (both permanent and transient) while preserving the quality supply to the load with V_{dc} almost constant. The battery converters can alternate from supplying the charge to charging the battery in a very short time, which permits to take advantage of all the transient surplus energy from the primary sources by storing them in the batteries, this is very difficult to comply with a classical system as the one shown in Fig. 4.5a.

For battery charging (converters working in step-down mode) two controllers have also been used, one for each battery converter that have not been treated in this work, since they are not related to the coupling of converters.

The ways to manage this system are many and are not intended to be contemplated in this work. It is only intended to show the possibilities of coupling DC sources, optimized by the converters proper design, connected with their outputs in series. The main contributions in this work are the coupling structure based on Z-source converters, the improvement of the design obtained from the converter stationary model as well as the dynamic model obtained, which has allowed us to obtain a controller with which all converters work synchronized in their step-up mode with a single controller.

If the traditional system is compared with the proposed in the traditional system, the voltage hardly exceeds 400 V at the DC bus. When the sources do not provide sufficient voltage, it is not possible to take advantage of all the energy generated, there are also transient states where it is not possible to take advantage of all the energy generated. As the system works with low voltages, this system is very limited in coupling power (a few kilowatts) and the distance between sources cannot be very long. To increase the power, more current is required and this increases the Joule losses and the cost of the converters.

In these systems, losses are estimated between 15 to 20%. Comparing the useful energy with the generated energy.

The proposed system can work at thousands of volts and it has the capacity to use almost all the energy generated, including that of the transient states, it can reach megawatt coupling powers. The generating branches can be interconnected over long distances, as it works with high voltages, the losses due to the Joule effect are greatly reduced, in this system it is estimated that 3 to 7% of the energy generated is lost (this varies with the distance between sources).

4.6. DISCUSSION

The classic DC sources coupling system is made by coupling the sources in parallel with each other and with the batteries, this technique severely limits the application of microgrids composed of small and medium power sources and low voltages. The sources for residential use (powers of a few kilowatts), with the classic system the working voltages are low, especially when batteries are necessary, normally of voltage below 100 V. It forces the use of current controllers for the coupling. Likewise, it is difficult to remove the oscillations of the generated power.

With the proposed system (based on a synchronized converters design) several sources of different types can be coupled (with different voltages and powers) and all the energy generated by the sources can be harnessed. The sources can be backed up by the batteries only when they do not cover the demand, ensuring that the randomness of the sources (especially wind turbines) does not affect the load.

The proposed system optimizes the coupling, taking advantage of all the energy generated, improving the efficiency of the system, obtaining a stable supply and being able to feed the load with higher voltage levels than the classic ones. Wind turbines, like all coupled sources, can also have their voltage uncontrolled at their terminals.

This new coupling technique opens up new possibilities, such as energy management (not studied in this work). This can be implemented in several different ways (with neural networks, artificial intelligence techniques, etc.). Similarly, the study of the microgrids stability composed of autonomous generating branches can extend this work and generate advances in renewable energy microgrids.

4.7. REFERENCES

1. Wang, F. A Novel Quadratic Boost Converter with Low Current and Voltage Stress on Power Switch for Fuel-Cell System Applications. *Renew. Energy* **2018**, *115*, 836–845, doi:10.1016/j.renene.2017.08.032.

2. Goudarzian, A.; Khosravi, A.; Raeisi, H.A. Analysis of a Step-up Dc/Dc Converter with Capability of Right-Half Plane Zero Cancellation. *Renew. Energy* **2020**, *157*, 1156–1170, doi:10.1016/j.renene.2020.05.088.

3. Kolli, A.; Gaillard, A.; De Bernardinis, A.; Bethoux, O.; Hissel, D.; Khatir, Z. A Review on DC/DC Converter Architectures for Power Fuel Cell Applications. *Energy Convers. Manag.* **2015**, *105*, 716–730, doi:10.1016/j.enconman.2015.07.060.

4. Babaei, E.; Shokati Asl, E. A New Topology for Z-Source Half-Bridge Inverter with Low Voltage Stress on Capacitors. *Electr. Power Syst. Res.* **2016**, *140*, 722–734, doi:10.1016/j.epsr.2016.04.010.

5. Khan, M.N.H.; Forouzesh, M.; Siwakoti, Y.P.; Li, L.; Kerekes, T.; Blaabjerg, F. Transformerless Inverter Topologies for Single-Phase Photovoltaic Systems: A Comparative Review. *IEEE J. Emerg. Sel. Top. Power Electron.* **2020**, *8*, 805–835, doi:10.1109/JESTPE.2019.2908672.

6. Dong, S.; Zhang, Q.; Chunbo, Z. Switched-Coupled-Inductor Z-Source Inverter with a High Boost Inversion Capability. *IET Power Electron.* **2020**, *13*, 2671–2674, doi:10.1049/iet-pel.2020.0204.

7. Ortega, M.; Ortega, M.V.; Jurado, F.; Carpio, J.; Vera, D. Bidirectional DC–DC Converter with High Gain Based on Impedance Source. *IET Power Electron.* **2019**, *12*, 2069–2078, doi:10.1049/iet-pel.2018.5385.

8. Spier, D.W.; Oggier, G.G.; da Silva, S.A.O. Dynamic Modeling and Analysis of the Bidirectional DC-DC Boost-Buck Converter for Renewable Energy

Applications. *Sustain. Energy Technol. Assessments* **2019**, *34*, 133–145, doi:10.1016/j.seta.2019.05.002.

9. Ortega, M.; Lanagrán, E.; Ortega, M.V.; Jurado, F. Design and Integration of Z-Source Converters for Energy Management with Series Operation: Applied to DC Microgrid. *Int. J. Electr. Power Energy Syst.* **2021**, *128*, doi:10.1016/j.ijepes.2021.106781.

10. Chen, D.; Deng, J.; Wang, W.; Wang, Z.; Wang, S. A Novel Voltage-Fed Hybrid Bridge Combining Semiactive Rectifier Converter for Wide Voltage Gain. *IEEE Trans. Ind. Electron.* **2022**, *69*, 365–375, doi:10.1109/TIE.2021.3051577.

11. Kan, J.; Xie, S.; Tang, Y.; Wu, Y. Voltage-Fed Dual Active Bridge Bidirectional. *IEEE Trans. Power Electron.* **2014**, *29*, 3582–3590.

12. Shi, F.; Song, D. A Novel High-Efficiency Double-Input Bidirectional DC/DC Converter for Battery Cell-Voltage Equalizer with Flyback Transformer. *Electron.* **2019**, *8*, doi:10.3390/electronics8121426.

13. Zhang, Y.; Wang, Z.; Li, Y.W.; Hou, N.; Cheng, M. A Leakage-Inductor Parameter Compensation Method for Paralleled Current-Fed Isolated DC/DC System. *IEEE Trans. Power Electron.* **2020**, *35*, 1160–1164, doi:10.1109/TPEL.2019.2930330.

14. Ortega, M.; Jurado, F.; Valverde, M. Novel Topology for DC/DC Unidirectional Converter for Fuel Cell. *IET Power Electron.* **2014**, *7*, 681–691, doi:10.1049/iet-pel.2013.0142.

15. Gao, S.; Wang, Y.; Guan, Y.; Xu, D. A High Step Up SEPIC-Based Converter Based on Partly Interleaved Transformer. *IEEE Trans. Ind. Electron.* **2020**, *67*, 1455–1465, doi:10.1109/TIE.2019.2910044.

16. Liu, Y.; Abu-Rub, H.; Ge, B. Front-End Isolated Quasi-Z-Source DC-DC Converter Modules in Series for High-Power Photovoltaic Systems-Part I:

Configuration, Operation, and Evaluation. *IEEE Trans. Ind. Electron.* **2017**, *64*, 347–358, doi:10.1109/TIE.2016.2598673.

17. Peng, F.Z.; Member, S. Z-Source Inverter. *IEEE Trans. Ind. Appl.* **2003**, *39*, 504–510.

18. Ahmad, A.; Bussa, V.K.; Singh, R.K.; Mahanty, R. Switched-Boost-Modified Z-Source Inverter Topologies with Improved Voltage Gain Capability. *IEEE J. Emerg. Sel. Top. Power Electron.* **2018**, *6*, 2227–2244, doi:10.1109/JESTPE.2018.2823379.

19. Stepenko, S.; Husev, O.; Vinnikov, D.; Fesenko, A.; Matiushkin, O. Feasibility Study of Interleaving Approach for Quasi- Z-Source Inverter. *Electron.* **2020**, *9*, 1–11, doi:10.3390/electronics9020277.

20. Barath, J.N.; Soundarrajan, A.; Stepenko, S.; Husev, O.; Vinnikov, D.; Nguyen, M.K. Topological Review of Quasi-Switched Boost Inverters. *Electron.* **2021**, *10*, doi:10.3390/electronics10121485.

21. Cha, H.; Li, Y.; Peng, F.Z. Practical Layouts and DC-Rail Voltage Clamping Techniques of Z-Source Inverters. *IEEE Trans. Power Electron.* **2016**, *31*, 7471–7479, doi:10.1109/TPEL.2016.2518807.

22. Florez-Tapia, A.M.; Vadillo, J.; Martin-Villate, A.; Echeverria, J.M. Transient Analysis of a Trans Quasi-Z-Source Inverter Working in Discontinuous Conduction Mode. *Electr. Power Syst. Res.* **2017**, *151*, 106–114, doi:10.1016/j.epsr.2017.05.022.

23. Zhu, X.; Zhang, B.; Qiu, D. Enhanced Boost Quasi-Z-Source Inverters with Active Switched-Inductor Boost Network. *IET Power Electron.* **2018**, *11*, 1–14, doi:10.1049/iet-pel.2017.0844.

24. Dehghanzadeh, A.R.; Behjat, V.; Banaei, M.R. Double Input Z-Source Inverter Applicable in Dual-Star PMSG Based Wind Turbine. *Int. J. Electr. Power Energy Syst.* **2016**, *82*, 49–57, doi:10.1016/j.ijepes.2016.02.017.

25. Wang, B.; Tang, W. A New Cuk-Based z-Source Inverter. *Electron.* **2018**, *7*, doi:10.3390/electronics7110313.

26. Papadimitriou, C.N.; Zountouridou, E.I.; Hatziargyriou, N.D. Review of Hierarchical Control in DC Microgrids. *Electr. Power Syst. Res.* **2015**, *122*, 159–167, doi:10.1016/j.epsr.2015.01.006.

27. Frances, A.; Asensi, R.; Garcia, O.; Prieto, R.; Uceda, J. Modeling Electronic Power Converters in Smart Dc Microgrids - An Overview. *IEEE Trans. Smart Grid* **2018**, *9*, 6274–6287, doi:10.1109/TSG.2017.2707345.

5. Conclusiones, aportaciones originales de la tesis y futuras líneas de investigación

5.1 Conclusions and original contributions.

The primary renewable energies, sun and wind, are not controllable by humans and have a high degree of randomness. Photovoltaic solar panels generate DC, wind turbines generate energy in the form of AC, but it can be easily rectified. It should be noted that DC can be stored for later use, so batteries or supercapacitors are needed for storage. DC can also be stored in the form of green hydrogen, obtained with electrolyzers.

In this way, green hydrogen can be produced with the energy left over during off-peak hours, and then used as fuel using fuel cell to produce electricity again, when renewable generation is not enough to feed the load. The green hydrogen can be transported and stored.

Green hydrogen can be considered a human-controlled renewable energy source just like biomass. The latter can be used to produce electrical energy through combustion or gasification processes, the latter being a less costly process than combustion.

To achieve the energy use of both random primary energies (sun, wind) and controllable secondary energies, DC/DC and AC/DC power converters are essential, as well as structures that allow us to integrate and control all these elements in the same microgrid, so that energy can be obtained from various sources, always prioritizing the non-controllable ones and reserving the controllable ones for times of scarcity of random renewable energies.

According to the described concept and as a specific result of this thesis, an innovative method of series coupling of several energy sources, being these controlled and uncontrolled renewable sources, has been presented in chapter 2. The primary uncontrolled (random) sources are: a wind turbine, a set of photovoltaic solar panels, also coupling a fuel cell which is controllable; for the coupling of these sources a unidirectional converter has been used for each of them. On the other hand, two bidirectional converters have been used for the integration in the coupling of two batteries. The integration of both sources and batteries has required calculating and designing the necessary converters and their impedance networks, depending on each of the sources and the coupling conditions and parameters. In the battery converters, starting from the design of the RZ for the step-up mode, the coupled inductor that adapts the RZ in the step-down mode has been obtained. The design method is justified in chapter 2.

To achieve the coupling, a controller acting on the duty cycle of all the converters at the same time is necessary. In Chapter 4, the dynamic model of the converter in boost mode was studied. Using this model, the average converter of all the coupled converters has been obtained and with the transfer function of the average converter, the controller used to control the coupling of converters in boost mode has been obtained.

Finally, in Chapter 3, the series coupling technique has been used to make a gasifier capable of working in island, with a quality supply and with good load following

capability, which is one of the problems that gasifiers have when they try to work in island. This has been achieved by integrating in series the gasifier generator with two batteries, through impedance source converters, with the outputs of the gasifier converter and battery converters coupled in series, thus, without changing the dynamic response of the gasifier-generator plant, a stable and quality power supply is achieved, with external actuation.

Specific results of this thesis include:

- A series coupling system, which allows us to couple several sources and ESSs. It improves the parallel coupling system, when it comes to coupling small and medium power sources, as is the case with the sources used in residential areas. The proposed coupling allows us to achieve a much higher coupling voltage than that obtained in parallel coupling, this also leads us to achieve greater coupling power and to expand the area of energy distribution, being able to integrate more subscribers (generators-consumers) within the same microgrid. Being a modular system that allows us to add several voltages in series, the voltage stress of the converter components is eliminated. Likewise, voltage disturbances are easily eliminated; they are even compensated between the different sources and those that are not compensated are eliminated by the converters of the ESSs.

- A method of designing and calculating impedance source converters in order to integrate a source with specific characteristics or a specific ESS into a coupling branch, with predefined parameters and targets.

- The dynamic model of the impedance source converter that allows us to design a controller.

- As an application of the coupling, a method is presented to stabilize and make independent a power supply based on a biomass gasifier. With this method, a gasifier can work as an island or can be coupled in a microgrid.

This research helps to improve renewable energy microgrids in general and in particular can be very useful to improve DC microgrids, especially in isolated or remote areas, where there is no possibility of public power grid. The integration of several

renewable sources of different types and ESS in series, configured as branches, can be coupled in parallel. This opens the door to new microgrid structures, which, starting from small and medium power sources, can achieve high coupling powers and provide electricity service to subscribers distributed over large areas.

Low quality DC supplies can also be improved, aided by an external system that does not affect the supply dynamics, but mitigates supply disturbances.

5.2 Futuras líneas de investigación.

5.2.1 Gestión del sistema.

El sistema de acoplamiento propuesto en esta tesis admite muchas técnicas de gestión, desde una gestión clásica basada en decisiones según unos criterios lógicos o prefijados, hasta otros tipos de gestión, basados en técnicas más avanzadas como la inteligencia artificial, donde las decisiones son tomadas por algoritmos con capacidad de aprendizaje, como las redes neuronales o el aprendizaje por refuerzo.

5.2.2 Aumento de la potencia convertida.

Los convertidores necesitan aumentar las potencias convertidas para ser aplicados cada vez a fuentes de mayor potencia. El convertidor puede ser mejorado en este sentido, desarrollando nuevas redes de impedancia que tengan capacidad para obtener ganancias mayores y convertir potencias mayores.

5.2.3 Reducción del estrés de tensión.

El estrés de tensión es uno de los problemas que más limita a los convertidores, ya que sus componentes soportan niveles de tensión limitados. El convertidor propuesto presenta muy buenas prestaciones en cuanto a potencia convertida y ganancia de tensión, pero está sometido a un estrés de tensión susceptible de ser mejorado. Pudiendo ser una futura línea de investigación el obtener redes de impedancia y técnicas de conmutación

que consigan mejorar el estrés de tensión, pero sin pérdida de linealidad de la salida respeto a ciclo de trabajo.

5.2.4 Mejora en las técnicas de control del acoplamiento de varios convertidores.

Para el control de convertidores pueden ser aplicadas diversas técnicas, y sobre todo, para su control del acoplamiento se ha aplicado una técnica clásica basada en un modelo promedio del convertidor, por lo que se propone como futura línea, la aplicación de otras técnicas que puedan mejorar el acoplamiento.

5.3 Publicaciones.

5.3.1 Artículos JCR

[1] M. Ortega, E. Lanagrán, M. V. Ortega, and F. Jurado, "Design and integration of Z-source converters for energy management with series operation: Applied to DC microgrid," Int. J. Electr. Power Energy Syst., vol. 128, no. January, 2021, doi: 10.1016/j.ijepes.2021.106781.

[2] E. Lanagrán, M. V. Ortega, M. Ortega, J. P. Roa, and P. García-Triviño, "Improvement of the Coupling of Renewable Sources through Z-Source Converters Based on the Study of Their Dynamic Model," Electron., vol. 11, no. 13, 2022, doi: 10.3390/electronics11132074.

[3] E. Lanagrán, M. V. Ortega, M. Ortega, D. Vera, and F. Jurado, "Design of an energy management system applied to an electric power plant based on a biomass gasifier," Renew. Energy, vol. 216, no. August, p. 119116, 2023, doi: 10.1016/j.renene.2023.119116.

5.3.2 Patente solicitada.

Solicitud de patente Nº P202031226

Título: Convertidores de corriente continua y rama generadora de corriente.